

Tailoring the Surface Chemistry of the Nanoparticles to Modulate their Interactions with Proteins and Cells

Dissertation

zur Erlangung des Doktorgrades

an der Fakultät für Mathematik, Informatik und Naturwissenschaften

Fachbereich Physik

der Universität Hamburg

Vorgelegt von

Saad Megahed

Hamburg

2022

This thesis is printed and published with the support of the German Academic Exchange Service.

Gutachter/innen der Dissertation:	Prof. Dr. Robert Blick Prof. Dr. Alaaldin Alkilany
Zusammensetzung der Prüfungskommission:	Prof. Dr. Florian Grüner Prof. Dr. Wolfgang Parak Prof. Dr. Gabriel Bester Prof. Dr. Alaaldin Alkilany Prof. Dr. Markus Klapper
Vorsitzende/r der Prüfungskommission:	Prof. Dr. Wolfgang Parak
Datum der Disputation:	25.05.2022
Vorsitzender Fach-Promotionsausschusses Physik:	Prof. Dr. Wolfgang Parak
Leiter des Fachbereiches PHYSIK:	Prof. Dr. Günter H. W. Sigl
Dekan der Fakultät MIN:	Prof. Dr. Heinrich Graener

Eidesstattliche Versicherung / Declaration of oath

Hiermit versichere ich an Eides statt, die vorliegende Dissertationsschrift selbst verfasst und keine anderen als die angegebenen Hilfsmittel und Quellen benutzt zu haben.

I hereby declare upon oath that I have written the present dissertation independently and have not used further resources and aids than those stated.

Hamburg, den 10.03.2022



Unterschrift des Doktoranden

DEDICATION

This study is wholeheartedly dedicated to those beloveds we lost, Prof. M. Elgohary, Dr. Theo Schotten, Herr. Horst Urbanski, and my grandfather Abdelmoneim Megahed.

And lastly, we dedicated this work to all those we lost because of the global pandemic around the world.

List of publications

- 1 **Saad Megahed**, Nicole Wutke, Markus Klapper, Wolfgang Parak, and Neus Feliu. Role of the surface chemistry on Protein adsorption and cellular uptake. *In progress*.
- 2 Huijie Yan, Michele Cacioppo, **Saad Megahed**, Francesca Arcudi, Luka Dordevic, Dingcheng Zhu, Maurizio Prato, Wolfgang J. Parak, Neus Feliu. Influence of the chirality of carbon nanodots on their interaction with proteins and cells. *Nat Commun* 12, 7208 (2021). <https://doi.org/10.1038/s41467-021-27406-1>.
- 3 Sanchez-Cano, Carlos; Alvarez-Puebla, Ramon A.; Abendroth, John M; **Megahed, Saad**;.....; Parak, Wolfgang J. X-ray-Based Techniques to Study the Nano–Bio Interface. *ACS nano*; 10.1021/acsnano.0c09563 (2021).
- 4 Stefania Garbujo; Elisabetta Galbiati; Lucia Salvioni; Matteo Mazzucchelli; Gianni Frascotti; Xing Sun; **Saad Megahed**; Neus Feliu; Davide Prospero; Wolfgang J. Parak; Miriam Colombo. Functionalization of colloidal nanoparticles with a discrete number of ligands based on a “HALO-bioclick” reaction. *Chem. Commun.* **56**, 11398–11401; 10.1039/D0CC04355A (2020).
- 5 Roy, Sathi; Liu, Ziyao; Sun, Xing; Gharib, Mustafa; Yan, Huijie; Huang, Yalan; **Megahed, Saad**; Schnabel, Maximilian; Zhu, Dingcheng; Feliu, Neus; Chakraborty, Indranath; Sanchez-Cano, Carlos; Alkilany, Alaaldin M.; Parak, Wolfgang J. Assembly and Degradation of Inorganic Nanoparticles in Biological Environments. *Bioconjugate Chemistry* **30**, 2751–2762; 10.1021/acs.bioconjchem.9b00645 (2019).

Conference contribution:

- 1 ‘How the surface charge of the nanoparticles modulates their protein and cell interactions?’ **Saad Megahed**, Nicole Wutke, Neus Feliu, Markus Klapper and Wolfgang J. Parak. AMA4MED <https://www.nanoge.org/proceedings/AMA4MED/624af337bbd506660170e2c8> [Oral]
- 2 “Universal approach to obtain colloidal stable Nanoparticles with different charge density” **Saad Megahed**, Nicole Wutke, Neus Feliu, Markus Klapper and Wolfgang J. Parak. Nanax9 Conference <http://www.nanax.org/nanax9.html> [Poster]

Acknowledgments

The present work would not be possible without the support and the contribution of many wonderful people. I would like, first of all, to thank my supervisors Prof. Wolfgang Parak, Prof. Robert Blick, and Dr. Neus Feliu. Thanks to Prof. Wolfgang Parak, for having me in his group at the University of Hamburg, where I have spent my Ph.D. studies. I would like to thank him for proposing the topic, his instructive guidance, and more important the way of thinking, interpreting, and criticizing the data. Where I have learned how to use basics and fundamental tools to answer a complex question.

I would like also to thank my mentor Dr. Neus Feliu for her suggestion, support, and discussion that enrich me during my Ph.D. work.

This work could not exist without our collaborators, therefore, I would like to thank Dr. Nicole Wutke, and Prof. Markus Klapper from Max Planck Institute for Polymer Research, for providing us with part of the amphiphilic polymers that have been used in the present study. Additionally, our collaborators from the Chemistry Department at the University of Hamburg and the Center of Applied Nanotechnology (CAN), Dr. Theo Schotten (we are so sorry to hear, he passed away at the beginning of 2021. Such a great person, I've enjoyed my short discussion with him, our condolences to his group and his family) and Ms. Öznur Tokmak, for supporting us with the QDs that has been used in the present work. I acknowledge also the work of Ms. Marta Gallego from CIC Biomagune for her assistance in recording the TEM of the nanoparticles.

Every journey starts with the first step, and my first step in the lab was under the guidance of Dr. Xing Sun, I would like here to thank him for helping me to make my first reaction and to adapt to the group. Thanks to Dr. Hujie Yan for her assistance and for introducing me to different techniques as Flow cytometer and SDS-PAGE gel electrophoresis, and special thanks to Ms. Yalan Huang for helping me with the Drop Shape Analyser machine and for taking care of our cell lab. Most of the ICP-MS samples have been recorded with the assistance of my colleagues Mr. Yang Liu and Mr. Bing Qi, I would like here to thank them for that.

Special thanks to Prof. Alaaldin Alkilany from the college of Pharmacy, Qatar University for his great support, fruitful discussion, and for his guidance whether in science or life. The Ph.D. life includes the good and the hard moments and without friends to share it with, the moments will be harder. Therefore, I would like to thank my colleague Dr. Mustafa ElGharib for sharing with me those moments throughout my Ph.D. time.

I would like to thank every current and former member of our group, the BiophotoniK group at the University of Hamburg for their support, sharing science, and cheerful atmosphere.

Acknowledgments

Each student normally has a mentor, in my case, I got many through my scientific life those who support me and encourage me to be a good student. I would like to use this chance to show my sincere gratitude to Prof. Tamer Gamal El-Din from the Department of Pharmacology, University of Washington, for his continuous support and guidance before I came to Germany and even through my Ph.D. time there. Additionally, I cannot forget my mentor Prof. Ahmed Eldib from the Department of Radiation Oncology, Fox Chase Cancer Center, for his support, advice, and guidance.

Sincere appreciation to the PIER Helmholtz Graduate School for giving me the opportunity to develop my skills, German language, and for their financial support. I would like to thank the German Academic Exchange Service (DAAD, Deutscher Akademischer Austauschdienst) and the Ministry of Higher Education and Scientific Research (MHESR) in Egypt for granting me the GERLS scholarship, and co-funding me throughout the entire Ph.D. time. Special thanks for their support during the pandemic time.

Finally, I want to thank my family, in Egypt and here in Germany for their unconditional support and love. Special thanks to my wife Asmaa Megahed for her support and for always being with me. During my Ph.D., we got our gift, my son Yahia Megahed. I would like to use this chance to thank him, he add meaning to my life. Your Dad loves you.

Abstract

Nowadays, nanomedicine is evolving faster and is already present in our daily life. Toward more efficient nanomedicine, we should understand in detail what happens at the nano-bio interface. Since 2007, the term protein corona is highlighted after the work of Dawson and co-workers, frequently in the literature, they refer to the delay in the clinical applications of the nanomedicine due to the interactions of the nanoparticles with the biological environment, including the formation of the protein corona. The surface of the nanoparticles plays a major role here regarding their interactions with biomolecules, that's why tremendous efforts were invested on how to manipulate or suppress the formation of protein corona by modifying the surface of the nanoparticles.

Starting from this point, we have established our research project by focusing on the surface of the nanoparticles – the first thing seen by cells and proteins – to study their protein and cellular interactions. In the present work, we have synthesized different inorganic nanoparticles and modify their surface using different charged amphiphilic polymers. As reported the surface charge of the nanoparticles has a significant impact on their protein interactions, and consequently their biological fate. Therefore, by using different charged polymers, while almost keeping the same surface chemistry; this has been achieved via using amphiphilic polymers to modify the surface of the nanoparticles, we were able to systematically compare the influence of the surface charge on the protein and cellular interactions of the nanoparticles. The physicochemical characterization of the coated nanoparticles has been studied using different techniques including, UV-Vis spectroscopy, photoluminescence spectrophotometer, dynamic light scattering, transmission electron microscopy, and drop shape analyzer.

Such techniques have been used to study the optical properties, the physical size including the core and the hydrodynamic diameter, and the hydrophilicity/hydrophobicity of the nanoparticles. The latter has been studied based on the fact that the hydrophobicity of the nanoparticles affects their biological interactions. Moreover, we have studied the in situ formation of the protein corona via measuring the minute change in their diffusion by fluorescence correlation spectroscopy, where we have achieved an overview of the effect of different charges on the protein adsorption. This was followed by studying the cellular interactions of these nanoparticles including, their biocompatibility and cellular uptake.

This work introduces a universal approach for the surface modification of the nanoparticles and shows at the same hydrophilicity degree, the protein and cellular interactions of the nanoparticles are governed mainly by the electrostatic interactions.

Zusammenfassung

Heutzutage entwickelt sich die Nanomedizin immer schneller und ist bereits in unserem täglichen Leben präsent. Um die Nanomedizin effizienter zu gestalten, sollten wir im Detail verstehen, was an der Nano-Bio-Grenzfläche passiert. Seit 2007 wird der Begriff Proteinkorona nach der Arbeit von Dawson und Mitarbeitern hervorgehoben. In der Literatur wird häufig auf die Verzögerung bei der klinischen Anwendung der Nanomedizin aufgrund der Wechselwirkungen der Nanopartikel mit der biologischen Umgebung, einschließlich der Bildung der Proteinkorona, hingewiesen. Die Oberfläche der Nanopartikel spielt dabei eine wichtige Rolle hinsichtlich ihrer Wechselwirkungen mit Biomolekülen, weshalb enorme Anstrengungen unternommen wurden, um die Bildung der Proteinkorona durch Modifizierung der Oberfläche der Nanopartikel zu manipulieren oder zu unterdrücken.

Von diesem Punkt aus haben wir unser Forschungsprojekt aufgebaut, indem wir auf die Oberfläche der Nanopartikel - das erste, was man sieht - konzentriert haben, um ihre Protein- und Zellinteraktionen zu untersuchen. In der vorliegenden Arbeit haben wir verschiedene anorganische Nanopartikel synthetisiert und ihre Oberfläche mit verschiedenen geladenen amphiphilen Polymeren modifiziert. Wie berichtet, hat die Oberflächenladung der Nanopartikel einen erheblichen Einfluss auf ihre Proteininteraktionen und folglich auf ihr biologisches Schicksal. Daher konnten wir durch die Verwendung unterschiedlich geladener Polymere bei gleichbleibender Oberflächenchemie - dies wurde durch die Verwendung amphiphiler Polymere zur Modifizierung der Oberfläche der Nanopartikel erreicht - den Einfluss der Oberflächenladung auf die Protein- und Zellinteraktionen der Nanopartikel systematisch vergleichen. Die physikochemische Charakterisierung der beschichteten Nanopartikel wurde mit verschiedenen Techniken untersucht, darunter UV-Vis-Spektroskopie, Photolumineszenz-Spektrophotometer, dynamische Lichtstreuung, Transmissionselektronenmikroskopie und Tropfenformanalyse.

Mit diesen Techniken wurden die optischen Eigenschaften, die physikalische Größe, einschließlich des Kerns und des hydrodynamischen Durchmessers, sowie die Hydrophilie/Hydrophobie der Nanopartikel untersucht. Letzteres wurde untersucht, weil die Hydrophobie der Nanopartikel ihre biologischen Wechselwirkungen beeinflusst. Darüber hinaus haben wir die Bildung der Proteinkorona in situ untersucht, indem wir die winzige Veränderung ihrer Diffusion mit Hilfe der Fluoreszenzkorrelationspektroskopie gemessen haben, wodurch wir einen Überblick über die Auswirkungen verschiedener Ladungen auf die Proteinadsorption erhielten. Anschließend wurden die zellulären Wechselwirkungen dieser Nanopartikel untersucht, einschließlich ihrer Biokompatibilität und zellulären Aufnahme.

Diese Arbeit führt einen universellen Ansatz für die Oberflächenmodifikation von Nanopartikeln ein und zeigt, dass bei gleichem Hydrophiliegrad die Protein- und Zellinteraktionen der Nanopartikel hauptsächlich durch elektrostatische Wechselwirkungen bestimmt werden.

Table of Contents

Eidesstattliche Versicherung / Declaration of oath	IV
DEDICATION	V
List of publications	VI
Acknowledgments.....	VII
Abstract.....	IX
Zusammenfassung	X
Table of Contents.....	XII
Abbreviation	XIV
List of Figures	XV
1 Introduction.....	1
1.1 Nanoparticles and nanotechnology	1
1.2 Bio-Applications of the Nanoparticles	4
1.3 Polymer Coating of the Nanoparticles.....	6
1.4 Protein Corona	11
1.5 Impact of Protein Corona at the Nano-Bio interface.....	15
1.6 Fluorescence Correlation Spectroscopy for Protein Adsorption	17
2 Aim of the Work	23
3 Results and Discussion	24
3.1 Amphiphilic polymers used in the present study	24
3.2 Physicochemical characterization of Gold nanoparticles	27
3.2.1 Transmission Electron Microscopy	28
3.2.2 UV-Vis absorption results of the gold nanoparticles	28
3.2.3 Dynamic light scattering results of the gold nanoparticles.	31
3.2.4 Zeta Potential Measurements (ζ).....	33
3.3 Physicochemical Characterizations of the QDs.....	35
3.3.1 Transmission Electron Microscopy of the QDs	36
3.3.2 UV-Vis absorption and photoluminescence PL results of the coated QDs.....	36
3.3.3 Dynamic light scattering results of the coated QDs.....	37
3.4 Colloidal stability of the Gold Nanoparticles	38
3.5 Dynamical Interfacial Tension.....	44
3.6 Protein Adsorption study using Fluorescence Correlation Spectroscopy.....	49
3.7 Biocompatibility of the Nanoparticles	61
3.8 Cellular uptake of the Nanoparticles	65

Table of Contents

3.8.1	Cellular Uptake using Flow Cytometry.....	65
3.8.2	Cellular Uptake using ICP-MS.....	66
4	Conclusion and Outlook	80
5	Materials and experimental protocols	82
5.1	Materials.....	82
5.2	Gold Nanoparticles synthesis.....	82
5.2.1	Synthesis of ≈ 17 nm Au NPs.....	82
5.2.2	Phase Transfer.....	82
5.2.3	Synthesis of the 4 nm Au NPs.....	83
5.3	Polymer Synthesis.....	84
5.3.1	Synthesis of the PMA-grafted dodecylamine.....	84
5.3.2	Synthesis of the PMA-DDA-DMAPA polymer.....	85
5.4	Polymer Coating.....	85
5.5	UV-Vis spectroscopy Measurements.....	86
5.6	Photoluminescence Measurements.....	86
5.7	Dynamic light scattering and ζ -potential measurements.....	86
5.8	Interfacial Tension measurements.....	87
5.9	Fluorescence Correlation Spectroscopy Measurements (FCS).....	88
5.10	Cellular Viability Study.....	90
5.11	Cellular Uptake Study.....	91
5.11.1	Cellular Uptake using Flow Cytometry.....	91
5.11.2	Cellular uptake using ICP-MS.....	92
6	Appendix	93
6.1	Gel Electrophoresis of the Au NPs.....	93
6.2	Quantification of the adsorbed protein.....	94
6.3	List of hazardous substances.....	96
7	References	97

Abbreviation

ACF	Autocorrelation function
APD	Avalanche photodiode
Au NPs	Gold nanoparticles
CLSM	Confocal laser scanning microscope
DDA	Dodecylamine
DDLS	Depolarized dynamic light scattering
DDT	Dodecanethiol
DLS	Dynamic light scattering
FA	Folic acid
FBS	Fetal bovine serum
FCS	Fluorescence correlation spectroscopy
Hela	Henrietta lacks cells
HSA	Human serum albumin
ICP-MS	Inductive coupled plasma Mass spectrometry
IFT	Interfacial tension
LSPR	Local surface plasmon resonance
MCF-7	Michigan cancer foundation-7
MPS	Mononuclear phagocyte system
NADH	Nicotinamide adenine dinucleotide phosphate
NMR	Nuclear magnetic resonance
NPs	Nanoparticles
PAL	Photoaffinity labelling
PBS	Phosphate buffer saline
PEG	Polyethylene glycol
PL	Photoluminescence
PMT	Photomultiplier tube
PPE	Poly(phosphateesters)
PSF	Point spread function
QDs	Quantum dots
Rh6G	Rhodamine 6G dye
SCS	Scattering correlation spectroscopy
SHLS	Second harmonic light scattering
SPR	Surface plasmon resonance
TEM	Transmission electron microscopy
Tf	Transferrin human protein
TOAB	Tetraoctylammonium bromide
UV-Vis	Ultraviolet-Visible spectroscopy
ζ	Zeta potential

List of Figures

Figure 1-1 Early example of nanotechnology. 2

Figure 1-2 Timeline for the development of nanoscience and nanotechnology. 3

Figure 1-3 Three C's layers that define the nanoparticles upon their bio-interactions. 5

Figure 1-4: Scheme of the amphiphilic polymer coating procedure. 7

Figure 1-5 Zwitterionic monomers that have been used frequently in the majority of polyzwitterions. 9

Figure 1-6 Cartoon representation of Nanoparticles-cell interactions. 15

Figure 1-7 Scheme of the FCS setup installed with the confocal microscope. 18

Figure 1-8 Timescales of different parameters measured by autocorrelation analysis. 20

Figure 3-1 Structure of the Amphiphilic polymers that have been used in the present study. 26

Figure 3-2 TEM Images of the NPs core. 28

Figure 3-3 Absorption Spectra of the 17 nm Au-NPs. 29

Figure 3-4 Absorption Spectra of the 17 nm Au-NPs coated with A) PMA, and B) PMAL. 30

Figure 3-5 Absorption Spectra of the 17 nm Au-NPs coated with A) PMA-DMAPA, and B) EDLF. 30

Figure 3-6 Absorption Spectra of the 4 nm Au-NPs. 31

Figure 3-7 Hydrodynamic Diameter of the 17 nm Au-NPs. 32

Figure 3-8 Hydrodynamic Diameter of the 17 nm Au-NPs coated with A) PMA, and B) PMAL. 32

Figure 3-9 Hydrodynamic Diameter of the 4 nm Au-NPs. 33

Figure 3-10 ζ - Potential Measurements of the 17 nm Au-NPs. 34

Figure 3-11 ζ - Potential Measurements of the 17 nm Au-NPs coated with A) PMA, and B) PMAL. 34

Figure 3-12 ζ - Potential Measurements of the 4 nm Au-NPs. 35

Figure 3-13 TEM image of the QDs. 36

Figure 3-14 UV-Vis and PL spectra of the coated QDs. 37

Figure 3-15 Hydrodynamic diameter obtained by DLS of the coated QDs. 37

Figure 3-16 Colloidal stability of the 17 nm Au NPs against different concentrations of NaCl. 39

Figure 3-17 Average of absorption values (600:650 nm) of Au NPs versus NaCl concentration. 40

Figure 3-18 Colloidal stability of Au-PMA and Au PMAL NPs. 40

Figure 3-19 Average of absorption values (600:650 nm) of 17 nm Au NPs versus NaCl concentration. 41

Figure 3-20 Colloidal stability of the 4 nm Au NPs. 41

Figure 3-21 Colloidal stability of the Au-PMA as a function of time. 43

Figure 3-22 Dynamical interfacial tension of QDs. 45

Figure 3-23 Dynamical interfacial tension of Au NPs. 46

Figure 3-24 Cartoon representation for the effect of the protein corona on the hydrodynamic radius of the nanoparticles. 50

Figure 3-25 HSA protein adsorption onto QDs coated with A) PMA (-), B) PH (-), C) PT (+), and D) PMAL (+/-). 51

Figure 3-26 Tf protein adsorption onto QDs coated with A) PMA (-), B) PH (-), C) PT (+), and D) PMAL (+/-). 52

Figure 3-27 Overview of the adsorption parameters of the QDs against A) HSA, and B) Tf protein. 54

Figure 3-28 Surface electrostatic distribution of HSA and Tf proteins. 55

Figure 3-29 Protein adsorption profile by FCS of QDs coated with PC (+/-) against A) BSA, B) HSA, and C) Tf. 57

Figure 3-30 Protein adsorption profile by FCS of QDs coated with SB (+/-) against A) HSA, and B) Tf. 57

Figure 3-31 Protein adsorption profile by FCS of QDs coated with EDLf against A) Tf and B) HSA protein. 58

Figure 3-32 Protein adsorption profile by FCS of QDs coated with PMA-DDA-DMAPA against HSA. 58

List of Figures

Figure 3-33 HSA adsorption on the QPC-FA QDs as obtained by FCS.	60
Figure 3-34 Graphic illustrations of the charge-dependent protein adsorption profiles of the NPs.	60
Figure 3-35 Scheme presenting the reduction of the resazurin into resorufin.	61
Figure 3-36 Cellular viability (V) of Hela Cells against different concentrations of QDs, after 24 hours exposure.	62
Figure 3-37 Cellular viability (V) of Hela cells against different concentrations of the 4 nm Au NPs, after 24 h exposure.	63
Figure 3-38 Cellular viability (V) of Hela cells against different concentrations of 17 nm Au NPs, after 24 h exposure.	63
Figure 3-39 Cellular viability (V) of Hela cells against different concentrations of 17 nm Au NPs and QDs.	64
Figure 3-40 Scheme of the cellular uptake and its quantification methods.	65
Figure 3-41 Cellular uptake of the QDs as measured by Flow cytometry.	66
Figure 3-42 Cellular uptake of 25nM QDs by Hela cells at 6h exposure time at two different serum conditions.	68
Figure 3-43 QDs content in the media after 6 h exposure time of the 25 nM QDs.	69
Figure 3-44 Cellular uptake of 50nM QDs by Hela cells at 6h exposure time at two different serum conditions.	69
Figure 3-45 QDs content in the media after 6 h exposure time of the 50 nM QDs.	70
Figure 3-46 Cellular uptake of Hela cells of QDs at two different concentrations for 24h exposure time with 10% FBS.	70
Figure 3-47 Cellular uptake of 17 nm Au NPs by Hela cells after 24 h exposure time at two different serum conditions.	71
Figure 3-48 Cellular uptake of 17 nm Au NPs coated with MAPA and ELDF.	72
Figure 3-49 Cellular uptake by Hela cells of 17 nm Au NPs coated with DMAPA vs PMA. after 24 h incubation time.	72
Figure 3-50 Cellular uptake of the 4 nm Au NPs by Hela cells at 24h exposure time.	73
Figure 3-51 Cellular uptake of Q-PC and Q-PC-FA by Hela cells at 6h exposure.	75
Figure 3-52 Cellular uptake of Q-PC and Q-PC-FA QDs by MCF7 cell line after 6h exposure.	76
Figure 3-53 Cellular uptake of different batches of Q-PC-FA by Hela cells for 6h incubation time.	76
Figure 3-54 Cellular uptake of the 4 nm Au NPs (PC and PC-FA) by Hela cells after 24 h.	77
Figure 3-55 Cellular uptake of the 4 nm Au NPs (PC and PC-FA) by Hela cells after 6h incubation.	77
Figure 3-56 Cellular uptake of the 4 nm Au NPs (PC and PC-FA) by MCF7 cells after 6h incubation.	78
Figure 3-57 Blocking experiment of the QDs at 25 nM in a serum-supplemented medium for 6h incubation time.	78
Figure 3-58 Blocking experiment of the QDs at 25 nM in serum-free medium for 6h incubation time.	79
Figure 5-1 Schematic of the Au NPs synthesis and phase transfer steps.	83
Figure 5-2 Schematic of the 4nm Au NPs synthesis and ligand exchange steps.	84
Figure 5-3 scheme of the main coating steps of the NPs by the amphiphilic polymers.	86
Figure 5-4 Intensity of the QDs as a function of the excitation power.	89
Figure 5-5 Scheme of the biocompatibility study.	91
Figure 5-6 Gating strategy for Hela cells.	92
Figure 6-1 Au NPs migration in agarose gel electrophoresis.	93
Figure 6-2 BSA protein adsorption as measured by Coomassie Bradford assay.	95
Figure 6-3 BSA adsorption as measured by SDS-PAGE gel electrophoresis.	95

1 Introduction

1.1 Nanoparticles and nanotechnology

"There is Plenty of Room at the Bottom."

Richard Feynman

Nanoscience, a well-established field with numerous applications in many areas including material science, water treatment, agriculture, anti-microbial, vaccines, cancer therapy, and many other applications. Recently, the world faced (still) a global pandemic (COVID-19), which is fought by developing nano-vaccines, using lipid nanoparticles NPs. Nanoscience holds lots of hope for many future applications from industry to medicine.

To define the term 'nanoparticles', there are many definitions, but we can simply refer to it as any material with at least one dimension ranging from 1 to 100 nm. As the material reduced in scale from bulk to the nanoscale, its properties dramatically changed. For instance, their surface-to-volume ratio and surface energy increased, and as a consequence, the electronic properties changed as the density of states and the spatial length of the electronic motion are reduced. This is physically transforming the optical properties of the nanomaterials into a new paradigm. So, what was in bulk state insulator transformed into a conductor, brittle into strength material, non-fluorescent into fluorescent material, and many new characteristics that define the new material at the nanoscale. Combining the property of solids; optical properties, and the property of molecules; the ability to move gives the nanoparticles their unique characteristics (Florence, 2021, Link, El-Sayed, 2003, Phan, Haes, 2019, Stark, 2011).

The existence of nanoparticles (NPs) dates back to the 4th century, in the masterpiece of Roman glass craftsmanship, the Lycurgus cup (British Museum). Where nanoalloys of the silver, copper, and gold NPs have been used in the Lycurgus cup, Figure 1-1. The cup shows the Greek and Roman mythical tale, where King Lycurgus attempted to kill Ambrosia – a follower of the god Dionysus (based on the myth). The cup shows two different colors the green color and the red color as a result of the presence of the Gold and Silver NPs. These two different colors are not only from a materialistic point of view that has a meaning or a reason (the presence of the NPs) but also describe the feeling and the status of King Lycurgus.

Dionysus has tried to fight Lycurgus by turning him mad, he firstly makes his son appear for Lycurgus as Ambrosia, making him kill his son unaware of what he is doing. Then, make him imagine his body parts are twined by Ambrosia leading to his death by killing himself. The green color represents the wise and the normal (sane) state of King Lycurgus before he got into the fight against Dionysus, and

the red light represents his madness. I'd like here to add, what is not shown in the figure, from another angle we can see inside the cup a little red color, representing a little madness already was there inside Lycurgus. Other parts of the cup tell the rest of the story, it is an irreplaceable human artifact.

In addition to that, gold NPs (Au NPs) were used to stain the Rose window of the Cathedral of Notre Dame, the bright red and purple colors are characteristics of the Au NPs as recognized by Faraday [Figure 1-1](#). Since then the evolution of nanoscience and its technology have emerged [Figure 1-2](#). By development of the electron microscope, with a higher resolution than the optical microscope, enables us to visualize the nanoparticles and helps in understanding the evolution of the nanoparticles' synthesis. (John Turkevich et al., 1951, Link, El-Sayed, 2003, Rossner et al., 2021)



Figure 1-1 Early example of nanotechnology. A) Lycurgus cup at the British Museum, lit from the outside (left) and the inside (right), B) The south rose window of Notre Dame Cathedral, ca 1250, and C) Polychrome lusterware bowl, 9th C, Iraq, British Museum (credit: Trinitat Pradell 2008). (Nanotechnology Timeline | National Nanotechnology Initiative, 2021)

Nanoparticles and nanotechnology

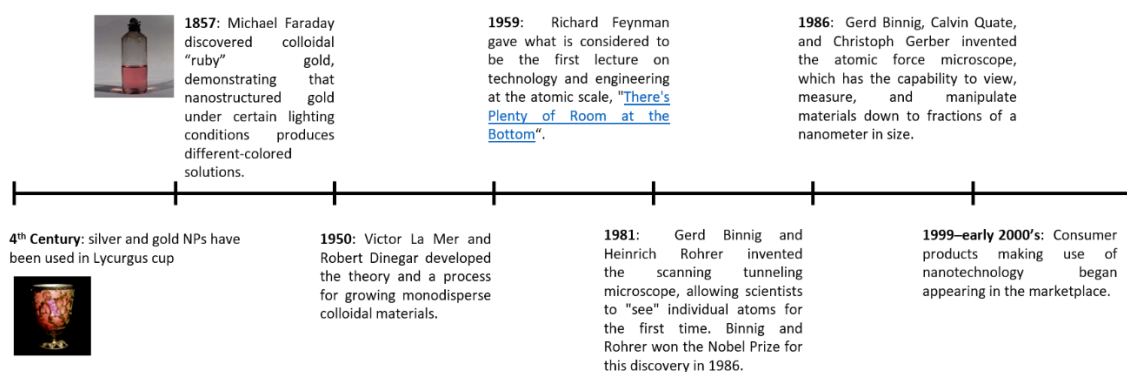


Figure 1-2 Timeline for the development of nanoscience and nanotechnology. (Nanotechnology Timeline | National Nanotechnology Initiative, 2021)

Starting from this point the scientific community was exposed to huge efforts toward understanding and developing the NPs. To finally have the NPs in every sub-scientific community and to be applied in many areas.

This simply highlights the importance of the NPs in terms of physical and chemical properties, which is dramatically added value and new synthetic nanomaterials with different shapes, cores, and physicochemical properties to the material science community. However, the application of the NPs did not stop at this level, as we have mentioned the nanoparticles are applied almost in our daily life. The bio-applications or biomedical applications of the NPs also gained so much attention and were recently applied in millions of patients' arms by introducing the corona-vaccine.

In the current work, we have tried to answer fundamental questions; Is it possible to have a universal coating approach for the nanoparticles? How the physicochemical identity of the nanoparticles influences their protein and cellular interactions? Are we able to obtain stealth-like nanoparticles? Does it keep its stealth property, when it is modified with a targeting ligand?

The present thesis is trying to answer these questions. The introduction chapter provides an overview of nanotechnology and its bioapplications, in addition to highlighting some of the challenges to achieving their targets. In the results and discussion chapter, present the results obtained while we have tried to answer the above-mentioned questions, followed by our conclusion and the future outlook. In the end, in the materials and experimental protocols chapter, where we have listed all the protocols we have used to perform our experiments.

1.2 Bio-Applications of the Nanoparticles

"Nanotechnology in medicine is going to have a major impact on the survival of the human race."

Bernard Marcus

The global pandemic helps in evolving the application of nanomedicine through the worldwide clinical introduction of the Moderna and Pfizer-BioNTech COVID-19 lipid-nanoparticle mRNA vaccines. This is a great success for the nanomedicine community; moreover, there are many clinical trials all over the world of nanomaterials, whether as vaccine vectors or imaging agents (Anselmo, Mitragotri, 2021).

In fact, the nanoscale is the natural scale of biology, as most of the processing and cellular networks are operating at the nanoscale, which includes the machinery itself and the biomolecules. (Dawson, Yan, 2021) This indicates why the nanoparticles gained much attention, particularly in their bio-applications. In contrast, and as expected working with biology was not an easy task, nature is so complex and gives us many challenges. In the past decades, the bio-applications of the nanoparticles were suffering from many barriers, including physiological; body fluid and the targeted tissue, colloidal; their stability over time, and manufacture barriers; as scaling up or having a standard protocol to be clinically approved. This is in many approaches still a challenge for the introduction of the nanoparticles into clinical applications. (Dawson, Yan, 2021, Feliu et al., 2016, Florence, 2021)

Upon introduction of the nanoparticles into biological media, they will be decorated by biomolecules present in the biological fluid, particularly the proteins. Such interactions, non-specific and non-desired adsorption of proteins significantly influence their final fate. It has been reported only 0.7% (Median) of the nanoparticles are successfully delivered to solid tumors, which is a lower value that explains the delay of the clinical translation of the nanoparticles (Ouyang et al., 2020) but, at the same time, it still shows an improvement of drug delivery compared to conventional methods. Poor understanding of the interactions of the nanoparticles upon introducing them into the biological medium is one of the main reasons for delaying the clinical translation of these nanoparticles. (Debayle et al., 2019, García-Álvarez, Vallet-Regí, 2021, Lundqvist, Cedervall, 2020, Mishra, Das, 2019)

Three main parameters that define and determine the identity of the nanoparticles, we call them here the three C's; Core, Coating, and protein Corona. These three levels of defining the nanoparticles will help not only in defining the identity of the NPs but also will improve our understanding of their upcoming interactions and stability.

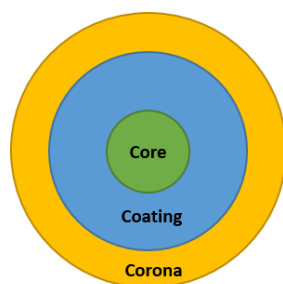


Figure 1-3 Three C's layers that define the nanoparticles upon their bio-interactions.

Starting by the core, and let us call it the 'physical identity' of the NPs. The core determines the basic physical properties of the NPs, whether they are plasmonic, magnetic, fluorescent, or any other properties that are governed by the core itself. The physical identity is in most cases determined by their application based on the property they own. The coating or 'the synthetic or chemical identity' determines the basic physicochemical properties of the NPs, such as size, shape, and surface charge, which significantly evaluate their colloidal and biological stability. It is well understood now the colloidal stability of the nanoparticle influences their further applications, including biomedical applications. The colloidal and biological stability of the NPs is a prerequisite for any potential candidate in nanomedicine. (Bevilacqua et al., 2021, Eagle et al., 2021, Feliu et al., 2016, Stefania Garbujo et al., 2020)

The protein corona or 'the biological identity' is the third level of our definition of nanoparticles. As reported before, the surface of the nanoparticles, within seconds, will be decorated with different biomolecules present in the biological fluid. Such a decoration layer affects the efficacy of the nanoparticles, by hindering their targeting ligand if there is one or forcing them to agglomerate or aggregate in larger clusters, which facilitates their identification by the immune system and shortens their lifetime inside the body. Therefore, by manipulating the protein corona or controlling its composition we can improve the blood circulation of the nanoparticles and subsequently its final fate. (Cho et al., 2011, Ding et al., 2018, Safavi-Sohi et al., 2016, Xu et al., 2018)

This protein corona was categorized into the soft and hard corona, based on the affinity and long-lasting of the protein molecules in the corona layer. The hard corona is defined as the protein that has a longer lifetime in the corona layer, which at the end describes the corona composition. Whereas, the soft corona is more dynamic and consists of loosely associated proteins and their dissociation rate is much faster. (Debayle et al., 2019, Feliu et al., 2016, Rampado et al., 2020) There are many approaches how to manipulating or suppressing the formation of the protein corona, which is mainly focused on the second level of the nanoparticles; the coating. By changing the coating or the surface chemistry of the nanoparticles helps in suppressing or reducing the effects of the protein corona. Within the next sections, we will highlight such techniques and their challenges.

1.3 Polymer Coating of the Nanoparticles

"God made the Bulk; the surface was invented by the devil."

Wolfgang Pauli

The surface chemistry of the nanoparticles is an essential parameter for any NPs prepared to be used in bio-applications. As we have discussed in the previous section, the chemical identity of the nanoparticles in a higher degree determines their stability and bio-interactions. Recently, Faria and co-workers suggested a minimum information standard for experimental work studying the bio-nano interactions, to further improve the outcome of the efforts invested in nanomedicine (Faria et al., 2018, Feliu et al., 2016, Morgese et al., 2017).

Fabricating NPs with an efficient surface chemistry that helps in stabilizing the NPs under different conditions is highly required. The surface chemistry of the NPs started from the synthesis, as normally most of the NPs are prepared in aqueous solutions through this process they are protected by chemical ligands. These chemical ligands define their initial property, as charge and stability. (Koll et al., 2019, Sperling, Parak, 2010)

For instance, the Au NPs are often synthesized via reduction methods, and often the reducing agent is at the same time the capping agent of the NPs. Due to the higher activity of the nanoparticles, it is highly recommended to coat the surface of the NPs with capping agents to reduce the inter-particle interactions, which is subsequently causing non-desired aggregation or agglomeration of the NPs. (Phan, Haes, 2019)

The stability of the nanoparticles means a lot of things, in terms of size, shape, core, and efficacy. (Phan, Haes, 2019) If we relate that with the three levels that define the NPs, it means we have different levels of defining and determining the stability of the NPs. From inside to outside, Is the core stable and retains its properties and degrades or not? Does the surface chemistry or ligand stabilize the core or not? Does the corona layer dissociate or not and influence the NP's fate or not?.

Deep understanding and investigating the stability of the NPs is crucial in nanomedicine. To enhance the colloidal stability of the NPs, there are different approaches introduced by using different ligands, such as peptides, proteins, small ligands, and polymer encapsulation. Each method has its challenge as scaling up the synthesis, reproducibility, restriction to specific cores, and biocompatibility. Among these approaches, we have selected amphiphilic polymers to functionalize the surface of the NPs. Pellegrino and co-workers were the first to develop a universal approach for wrapping the surface of

the nanoparticles with an amphiphilic polymer, yielding NPs with different cores (physical identity) but with identical surface chemistry (chemical identity). (Pellegrino et al., 2004)

Since then, different research groups have followed the same strategy to produce different NPs with the same surface chemistry and the approach was improved by introducing to the polymers a cross-linker or polyethylene glycol (PEG) to help in stabilizing the coated NPs. This amphiphilic shell can be further functionalized with different molecules or ligands to add more properties to the NPs, such as imaging agent; if we introduce fluorescent molecule, targeting; if we apply targeting molecule, and sensing. (Abdelmonem et al., 2015, Pellegrino et al., 2005, Roy et al., 2019, Soliman et al., 2015, Sperling, Parak, 2010, Stefania Garbujo et al., 2020) The coating strategy of this polymer simply depends on the hydrophobic intercalation of the alkyl chain on the polymer with that on the surface of the NPs, leaving the hydrophilic group of the polymer toward the solvent, yielding negatively charged NPs stabilized in water by the electrostatic repulsion, Figure 1-4.

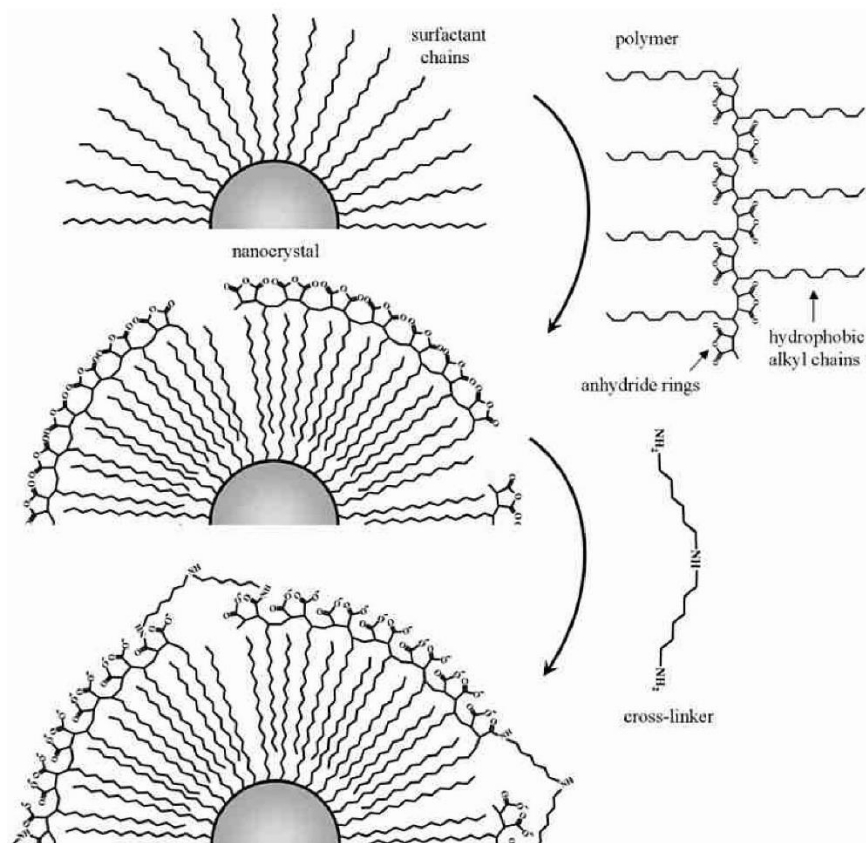


Figure 1-4: Scheme of the amphiphilic polymer coating procedure. Copyright (Pellegrino et al., 2004)

Having the water-dispersed NPs is a prerequisite for any biomedical applications, but as we have discussed in the previous section, the surface chemistry of the nanoparticles is an important factor in determining their stability and future bio-applications. The negatively charged NPs are in high chance

will be decorated with proteins as reported elsewhere. To reduce the formation of the protein corona, we need to modify the surface chemistry, it has been reported the neutral or zwitterionic surface suppresses the formation of the protein corona, pre-coating with proteins helps in selecting the composition of the corona, and coating with polymers; as polysaccharides, polyacrylates, polyacrylamides, and in addition to the PEG; which is the gold standard for reducing the protein adsorption and improving the stability of the NPs. (Debayle et al., 2019, Galdino et al., 2019, Nsubuga et al., 2018, Sanchez-Cano, Carril, 2020, Sperling, Parak, 2010)

On the other hand, PEG does not only improve the lifetime of the nanoparticles but also reduce their uptake by the target cell and multiple introductions induce an immune response (anti-PEG) that limits their applications (Rampado et al., 2020), it is worth to mention that the PEG itself is not immunogenic but its ordered pattern on the NPs surface that induced higher immunoreactivity against PEG-coated NPs, which has been shown by Grenier et al. (Grenier et al., 2018). It has been already reported that many people who have never taken pegylated medicine, have anti-PEG antibodies. The recently used SARS-COV-2 vaccines (BNT162b, and mRNA-1273 from BioNTech, and Moderna, respectively) have in their formulation a PEG2000. The global introduction of these vaccines raises a concern that pre-existing anti-PEG antibodies cause allergic reactions. In addition to that such development of anti-PEG may affect the other pegylated medicine, leading to a more critical situation similar to what we facing right now regarding antimicrobial resistance. (Chen et al., 2021)

Because PEG was not satisfying in fabricating corona-free NPs alongside their side effects, the need for another efficient surface modification increased and other potential candidates are introduced and seemed to be more promising.

Zwitterion and other strategies

Another strategy to overcome or manipulate the protein corona is the pre-coating of the NPs by selected proteins to recruit similar proteins from the plasma via protein-protein interactions, which will be utilized to facilitate the uptake and the targeting of the NPs. (Mahmoudi et al., 2016) Poly(phosphateesters) (PPEs) attract more attention because of their biodegradability, biocompatibility, and stealth properties. Recently, Müller et al. (Müller et al., 2017) have studied the protein adsorption of four different PPEs polymers that non-covalently coat the NPs, all the NPs were able to reduce the adsorption of human serum albumin (HSA), and partially stabilize the NPs by preventing their aggregation in serum.

On the other hand, the zwitterionic surface has recently attracted more attention due to its anti-fouling properties, higher hydrophilicity, and the formation of a thermodynamically favored hydration

layer, which acts as a barrier to protein adsorption. Based on the IUPAC definition of zwitterionic polymers, they are a subclass of ampholytic polymers that have ionic groups of opposite signs commonly on the same pendant groups. Zwitterionic polymers exhibit unique properties such as charge neutrality and their higher hydrophilicity. The first synthesis of zwitterionic material was reported in the 1950s, aiming to have a protein-like structure. (Alfrey et al., 1950) Polyzwitterions are mainly based on five monomers, including one is phosphobetaine (combining ammonium and phosphate groups), two are carboxybetaines (combining ammonium and carboxylate groups), and two are sulfobetaine (SB) (combining ammonium and sulfonate groups) as shown in Figure 1-5, such polyzwitterions do not occur in nature but were inspired by nature. (Laschewsky, Rosenhahn, 2019)

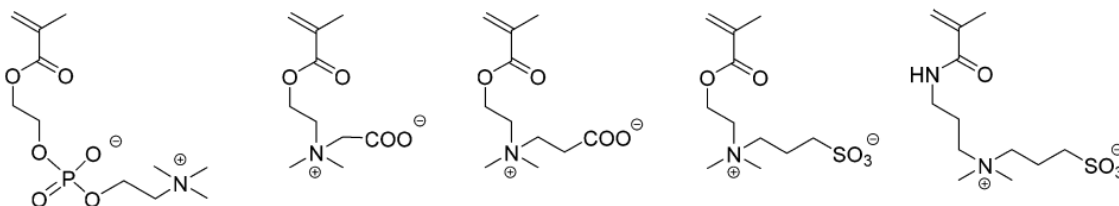


Figure 1-5 Zwitterionic monomers that have been used frequently in the majority of polyzwitterions. From left to right, phosphobetaine structure, two structures of carboxybetaines, and two structures of sulfobetaine polymers. Copyright (Laschewsky, Rosenhahn, 2019)

Polyzwitterions as polysulfobetaines attract more attention because of their permanent zwitterionic character over a broad range of pH, higher hydrophilicity, and high chemical inertness; against oxidation in air or hydrolysis. In addition to their higher dipole moments, indicating the strong binding interactions between the headgroups and the strong hydration layer, making them effective anti-fouling materials. (Wu et al., 2019) The interactions of polyzwitterions with macromolecules depend on the precise structure of the zwitterionic polymer; including the nature of the zwitterionic moieties, the anchoring geometry, the spacer group, the backbone, and the nature of the backbone itself. All of these factors contribute in an attractive or repulsive way to the interactions of zwitterionic polymers with macromolecules, which should be considered in the surface modification process of the NPs. (Laschewsky, Rosenhahn, 2019)

In a recent study by, Debyale et al. (Debyale et al., 2019), QDs that have been coated with different zwitterionic polymers suppressed the formation of protein corona (soft corona) as measured by FCS. Moreover, Loiola et al. (Loiola et al., 2019), showed a substantial decrease of BSA adsorption on the surface of silica NPs when they are functionalized with SBS, as a zwitterionic moiety, and even at double functionalization with what is called biologically active groups (BAGs) as $-NH_2$, $-SH$ or $-COOH$, the silica NPs were able to retain their stealth properties because of the zwitterionic functionalization that shields possible interactions of these BAGs.

Furthermore, Moyano et al. (Moyano et al., 2014) used a series of zwitterionic NPs with tunable hydrophobicity and have observed no formation of the hard corona, suggesting the zwitterionic surface could be a good candidate that facilitates the interaction between the NPs and the biological compartments without the interference of protein corona.

Moreover, poly(carboxybetaine) a zwitterionic polymer is currently in a pre-clinical stage to be another PEG alternative. Its super-hydrophilic properties give it more advantage over PEG in terms of interactions with proteins and lipid bilayer. (Cao, Jiang, 2012, Chen et al., 2021)

In contrast, it was reported that the zwitterionic surface has not the same anti-fouling efficacy against the charged proteins, by suppressing the adsorption of the negative proteins and showing less effectiveness against positive proteins, adding to that the possible hydrolysis of the zwitterionic moieties that will pose a problem and should be considered while designing the polymer encapsulation for the NPs, and the precise structure of the zwitterion; linear orientation of the zwitterion led to better resistance to protein adsorption than nonlinear analog. As we have mentioned before, the stability of the coating (chemical identity) is a crucial factor that determines the bio-stability of the nanosystem and governs their nano-bio interactions, any degradation to this layer or this level causes misinterpretation of the outcome and this step should be taken carefully into account. (Koc et al., 2019)

1.4 Protein Corona

We have discussed the concept of protein corona and its effect on the final fate of the nanoparticles. In the current section, we elaborate more on the protein corona, how to characterize it, and why the zwitterionic surface could help in suppressing the formation of the protein corona.

The term 'corona' itself means a crown and has been used in different fields as physics; for example by referring to the solar corona, which is the gas layer (plasma) that surrounds the sun. Therefore, the protein corona is the crown of proteins that surround or adsorb onto the NPs and this term is firstly introduced by Dawson and co-workers. (Cedervall et al., 2007, Ke et al., 2017) By knowing that, it is clear that only the second level (surface chemistry or coating) of the NPs is in direct contact with the proteins to form the third level (protein corona). The protein corona was categorized into, soft and hard corona, based on the kinetics of adsorption and its strength. The proteins that last for a longer time and strongly interact with the nanoparticles are categorized as the hard corona, while that dissociate easily even if they have adsorbed to the nanoparticles faster than other proteins are referred to as the soft corona. The soft corona is known to be more dynamic than the hard corona. (Debayle et al., 2019, Ke et al., 2017, Kharazian et al., 2016, Rampado et al., 2020)

The corona formation is independent of the type of the NPs, it has been reported to be formed on metal (Casals et al., 2010), polystyrene (Tenzer et al., 2013), and lipids NPs (Barrán-Berdón et al., 2013).

Influence of protein corona and NPs on each other

As the protein corona influences, the fate of the nanoparticles, the protein itself undergoes structural rearrangement (conformational changes), which is thermodynamically favored. (Kharazian et al., 2016) The existence of protein corona is not only could affect the biological fate of the nanoparticles but can also influence their colloidal stability in two different ways, stabilizing or destabilizing impact, stabilizing the NPs by their steric repulsion, and destabilizing them by forming a bridge, and changing the surface charge homogeneity. (Feliu et al., 2016)

For instance, the citrate-Au NPs aggregate in phosphate buffer saline, but they are stable in presence of proteins (Dobrovolskaia et al., 2009). In contrast, Mishra and Das (Mishra, Das, 2019) found that only a small amount of protein was enough to induce a bridging followed by aggregation of the citrate-Au NPs, keep in mind they have used Lysozyme, which is a positive protein. Such instability may be related to the concentration of proteins, as Ho et al. (Ho et al., 2018) observed, at lower concentrations of proteins NPs aggregation was observed, in contrast at higher concentrations the

NPs were stabilized. Furthermore, Mishra and Das (Mishra, Das, 2019) have found that the SPR peak of the cationic Au NPs after adding lysozyme protein is red-shifted, a decrease in the peak intensity, the appearance of another peak in the red region, and changing the color, which is attributed to the aggregation of the Au NPs.

The composition of the protein corona depends on many factors including that of the physicochemical properties of the NPs; as size, shape, hydrophilicity, and surface chemistry and that of the environment; as blood, interstitial fluid, cell cytoplasm, the duration or the exposure time, and also the incubation dynamics. (Kharazian et al., 2016, Rampado et al., 2020) For instance, it was reported the hydrophobic NPs are more attractive to proteins and opsonized more quickly than hydrophilic NPs. (Lck et al., 1998). The topology of the surface influences the corona formation, as reported by Schroffenegger et al., (Schroffenegger et al., 2020) they found that the protein corona adsorbed more on the linear polymer than the cyclic one. The curvature of the NPs has an impact on the corona conformation, proteins adsorbed on highly curved NPs tend to have fewer conformation than those adsorbed onto less curved NPs. (Kharazian et al., 2016)

In the study by Bonvin et al. (Bonvin et al., 2017) they concluded that the incubation condition, static or dynamic, has an impact on the formation of the protein corona, they found that at higher flow rates the protein adsorbed are more structurally flexible, suggesting a conformation change to have a stable binding to the NPs and by alternating the incubation medium (blood and then lymph, and vice versa) the corona content was different depending on the order of incubation, which means the protein corona is evolving, based on the environment. On the other hand, (Hadjidemetriou et al., 2019) reported that the amount of adsorbed protein, when NPs injected into mice, did not change over time, and most of the identified proteins were constant. It is worth mentioning, they observed the formation of protein corona as soon as 10 min from the injection.

Forces and the process kinetics

The process of protein adsorption is a spontaneous process that involves enthalpy and entropy to produce the negative Gibbs free energy. Forces involved as van der Waal, H-bonding, electrostatic forces (considered as enthalpic governed), and hydrophobic interactions (tend to increase the entropy) among others. (Feliu et al., 2016, Galdino et al., 2019, Kharazian et al., 2016, Mahmoudi et al., 2016)

The van der Waal is a weak force and acts at a short distance by electrostatic attraction between dipoles, H-bonding is mainly formed between uncharged hydrophilic parts of the proteins and polar sites on the surface of the NPs, hydrophobic interactions could happen between the hydrophobic

residues of the proteins and the NPs if they are in close contact and may affect the conformation of the proteins as mentioned before, and the electrostatic forces are the more crucial one. It is believed to be the most effective in the protein adsorption process, as reported elsewhere. (Mahmoudi et al., 2016, Mishra, Das, 2019)

In a recent study by Moustouli et al. (Moustouli et al., 2019), where they have studied the adsorption of different charged plasma proteins with negatively charged Au NPs, they found that the adsorption is driven by Coulomb interactions between the negatively charged Au NPs and the positive sites on the different proteins, as estimated from the thickness of the corona layer and the charge distribution on the proteins.

How to detect protein corona?

There are many methods already reported in the literature regarding identifying and measuring the protein corona, this review of Carrillo-Carrion et al. (Carrillo-Carrion et al., 2017) is a good start. Where they have compared different techniques that have been used to measure the protein corona, whether directly or indirectly. Typically, most direct methods involve the separation of the NPs from the medium after incubation whether by centrifugation or other separation techniques. Such approaches could mislead or give biased results regarding the corona formation, and this is simply because of the purification steps that could cause aggregation/agglomeration, desorption of proteins, and disturb the overall process dynamic. Recently, Pattipeiluhu et al. (Pattipeiluhu et al., 2020) found that for different liposome formulations, the number of proteins in the protein corona was higher, when centrifugation was used as an isolation method compared to the photoaffinity method.

That's why, the need for in situ techniques is essential to avoid many artifacts, one of these methods includes the optical method. For in situ quantifying the protein corona based on diffusion coefficient measurements, there are different techniques including, fluorescence correlation spectroscopy (FCS), dual-focus fluorescence correlation spectroscopy (d-FCS) (Maffre et al., 2011), depolarized dynamic light scattering (DDLs) (Balog et al., 2015), diffusion nuclear magnetic resonance (NMR) (Carril et al., 2017), and scattering correlation spectroscopy (SCS) (Moustouli et al., 2019).

Moreover, Mishra and Das (Mishra, Das, 2019) have used second harmonic light scattering (SHLS) to detect the formation of protein corona on citrate-Au NPs. They found that the lysozyme protein, only a small amount of it was enough to form a bridging which is followed by aggregation of the NPs. They suggested that the protein adsorption is driven by electrostatic attraction and there are no Au-S bonds formed, that's why they categorized this interaction as physisorption.

For measuring the protein corona in more complex media, Carrillo-Carrion and coworkers have used the NMR to detect the formation of protein corona in a complex media as blood by measuring the change in the diffusion coefficient of the fluorine-labeled NPs. (Carril et al., 2017)

Apart from this Pattipeiluhu et al. (Pattipeiluhu et al., 2020) has introduced the photoaffinity labeling (PAL) method to the nanomedicine community for the first time as an unbiased technique that helps in capturing the protein corona of liposomes in their native state. Understanding and measuring protein corona require the integration of many different methods to deeply understand the nano-bio interactions and to predict them. Such requirements may make the process more complex to analyze, adding to that the need for having a precise method to measure the protein adsorption onto the NPs in more complex media is highly needed and more efforts should be invested there.

1.5 Impact of Protein Corona at the Nano-Bio interface

The two main routes of entry into cells are passive diffusion or direct fusion with the plasma membrane and endocytosis, however, the main route of the entry of the NPs is via endocytosis. See Figure 1-6. (Rennick et al., 2021)

The biological fate of the nanoparticles depends on many different things including; the administration route, their size, their shape, and their biological identity (the third level). But once the NPs reached the blood, their fate will highly depend on their protein corona, protein corona enriched with complement factors, immunoglobulins, and coagulation factors will shorten the lifetime of the NPs. (Rampado et al., 2020)

The existence of protein corona not only changes the overall hydrodynamic size of the NPs but also changes their surface charge into a negative charge; regardless of the initial surface charge, which in turn may affect their cell interactions. (Cho et al., 2011) This is supported by the results obtained by Ding and co-workers (Ding et al., 2018), where they have studied the effect of size, shape, and protein corona on the cellular uptake and exocytosis. They have observed almost no change regarding the exocytosis mechanisms, only the rate is a function of size, while they found that the protein corona influences the uptake pathway. Therefore, we could say the endocytosis of the NPs is mainly governed by the protein layer rather than the NPs itself, meaning the third layer (Protein corona) plays a major role in determining the biological fate of the NPs. (Maffre et al., 2014)

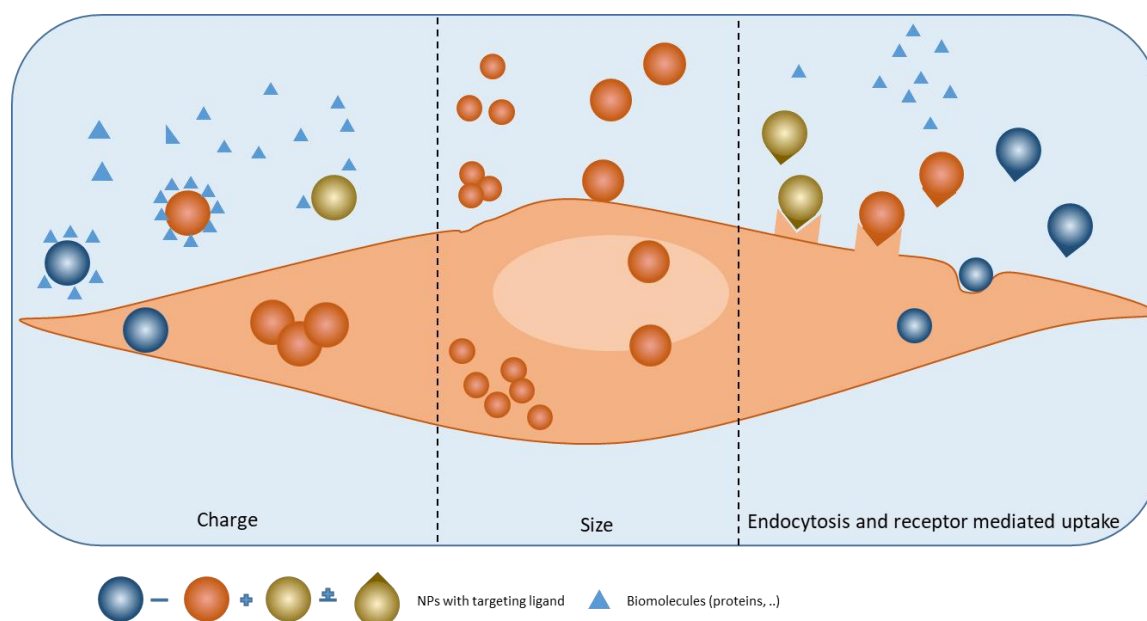


Figure 1-6 Cartoon representation of Nanoparticles-cell interactions. Showing the effect of charge on the protein and cellular internalization, the effect of size of the NPs on their uptake; showing how smaller NPs may be internalized in a higher amount than the larger size while sometimes they have to form clusters first to be internalized, and the possible internalization pathways for the NPs including the receptor-mediated uptake and the endocytosis by cells.

In addition to influencing the uptake profile of the NPs, it has been reported the existence of protein corona reduces the targeting efficacy of the NPs by 94% even at a low level of serum. (Mirshafiee et al., 2013)

In Wolfram et al. (Wolfram et al., 2014) work, they have discussed the different biological effects of the protein corona; protein corona helps in reducing the toxicity of the NPs, but at the same time it may affect the function of the plasma proteins, majority of proteins in the corona layer are immunostimulatory proteins causing rapid immunorecognition of the NPs as shown also by Mahmoudi and co-workers (Mahmoudi et al., 2016), which is negatively affect the targeting of the NPs as previously proven by Mirshafiee et al. (Mirshafiee et al., 2013), and in general, affects the biodistribution and efficacy of the nanomedicine.

Apart from the corona effect on the biological interactions of the NPs, the size of the NPs also determine their endocytosis path, for example, the smaller 5 nm NPs can flow directly into lymph nodes follicles, while the 100 nm requires cell-mediated transport into the follicles, as shown in Zhang et al. (Zhang et al., 2019) work. In contrast, smaller NPs are not widely used in biological applications, cause of their faster dynamics to form aggregates than the larger size, which explains their poor distribution in the exposed organism and their faster rate of exocytosis. (Chithrani, Chan, 2007, Stark, 2011)

The ratio of adhesion, membrane stretching, and membrane's bending energy determine the size-dependent uptake of the NPs. Therefore, the 50 nm Au NPs are more efficient to be internalized into the cells in comparison to the larger and the smaller size (Chithrani, Chan, 2007), and the smaller NPs tend to accumulate first on the plasma membrane before gradually entering the cell. (Shang et al., 2014) On the other hand, it has been reported the smaller NPs have been internalized into the cells with higher numbers than the bigger ones. (Cho et al., 2011)

1.6 Fluorescence Correlation Spectroscopy for Protein Adsorption

"With four parameters I can fit an elephant, and with five I can make him wiggle his trunk."

Johnny von Neumann

Among different techniques that have been used to measure the existence of protein corona as we have introduced before, we have used fluorescence correlation spectroscopy (FCS) to in-situ study the NPs-protein interactions. FCS is a powerful technique that can be used to determine minute changes in diffusion of the fluorescent molecules precisely. Because the formation of protein corona forms a layer in nanometer thickness, the need for such techniques was a prerequisite to have more precise measurements.

FCS was developed in the early of 1970s, since then it has been used to measure chemical reaction rates, molecular mobility, particle size, and concentration. FCS is a fluctuation technique, we can say the motto of the FCS compared to the Confocal Laser Scanning Microscopes (CLSM), is 'Intensity is not enough' or 'Making signal out of noise', this is based on the fact that for laser scanning approach we need to collect many photons as much as we can to obtain a good image, while in case of FCS we are collecting the fluctuations of the fluorophore signal. Basically, the FCS unit is installed with Confocal Laser Scanning Microscopes (CLSM), where the excitation laser beam is focused into a smaller excitation volume, the light emitted from the fluorescent sample will be collected by the same objective used for excitation and the non-desired signal are blocked by the pinhole at the back of the objective, then the signal is directed to a single-point detector, such as photomultiplier tube (PMT), an avalanche photodiode (APD), or a hybrid detector, see [Figure 1-7](#). (Krieger et al., 2015, Slenders et al., 2021)

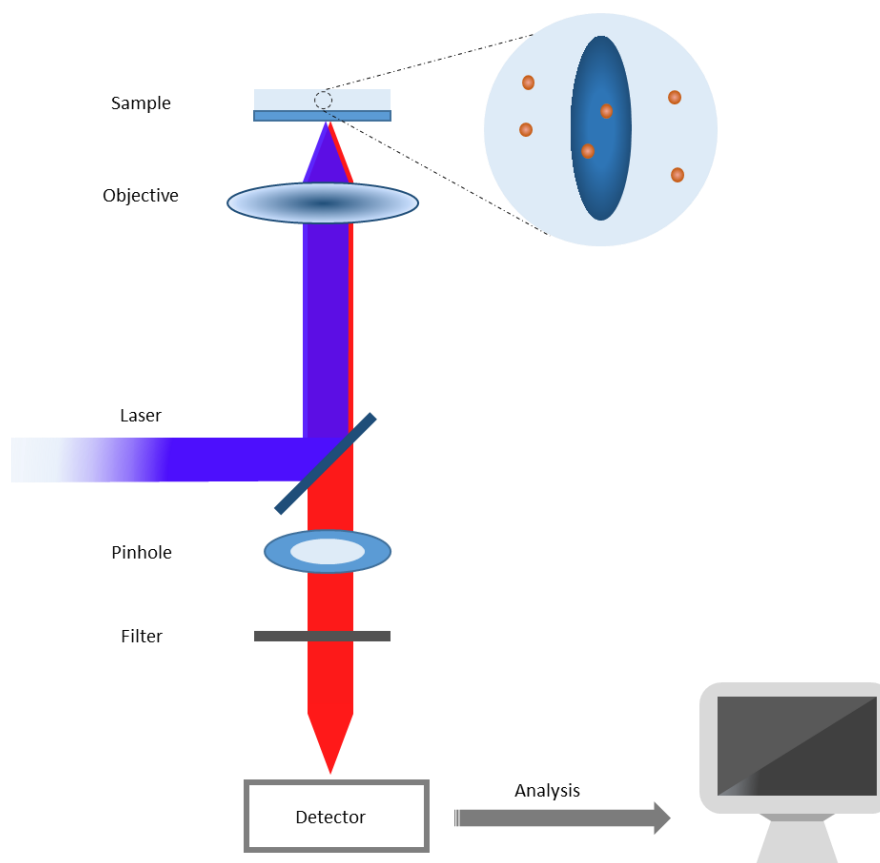


Figure 1-7 Scheme of the FCS setup installed with the confocal microscope.

The fluctuation of the signal has many sources, including those that reflect the physical evolution; such as varying number of emitters in the confocal volume, variation of the emission cause of interactions, reorientation or internal dynamics, or that carry non-useful information as shot noise, which occurs at very short time scale, and the other fluctuation sources are that from the background fluorescence or the scattering, and the noise attributed to the detector device. (Petrášek, Schwille, 2009)

In FCS the fluctuation (δI) is mathematically analyzed, this fluctuation is caused by particles leaving and entering into the confocal volume (its Brownian motion), if the average particle number (N) increases, becomes more difficult to distinguish these fluctuations. Therefore, working at nanomolar concentration or even lower is preferred in FCS to obtain valid information.

Any molecule entering the confocal volume will leave it after a certain time, on average. Therefore, in FCS the mathematical treatment relies on the average notion, correlation. This is understood in a way to quantify how much signal is still similar to itself after a certain delay time or what is the probabilities to have the same signal from the same molecule. (Ferrand et al., 2011)

As the fluctuation of the signal measured by the detector is related to the particles inside the confocal volume, then the reading intensity $I(t)$ will fluctuate in the same way as the number of particles $N(t)$

do, therefore every property derived for $N(t)$ is also valid for $I(t)$. These fluctuations could be described by the autocorrelation function (ACF);

$$g(\tau) = \frac{\langle I(t) I(t + \tau) \rangle}{\langle I(t) \rangle^2} \quad (1-1)$$

In case the τ is much smaller than the residence time of the molecule, then the signal does not have the time to change. This means, $\langle I(t) I(t + \tau) \rangle \approx \langle I(t)^2 \rangle > \langle I(t) \rangle \langle I(t) \rangle$ and therefore $g(\tau) > 1$. In case τ is very large, then there is no similarity and the ACF amplitude will approach 1. The intermediate value carries the information on the duration and the resident time of the molecule.

The shape of the observation volume is described by the point spread function (PSF) of the confocal microscope. The exact description of the PSF is complicated but for FCS studies, it is generally assumed by a Gaussian approximation to be defined as

$$V_{eff} = \pi^{\frac{3}{2}} \omega_{xy}^2 \omega_z \quad (1-2)$$

Where, ω_{xy} and ω_z denote the lateral and axial waist, respectively.

By writing the fluctuating intensity as $I(t) = \langle I \rangle + \delta I(t)$, equation 1 becomes,

$$G(\tau) = 1 + \frac{\langle \delta I(t) \delta I(t + \tau) \rangle}{\langle I(t) \rangle^2} \quad (1-3)$$

Cause the FCS signal is following Poisson distribution (meaning the variance equals the average), the ACF at a very short time could be written as

$$G(\tau \rightarrow 0) = 1 + \frac{1}{\langle N \rangle} \quad (1-4)$$

This emphasizes that the ACF amplitude depends on the number of molecules in the confocal volume, and as the number increased it becomes more difficult to observe the fluctuation.

It's clear now, why we have the 'fluorescence' and 'correlation' terms in the name of the FCS technique, but what about the 'spectroscopy' term. FCS is able to monitor different physical states of the molecule which is happening at different time regimes, as shown in the following figure, which could be described by equation 1-5.

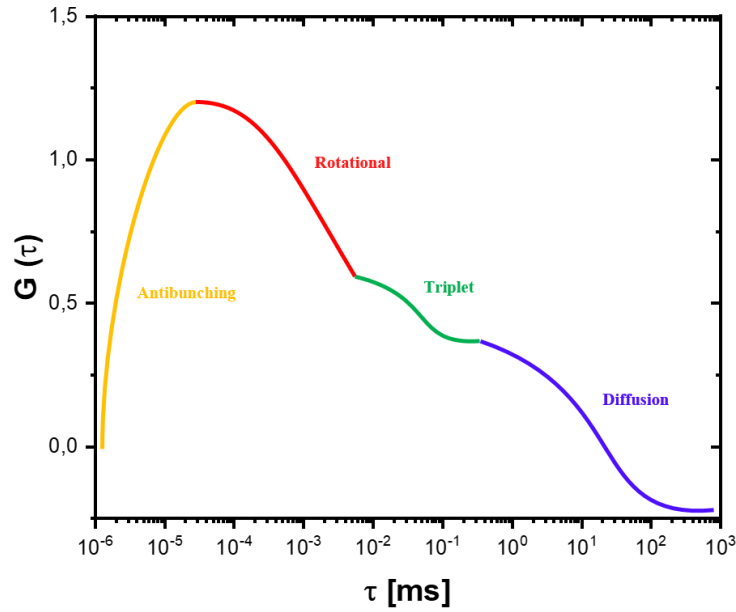


Figure 1-8 Timescales of different parameters measured by autocorrelation analysis.

$$G_{tot}(\tau) = B^2 \cdot A \cdot G_T(\tau) \cdot G_{dxy}(\tau) \cdot G_{dz}(t) \cdot G_r(\tau) \cdot G_a(\tau) \quad (1-5)$$

Where B is the background, A is the amplitude, G_T is the correlation term for the triplet state, G_{xy} and G_z are the translation diffusion term in xy and z-direction, respectively, G_r is the correlation term of the rotational diffusion, and G_a is the antibunching correlation term.

In the free diffusion case and for our interest we will focus only on the translation diffusion and the triplet state of the fluorophore, to have an ACF as follow,

$$G_\tau = \frac{1}{N} \left(1 + \frac{T}{1-T} e^{-\frac{\tau}{\tau_T}} \right) \sum_{i=1}^M \frac{f_i}{1 + \frac{\tau}{\tau_{Di}}} \frac{1}{\sqrt{1 + \frac{\tau}{\tau_{Di}} S^2}} \quad (1-6)$$

Where N is the average number of fluorophores within the observation volume, M is the number of the different fluorescent components (here $M = 1$), f_i determines the contribution of the different fluorescent components to the ACF, T is the fraction of the fluorescence decay from the triplet state and τ_T is the lifetime of the triplet state, τ_D is the diffusion time of the fluorescent molecule, and S is the structural parameter, the ratio of the axial and lateral radius of the effective observation volume

$$S = \frac{\omega_z}{\omega_r}$$

The dimension of the observation volume can be determined through the calibration process by using a high quantum yield dye with known diffusion coefficient D , and for 1 photon excitation system, the calibration of the lateral radius is governed by the following relation.

$$\tau_D = \frac{\omega_r^2}{4 \cdot D} \quad (1-7)$$

Once the calibration is performed, we will be able to determine the diffusion coefficient of an unknown sample.

FCS experiments are normally performed on fluorescent molecules (here are the NPs) at nanomolar concentration moving freely through the confocal volume of the order of 1 fL. The fluctuation of the fluorescence emission is analyzed by the ACF to obtain the diffusion time of the NPs, which change stepwise in the presence of protein corona. From the Stokes-Einstein relation, we can calculate the hydrodynamic radius of the NPs and the thickness of corona layer can be easily estimated.

In addition to that, to get more quantitative results regarding the adsorption process fitting of the change in the hydrodynamic radius using one of the thermodynamic models (Hill model) is required. To briefly show the relation between the adsorption of protein corona onto the NPs and the well-known Hill model, that originally formulated in 1910 to describe the oxygenation of the hemoglobin (Del Pino et al., 2014, HILL, 1910).

We need here to state that the fraction of the saturated NPs is equivalent to the fraction of the occupied sites on the NPs surface by proteins, and according to the law of mass action. For NPs are interacting with n of proteins P , to form a complex of protein-NPs.



The dissociation coefficient K_d of that will be,

$$K_d = \frac{[NP][P]^n}{[P_n NP]} \quad (1-9)$$

The initial concentration of the NPs, in this case, will be the free NPs in solution $[NP]$ and the ones that formed complex $[P_n NP]$. Accordingly, the fraction of the saturated NPs or the fraction of the occupied sites on the NPs can be expressed by the following.

$$\frac{N}{N_{max}} = \frac{[P_n NP]}{[NP] + [P_n NP]} \quad (1-10)$$

Instead of using the dissociation coefficient, we can use the concentration producing half-saturation, where $k_d = (K_D)^n$, the number of occupied sites could be described as.

$$N = \frac{N_{max}}{1 + \left(\frac{K_D}{[P]}\right)^n} \quad (1-11)$$

The Hill-coefficient here is an empirical parameter, which measures how steep the adsorption profile is and may describe the cooperativity of protein adsorption. In case $n > 1$, is a positive cooperative binding, once the proteins are adsorbed the affinity for others increases. $n < 1$, is a negative cooperative binding or anti-cooperative, once the proteins are adsorbed the affinity for others is suppressed. $n = 1$, is a non-cooperative binding, completely independent adsorption.

By knowing how many proteins are adsorbed on the NPs surface, we can calculate the change of size or the hydrodynamic size of the NPs. In case N of proteins with protein volume V_P are adsorbed on the NPs, the dependency of the volume of the NPs on the proteins adsorbed described by.

$$V_{(N)} = V_0 + N \cdot V_P \quad (1-12)$$

In this case, if we call the ratio of the volume of protein to the volume of the NPs before any protein adsorbed to be $c = \frac{V_P}{V_0}$, and recalling equation 11, we can describe the hydrodynamic radius of the NPs in dependence on the number of proteins adsorbed by.

$$R_{h(N)} = R_{h(0)} (1 + c \cdot N)^{\frac{1}{3}} \quad (1-13)$$

By using this equation to fit the change of the hydrodynamic radius obtained by FCS, we can derive different quantitative parameters to be used to describe and compare different protein adsorption profiles, as will be discussed in the following sections.

2 Aim of the Work

In view of what we have discussed in the introduction chapter, our motivation was mainly to develop a potential approach for more efficient nanomedicine. Therefore, our project aims to develop a universal method for surface modification of the nanoparticles, where we can modify the surface chemistry of the nanoparticles, independent of the core, with different surface charges, imaging agents, or targeting ligand.

Moreover, understanding the impact of the surface charge and the physicochemical character of the nanoparticles on their cellular and protein interactions. This could be achieved with a detailed physicochemical characterization of the synthesized NPs, before and after surface modifications. In addition to studying their surface properties upon using different amphiphilic polymers to modify the surface of the NPs.

As a prerequisite now for any nanomedicine candidates, a deep understanding of their protein interactions is highly required. From this perspective, single-molecule biophysics techniques as fluorescence correlation spectroscopy would provide us with indirect measurements of the protein adsorption with the NPs. Furthermore, by using a specific thermodynamic model to deduce more quantitative parameters upon the protein adsorption.

The cellular interactions of these polymer-coated NPs quantified using different techniques to obtain a comparative view of the effect of using different-charged amphiphilic polymers. We, in the end, aim to introduce potential candidates for nanomedicine applications.

3 Results and Discussion

Herein, we are presenting and discussing the results obtained in our way to answer the research question stated before. The current chapter is divided into sub-sections, the polymer library that has been used in the present work, the physicochemical characterization of the successfully coated NPs; this includes the Au NPs and the QDs, the colloidal stability test for the polymer-coated Au NPs, the dynamical interfacial tension results, the *in situ* protein adsorption results as measured by the fluorescence correlation spectroscopy (FCS), and at the end of this chapter, we are presenting the cellular interactions of these NPs including their biocompatibility and their cellular uptake.

3.1 Amphiphilic polymers used in the present study

In this study, we have used amphiphilic polymers with different charges, the structure of these polymers is shown in [Figure 3-1](#) and their parameters are listed in [Table 3-1](#). We have used these amphiphilic polymers to modify the surface chemistry of the NPs, based on the hydrophobic interactions between the alky chain of the polymer to that on the surface of the NPs (this means we have to get NPs dispersed in an organic solvent, whether as-synthesized or we carrying out ligand exchange followed by phase transfer to have them in hydrophobic media, as we did with the 17 nm Au NPs) leaving the hydrophilic chain (which bears the charge) exposed to the aqueous solution.

This ensures applying the same surface modification or the same chemistry to the NPs, regardless of the core, and at the same time having different surface charges. This approach was a prerequisite to help in answering our research questions stated before, we need to study the effect of the surface charge upon the different interactions of the NPs while trying to normalize other factors. This has been achieved by having universal surface chemistry on the NPs surface (the second layer, Coating), which is possible in the case of the amphiphilic polymers. More details regarding these polymers, and how we did the polymer coating to different NPs are described in the experimental chapter.

In addition to that, the amphiphilic polymers with phosphonate ($pK_{a1} = 2.4$), carboxylates ($pK_a = 4.3$), and ammonium groups ($pK_a = 9.25$) show permanent charge at the physiological pH. (Hühn et al., 2013)

On the other hand, one other advantage of working with these polymers, particularly in tumor therapy, these polymers are considered as charge-reversal polymers. Where they are able to switch their charge upon stimuli, like pH or enzymes. This in turn helps in increasing their local internalization in the tumor based on the fact that the tumor environment is more acidic than the normal physiological fluid. Transforming their surface charge from negative or neutral into positive facilitates

their localization into the targeted tissue. As reported, the sulfobetaine SB polymers for example, where the negative charge on the sulfonate group reversed into positive upon the acidic condition of the environment. Moreover, the polymers have the amide bond, which is believed to be non-degradable or only at a harsh pH value. However, the amide bond of the maleic derivatives can be cleaved at a slightly acidic pH value. (Da Huang et al., 2016, Da Huang et al., 2017, Dai et al., 2008, Du et al., 2010, Du et al., 2018, Pang et al., 2016, Wang et al., 2015)

Amphiphilic polymers used in the present study

Table 3-1 Amphiphilic Polymers that have been used in the present study.

Polymer	Label	Mw [g/mol]	x: y: z*	Charge
PTMAEMA-stat-PLMA-stat-PPgMA	PT	15576	48:48:04	+
	PTL	7200	54:43:03	+
PSB-stat-PLMA-stat-PPgMA	SBL	3905	62:36:02	+/-
	SB	7200	54:43:03	+/-
PMPC-stat-PLMA-stat-PPgMA	PC	21841	48:50:02	+/-
PMAPHOS-stat-PLMA-stat-PPgMA	PH	11098	56:41:03	-
Poly (isobutylene-alt-maleic anhydride)-grafted-dodecylamine	PMA	11400	25:75	-
Poly (maleic anhydride-alt-1-octadecene), 3-(Dimethylamino)-1-propylamine derivative	PMAL [#]	12000	50:50	+/-
Poly (isobutylene-alt-maleic anhydride)-grafted-dodecylamine-3-(dimethylamino)-1-propylamine	DMAPA	11460	50:50	+/-

* x:y:z, is the ratio of the Hydrophilic (charged) to Hydrophobic to functionalized monomer units, respectively.

[#]PMAL is a commercial polymer.

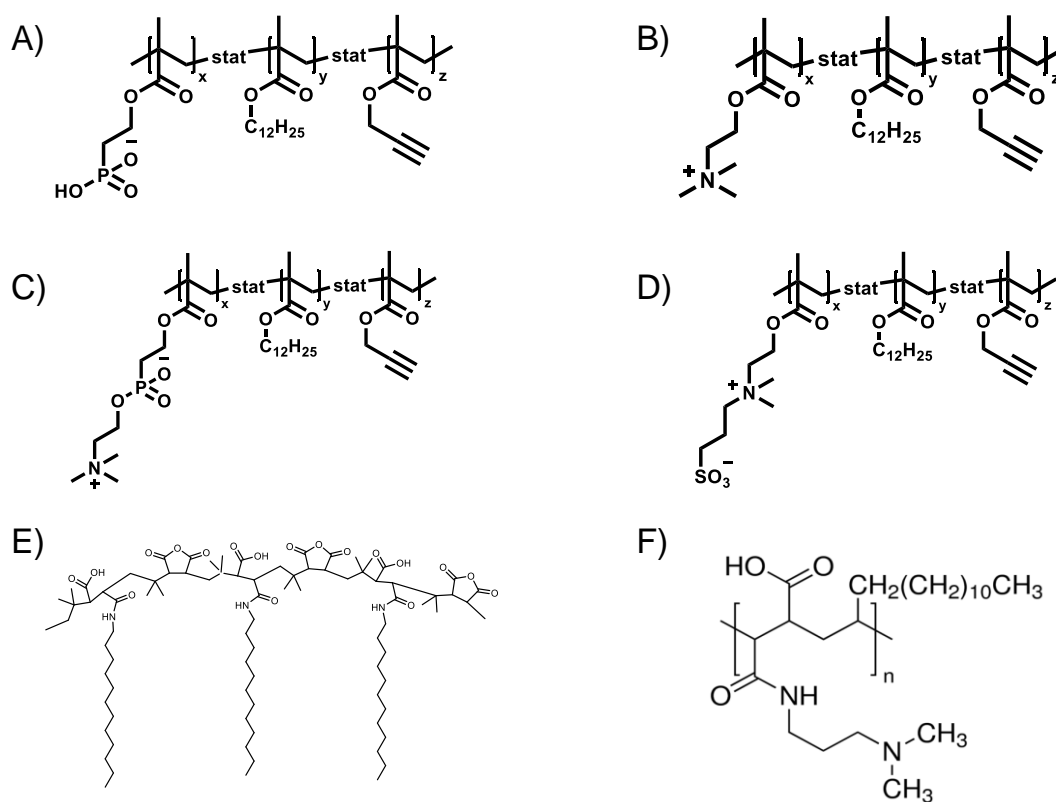


Figure 3-1 Structure of the Amphiphilic polymers that have been used in the present study. A) PH, B) PT or PTL, C) PC, D) SB or SBL, E) PMA, and F) PMAL polymer. PMAL is a commercial polymer.

3.2 Physicochemical characterization of Gold nanoparticles

The physicochemical characterizations of the coated Au nanoparticles have been studied using different techniques as UV-Vis spectroscopy, Transmission electron microscope (TEM), ζ -potential, and Dynamic light scattering (DLS). Table 3-2 and Table 3-3 show the summary of the physicochemical characterization of the coated 17 nm and 4 nm Au NPs, as obtained by DLS, UV-Vis, and ζ -potential measurements.

Table 3-2 Summarized Characterization of the 17 nm Au-NPs coated with different polymers. $d_{H(N)}$ is the hydrodynamic diameter as measured by DLS, ζ is the zeta potential of the samples, LSPR is the center of the localized surface plasmon peak as measured by UV-Vis spectroscopy, and FWHM is the full width at half maximum of the SPR peak.

Sample code	Charge	$d_{H(N)}$ [nm]	ζ [mV]	SPR [nm]	FWHM [nm]
Au-SBL	+/-	23±1	-32±3	524	50
Au-SB	+/-	23±1	12±3	524	50
Au-PC	+/-	21±2	7±2	521	46
Au-PH	-	20±1	-42±1	521	47
Au-PT	+	28±4	48±3	527	50
Au-PTL	+	25±1	36±1	529	52
Au-PMA	-	21±2	-52±5	520	45
Au-PMAL	+/-	20±5	4±1	524	48
Au-MAPA	+/-	30±1	5±1	521	45
Au-EDLF	+/-	20±1.6	19±3	522	50

Table 3-3 Summarized Characterization of the 4 nm Au-NPs coated with different polymers. $d_{H(N)}$ is the hydrodynamic diameter as measured by DLS, ζ is the zeta potential of the samples, and LSPR is the center of the localized surface plasmon peak as measured by UV-Vis spectroscopy.

Sample Code	Charge	$d_{H(N)}$ [nm]	ζ [mV]	SPR [nm]
4Au-SBL	+/-	12±3	-25±2	517
4Au-PH	-	13±1	-28±2	518
4Au-PT	+	13±1	13±1	525
4Au-PC	+/-	14±5	-5±0.2	522
4Au-PMA	-	15±1	-36±3	520

3.2.1 Transmission Electron Microscopy

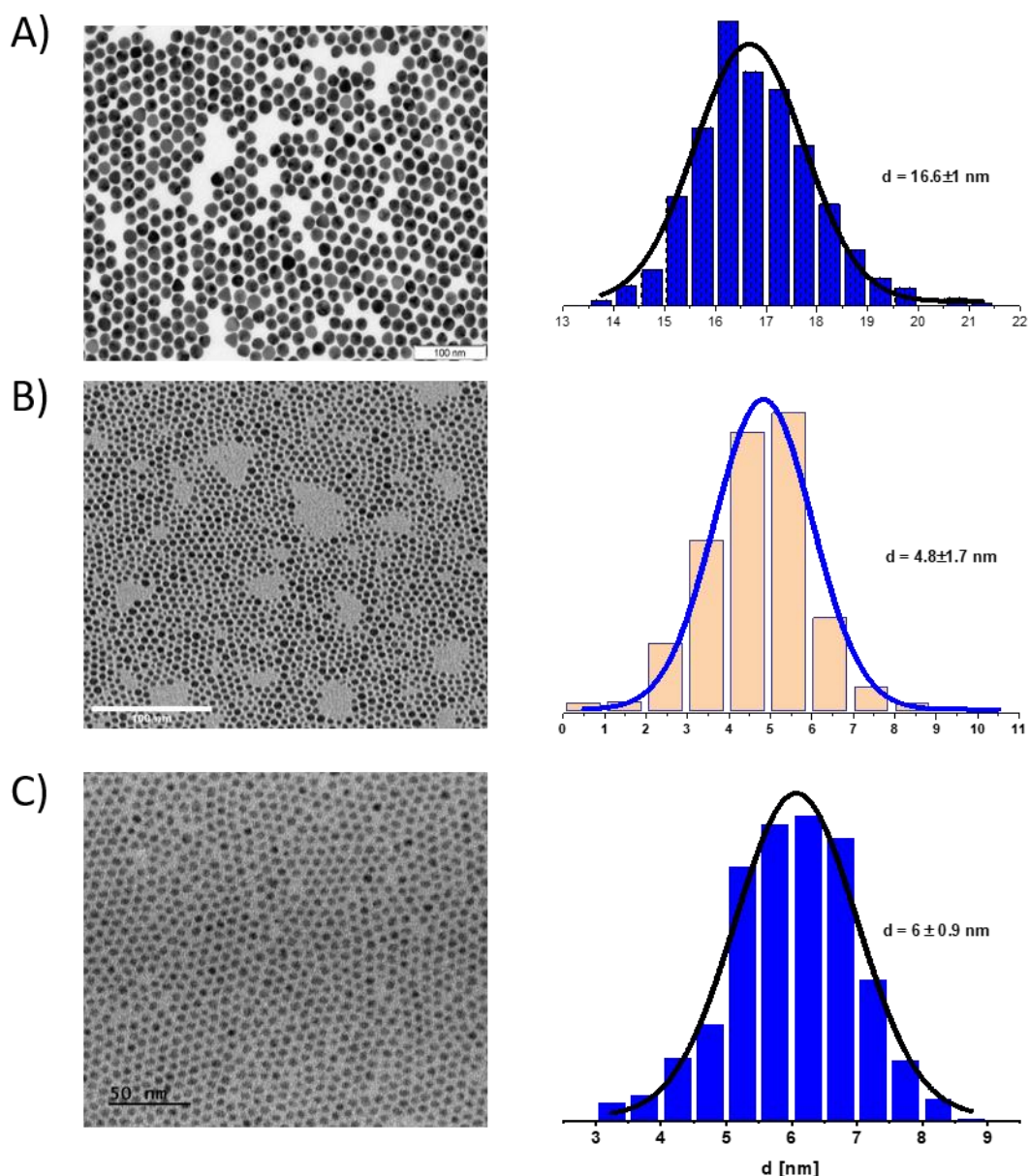


Figure 3-2 TEM Images of the NPs core. The core of A) 17 nm Au NPs calculated out of 573 NPs B) 4 nm Au NPs calculated out of > 2000 NPs, and C) QDs calculated out of > 1000 NPs.

3.2.2 UV-Vis absorption results of the gold nanoparticles

The coated Au NPs were characterized using different techniques to evaluate their physicochemical properties. Herein, we are showing the results obtained for the gold nanoparticles coated with different polymers. Figure 3-3: 5 show the UV-Vis absorption spectra of the Au NPs coated with different polymers. Figure 3-3 shows the Au NPs coated with PC (+/-), PTL (+), PT (+), SB (+/-), SBL (+/-), and PH (-) polymers, while Figure 3-4 shows those coated with PMA (-) and PMAL (+/-) polymer and Figure 3-5 shows the Au NPs coated with PMA-DMAPA and EDLF polymer.

Table 3-2 summarizes the physicochemical parameters of the coated NPs obtained using different techniques such as DLS and UV-Vis spectroscopy. The LSPR peak of the coated samples located at 524 ± 3 nm, as an average of all the samples with FWHM of the LSPR peak of 48 ± 3 nm. This ensures the existence of the polymer on the NPs did not significantly change their optical properties and the redshift of the peak is only around 3 nm if compared with the core.

For the 4 nm Au NPs, Table 3-3 shows the characterization parameters of the coated NPs and as shown the LSPR at 518 nm, with an exception for the positively coated NPs which are red-shifted by 7 nm. This shift is also observed for this polymer with the larger size of the Au NPs as shown in Table 3-2. Which is could be related to a local environment change cause of this polymer that induced such red-shift in the SPR peak. (Zijlstra et al., 2012)

Based on the optical properties of the coated NPs, we can conclude that the polymer coating is successful in keeping the optical properties of the Au NPs without significant change for the smaller and larger size.

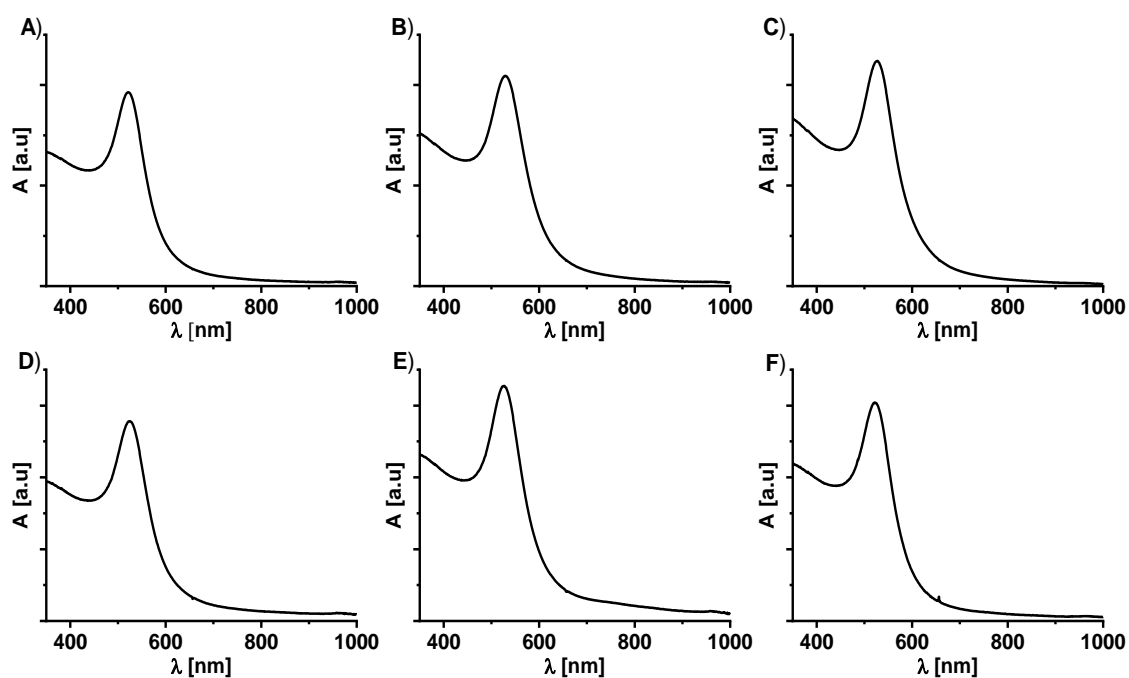


Figure 3-3 Absorption Spectra of the 17 nm Au-NPs. NPs coated with A) PC, B) PTL, C) PT, D) SB, E) SBL, and F) PH.

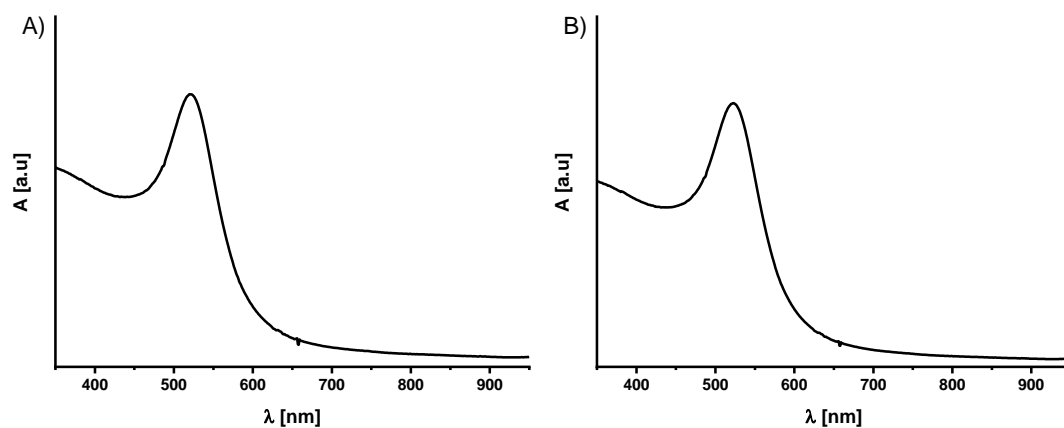


Figure 3-4 Absorption Spectra of the 17 nm Au-NPs coated with A) PMA, and B) PMAL.

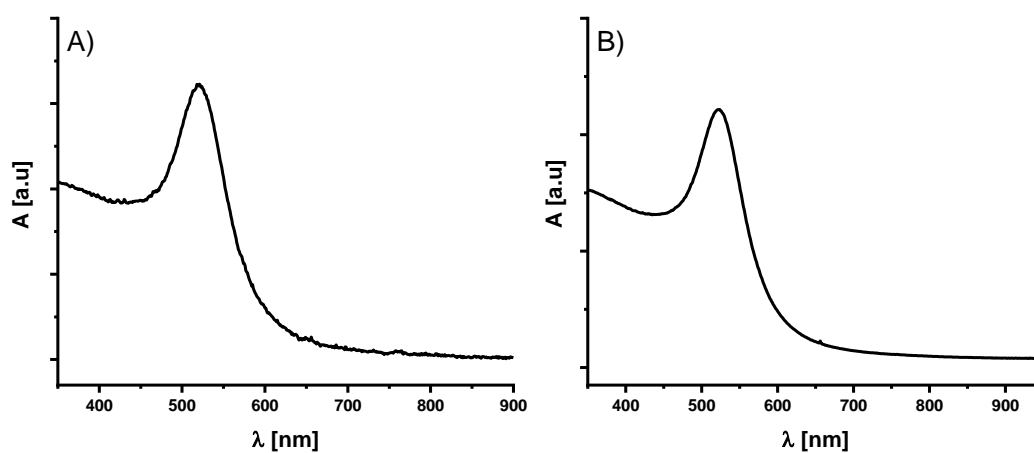


Figure 3-5 Absorption Spectra of the 17 nm Au-NPs coated with A) PMA-DMAPA, and B) EDLF.

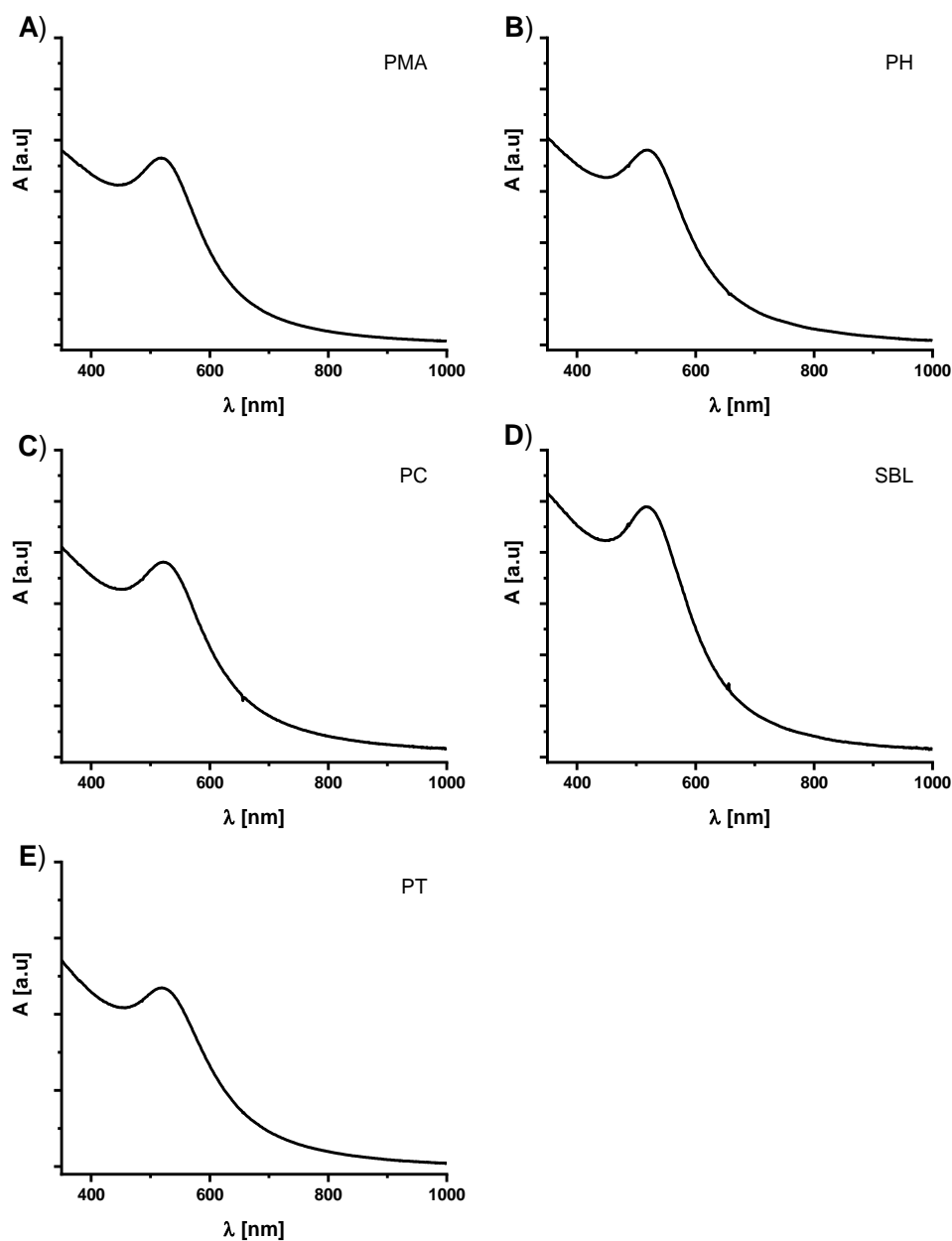


Figure 3-6 Absorption Spectra of the 4 nm Au-NPs. NPs coated with A) PMA, B) PH, C) PC, D) SBL, and E) PT polymer.

3.2.3 Dynamic light scattering results of the gold nanoparticles.

The sensitivity to detect any size agglomeration is commonly achieved by using the DLS apparatus, which determines the hydrodynamic radius of the NPs based on a scattering approach, a good indicator, and sensitive to the agglomeration of the NPs. Table 3-2 shows the summary of the hydrodynamic results of the 17 nm Au NPs and the results are also graphically shown in Figure 3-7 and Figure 3-8. The average Hydrodynamic diameter d_h of the samples is 22 ± 3 nm, which indicates and supports the optical results of these samples. For most of the polymers, the average size is nearly the same with a slight deviation.

Table 3-3 is showing the d_h of the 4 nm Au NPs, and these results are also graphically shown in Figure 3-9. Here, the average of the d_h is around 12 ± 1 nm. The existence of the polymers onto the NPs leads to the formation of a hydration layer around it this, in turn, results in a larger radius than the core itself, which is known for such polymers.

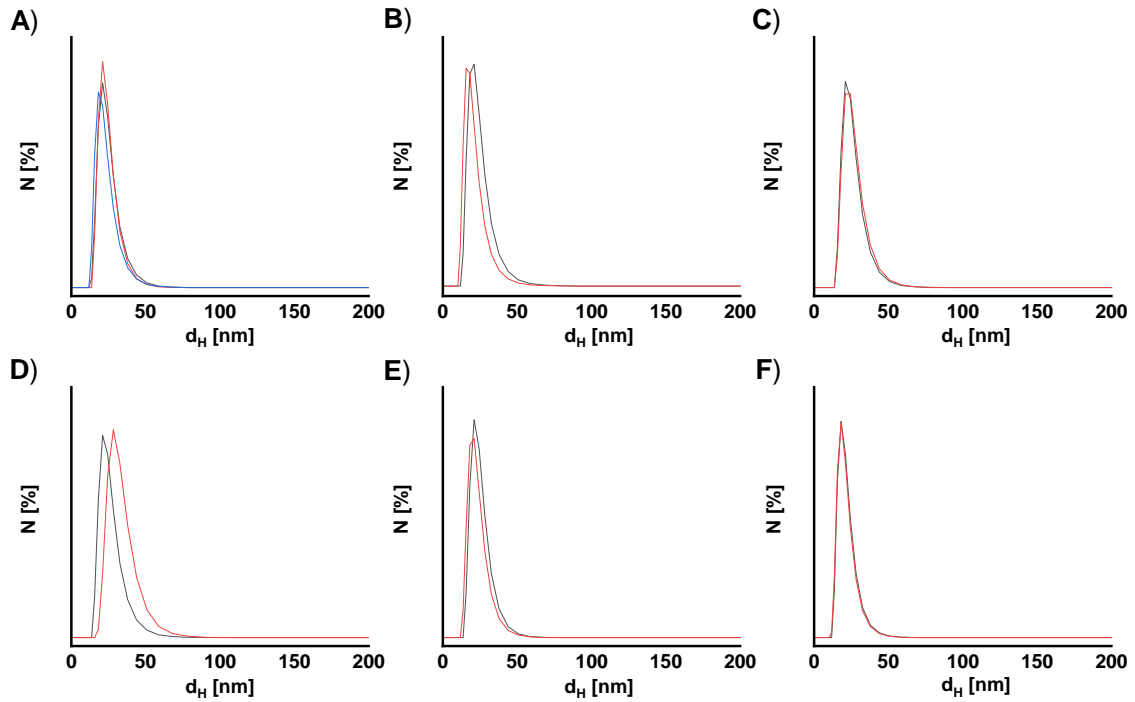


Figure 3-7 Hydrodynamic Diameter of the 17 nm Au-NPs. NPs coated with A) SBL, B) PC, C) PTL, D) PT, E) SB, and F) PH.

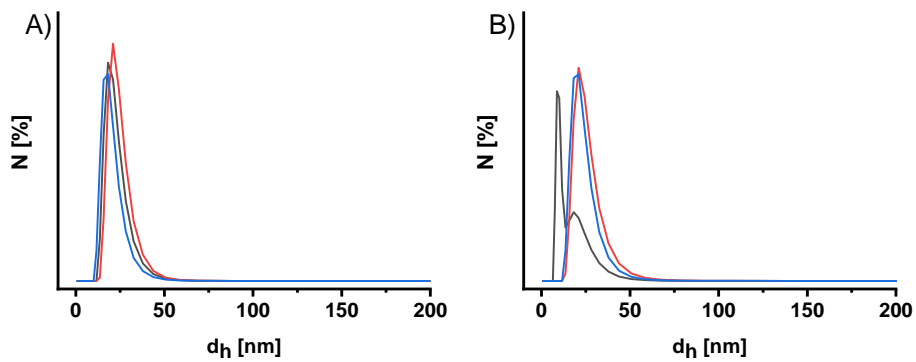


Figure 3-8 Hydrodynamic Diameter of the 17 nm Au-NPs coated with A) PMA, and B) PMAL.

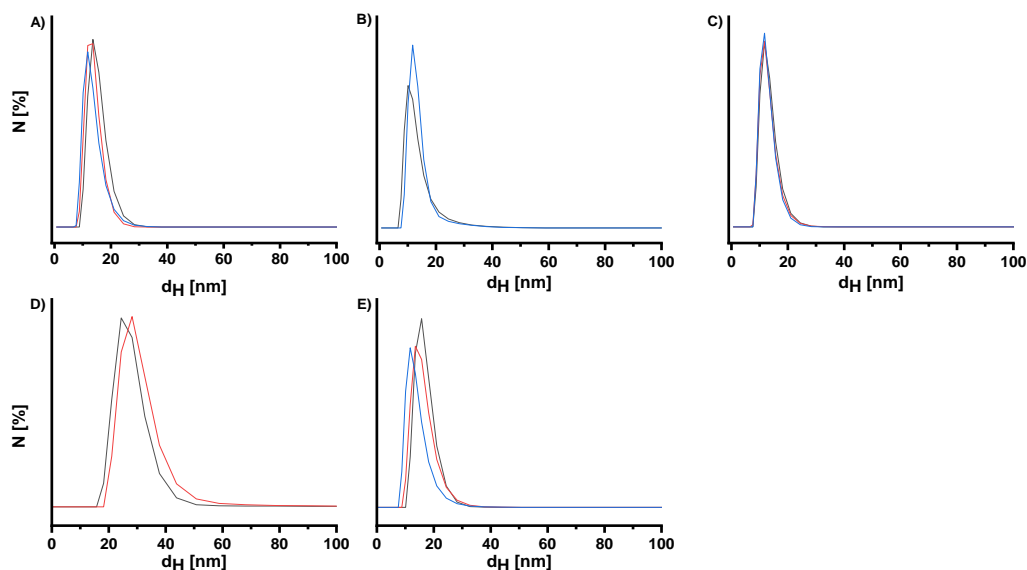


Figure 3-9 Hydrodynamic Diameter of the 4 nm Au-NPs. NPs coated with A) PH, B) PT, C) SBL D) PC, and E) PMA.

3.2.4 Zeta Potential Measurements (ζ)

Zeta potential ζ is one of the major factors that determine the long-term colloidal stability of the NPs. Having a lower value for the ζ -potential, which is reported to be between +25 to -25 mV, is significantly affects the colloidal stability of the NPs. However, this is not the full story of the colloidal stability; the colloidal stability could be enhanced with other factors; for example, the steric repulsion. Steric repulsion came from the formation of a thicker hydration layer around each NPs, this layer is frequently formed around the polymers. That's why in our case if the surface charge is within the lower limit to make the NPs stable for a longer time, as in the case of the zwitterionic polymers, the steric repulsion plays the major role to keep these NPs stable for a longer time. It is worth mentioning here that these NPs were colloidal stable for more than two years on the bench. (Sakura et al., 2005, Sperling, Parak, 2010)

As presented in Table 3-2 and Table 3-3, the zeta potential of the coated NPs is in good agreement with their structure and was above the critical range (± 25 mV) for longer stability. With exception to the zwitterionic NPs, which is expected to have a very low value (< 20 mV), but as stated before such cases are also stabilized based on their steric effect. We have also observed, a negative value for the NPs coated with the SB family, although, it is normally for SB structures to be fully deprotonated at a broad range of pH and permanently charged. One of the possibilities to have such a negative value is a phenomenon called the chameleon effect, described by the higher affinity of the anions than cations towards zwitterionic groups, which leads to the overall negative zeta potential value. We have proved their zwitterionic character by testing their migration in gel electrophoresis as shown in the appendix.

We have observed no migration for the zwitterionic NPs, and the positive ones, whereas the negative NPs showed a significant migration into the gel toward the positive pole, Figure 6-1.

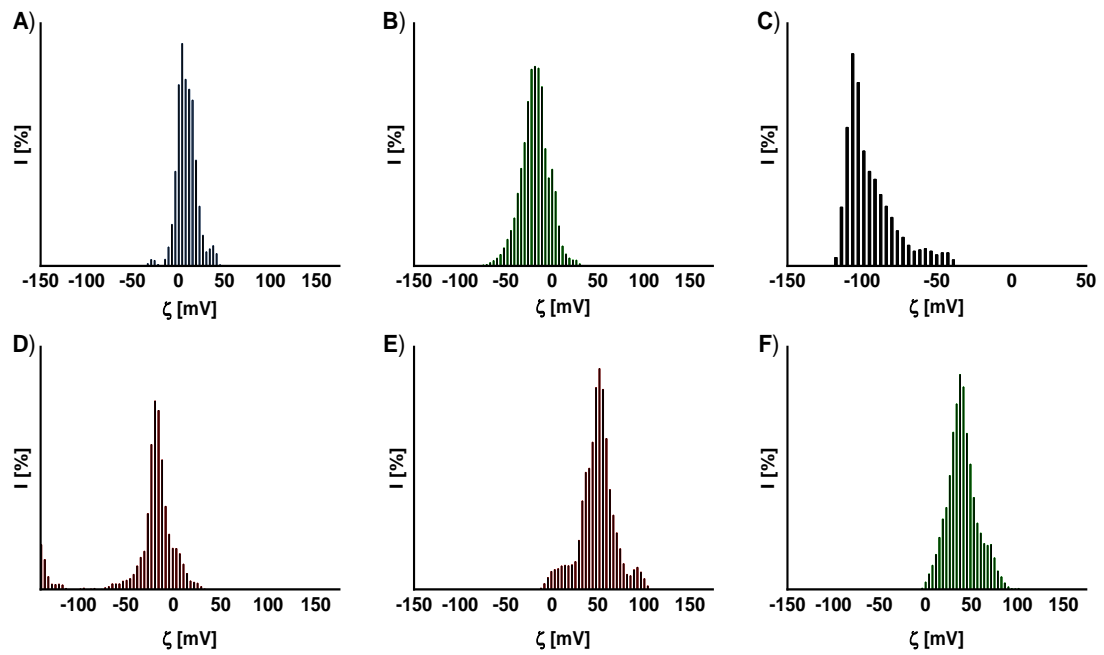


Figure 3-10 ζ - Potential Measurements of the 17 nm Au-NPs. NPs coated with A) PC, B) SBL, C) SB, D) PH, E) PT and F) PTL.

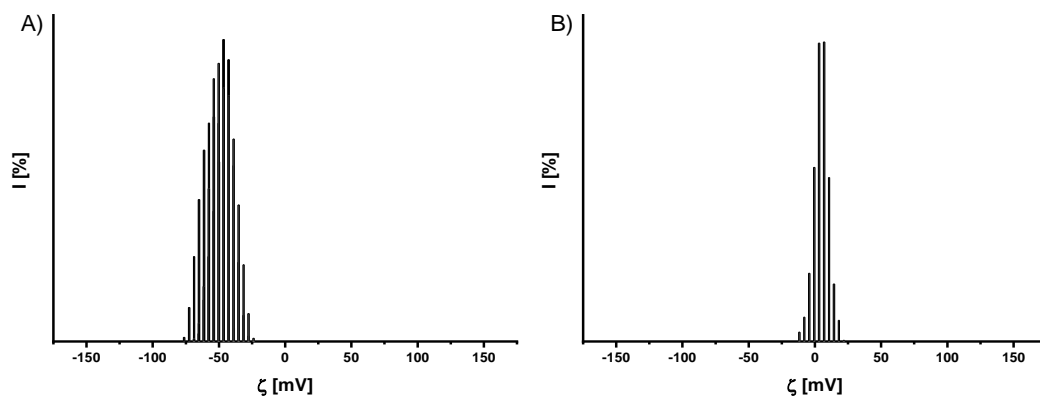


Figure 3-11 ζ - Potential Measurements of the 17 nm Au-NPs coated with A) PMA, and B) PMAL.

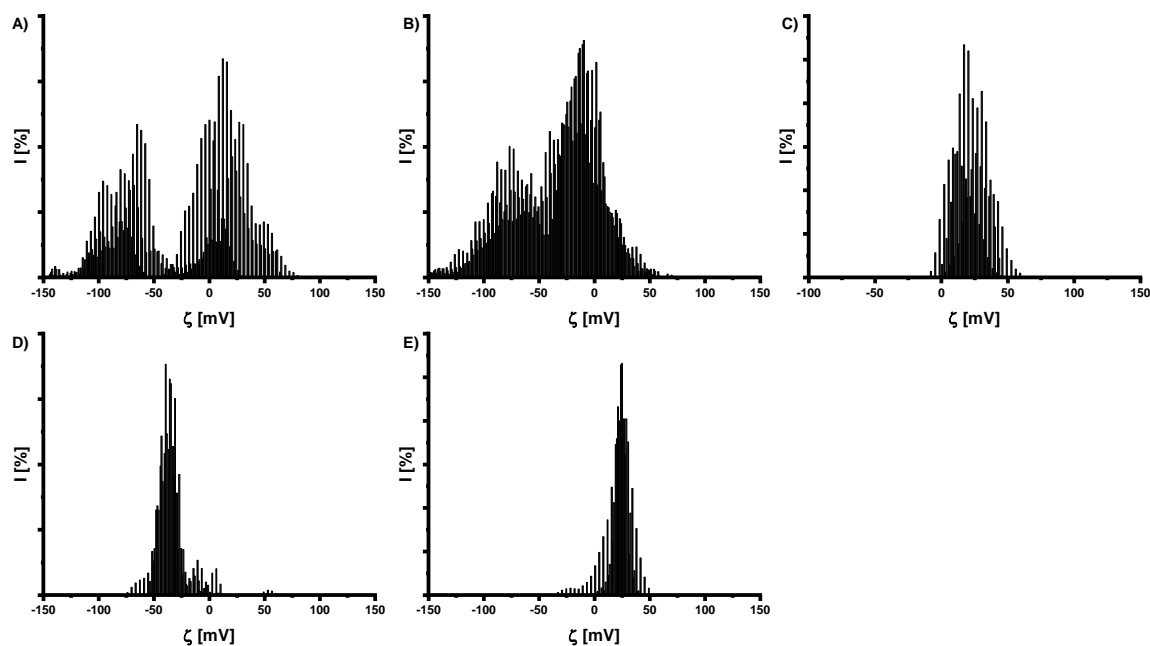


Figure 3-12 ζ - Potential Measurements of the 4 nm Au-NPs. NPs coated with A) PMA, B) PH, C) PC, D) SBL, and E) PT polymer.

3.3 Physicochemical Characterizations of the QDs

Herein, we are showing the characterization results of the polymer-coated QDs. Table 3-4 shows the summary of the characterization parameters of the coated QDs as measured by DLS, and FCS, while Figure 3-13:14 show graphically these characterization parameters, including the TEM images, Optical characterization, and DLS results.

Table 3-4 Characterization parameters of the coated QDs. Where R_{hN}^{DLS} is the hydrodynamic radius as measured by DLS, R_{hN}^{FCS} is the hydrodynamic radius as calculated from FCS measurements, ζ is the zetal potential of the QDs, and PL_{FWHM} is the full width at half maximum of the PL peak.

Sample	Charge	R_{hN}^{DLS} [nm]	R_{hN}^{FCS} [nm]	ζ [mV]	PL_{FWHM} [nm]
Q-PMA	-	5±0.4	6.9±0.1	-11±3	35
Q-PH	-	7±0.9	7±0.4	-42±4	33
Q-PT	+	8±0.3	11±0.3	50±2	40
Q-PMAL	+/-	5±0.2	8.4±0.2	4±1	39
Q-PC	+/-	9±0.2	11±0.2	-1±0.1	40
Q-SB	+/-	7±1	12±0.5	-22±1	32
Q-PC-FA	+/-	11±3	9±0.02	20±0.8	31
Q-DMAPA	+/-	8±3	7.6±0.02	6±0.5	35
Q-EDLF	+/-	11±2	8±0.2	0.4±1	33

3.3.1 Transmission Electron Microscopy of the QDs

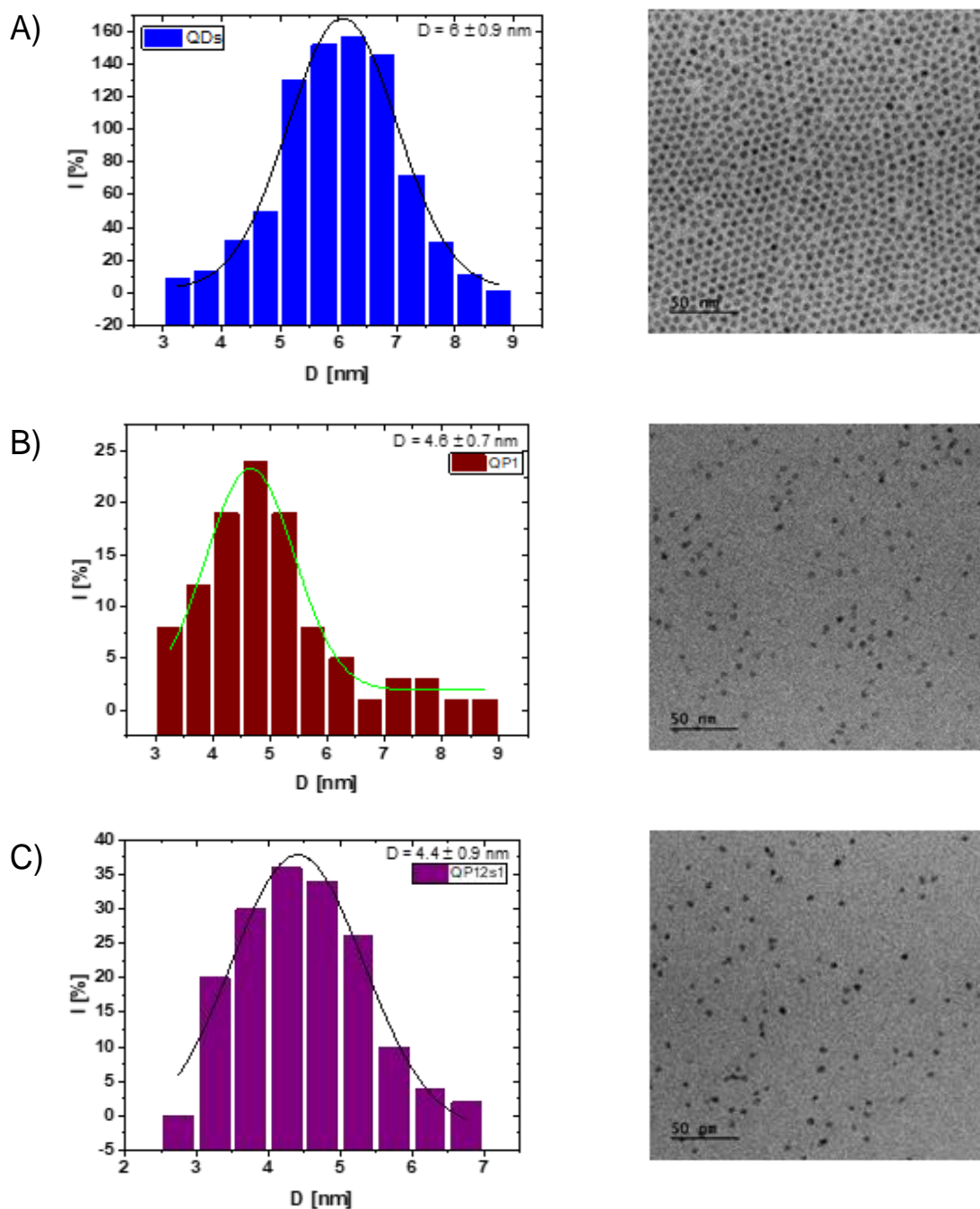


Figure 3-13 TEM image of the QDs. A) Core, B) Q-PMA, and C) Q-PC and their histogram.

3.3.2 UV-Vis absorption and photoluminescence PL results of the coated QDs

The coated QDs were characterized using UV-Vis and PL spectrophotometer for determining the quality and success of the coating. As shown in Figure 3-14 the QDs retain their optical properties as one can see from the UV-Vis and the fluorescence spectra of the QDs coated with different polymers. The FWHM of the PL peak is in the same range as the core with an average value of 36 nm that is only

a 4 nm difference from the core itself, indicating no significant variation happens to the core after the polymer coating. Therefore, the QDs still preserve their properties and their emission peak is at the same position as the core 615 ± 10 nm. This indicates that the polymer coating of the QDs was successful to keep the optical and the structural properties of the QDs with no significant change and did not alter their emission peak window. These results are further supported by the TEM images as there is no deviation in their core size, and by the DLS, as shown in Figure 3-13:14.

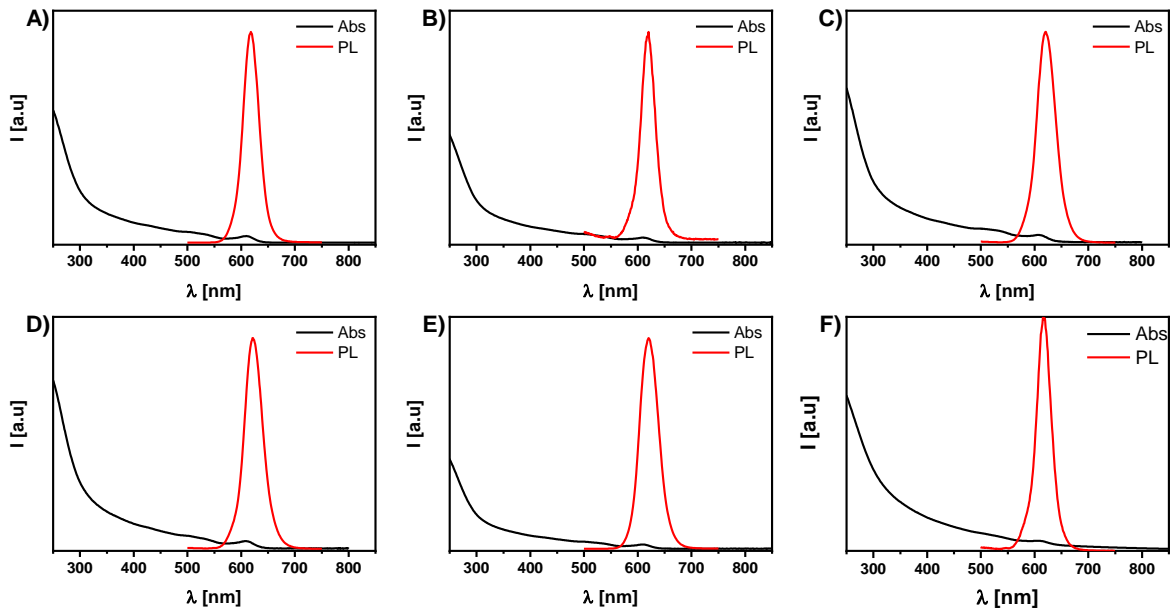


Figure 3-14 UV-Vis and PL spectra of the coated QDs. QDs coated with a) PMA (-), b) PH (-), c) PT (+), d) PC (+/-), e) PMAL (+/-) and f) SB (+/-).

3.3.3 Dynamic light scattering results of the coated QDs

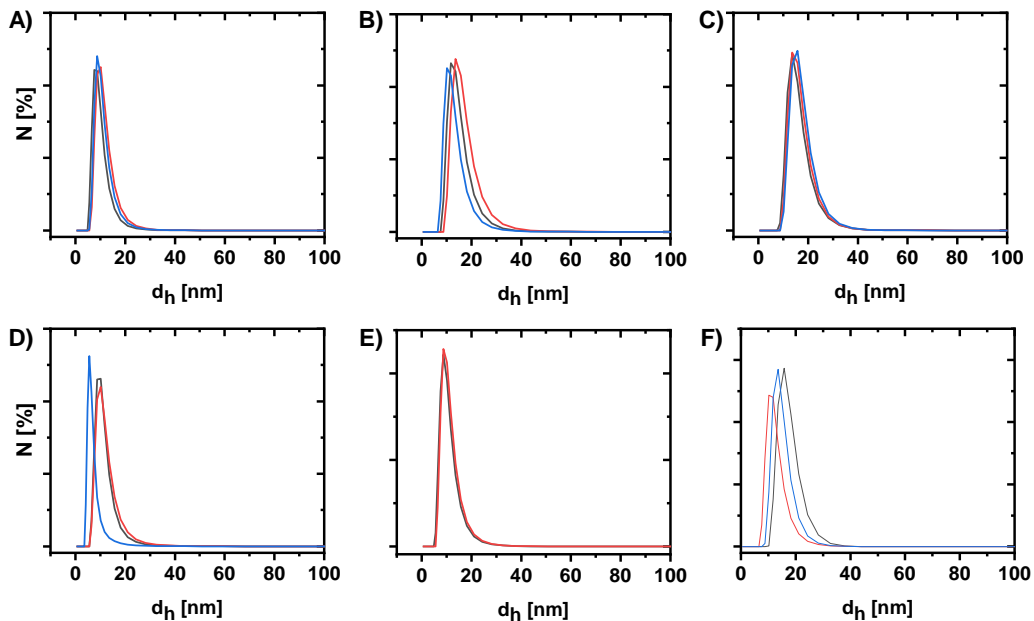


Figure 3-15 Hydrodynamic diameter obtained by DLS of the coated QDs. QDs coated with a) PMA (-), b) PH (-), c) PT (+), d) PC (+/-), and e) PMAL (+/-).

3.4 Colloidal stability of the Gold Nanoparticles

The colloidal stability of the nanoparticles is an essential property of the NPs to be used in bio-applications. This could be examined by exposing the nanoparticles to a high ionic strength media that screen the charge of the nanoparticles and leads to agglomeration and instability of the nanoparticles. One of the other possible ways to keep the nanoparticles stable is the steric repulsion - the hydration shell around the nanoparticles that work as a barrier toward the nanoparticle's agglomeration. This could be achieved by the polymer shell encapsulating the nanoparticles. (Hühn et al., 2016, Phan, Haes, 2019, Sakura et al., 2005, Stark, 2011)

We have examined the colloidal stability of the nanoparticles when exposed to a high ionic strength media, which in our case is NaCl, at two different time points and with two different techniques. The obtained results are shown in the following figures.

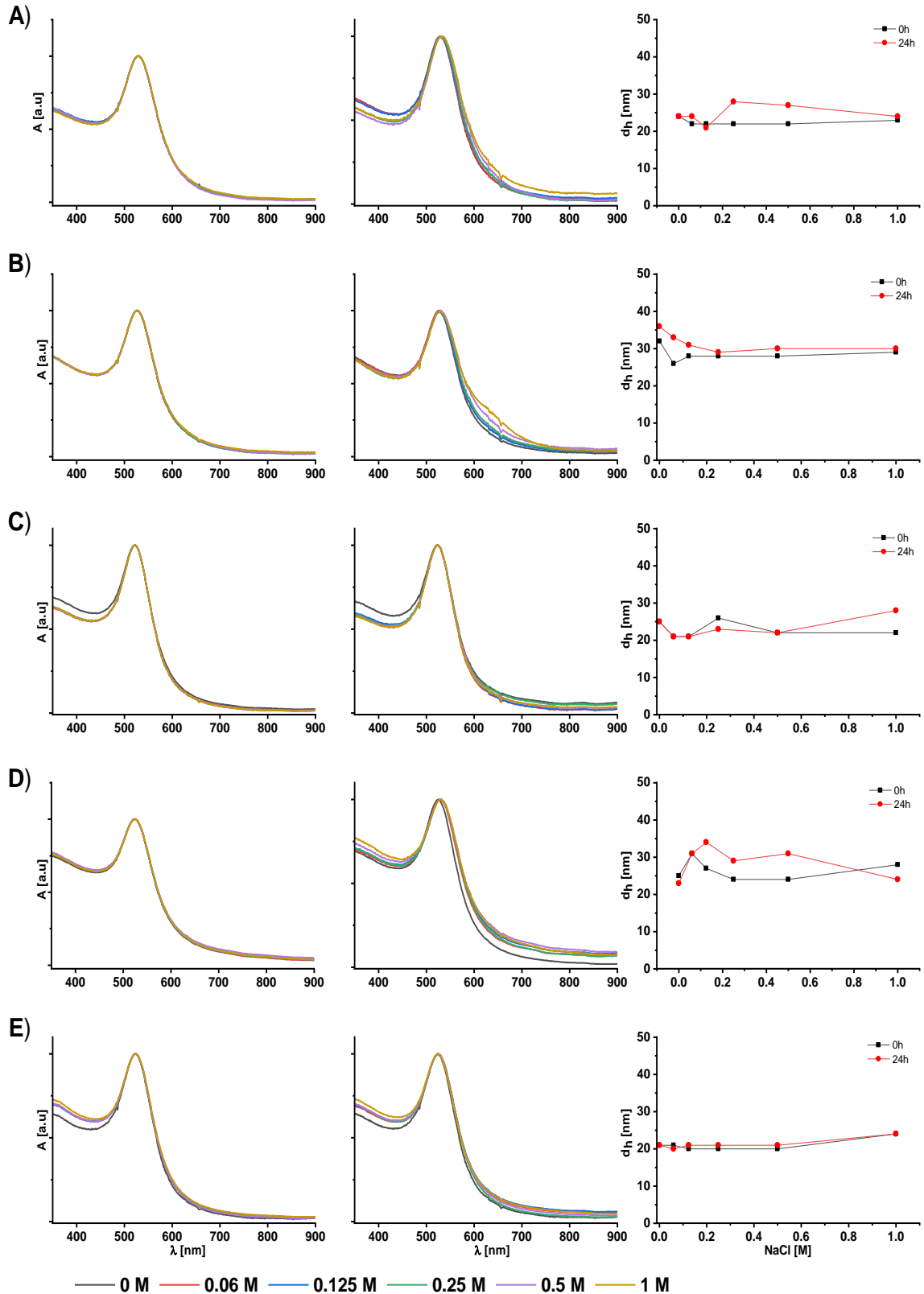


Figure 3-16 Colloidal stability of the 17 nm Au NPs against different concentrations of NaCl. The colloidal stability studied at 0 h and 24 h (left and middle panel) as investigated by UV-Vis and DLS of the 17 nm Au-NPs coated by A) PTL (+), B) PT (+), C) PC (+/-), D) SB (+/-), and E) PH (-).

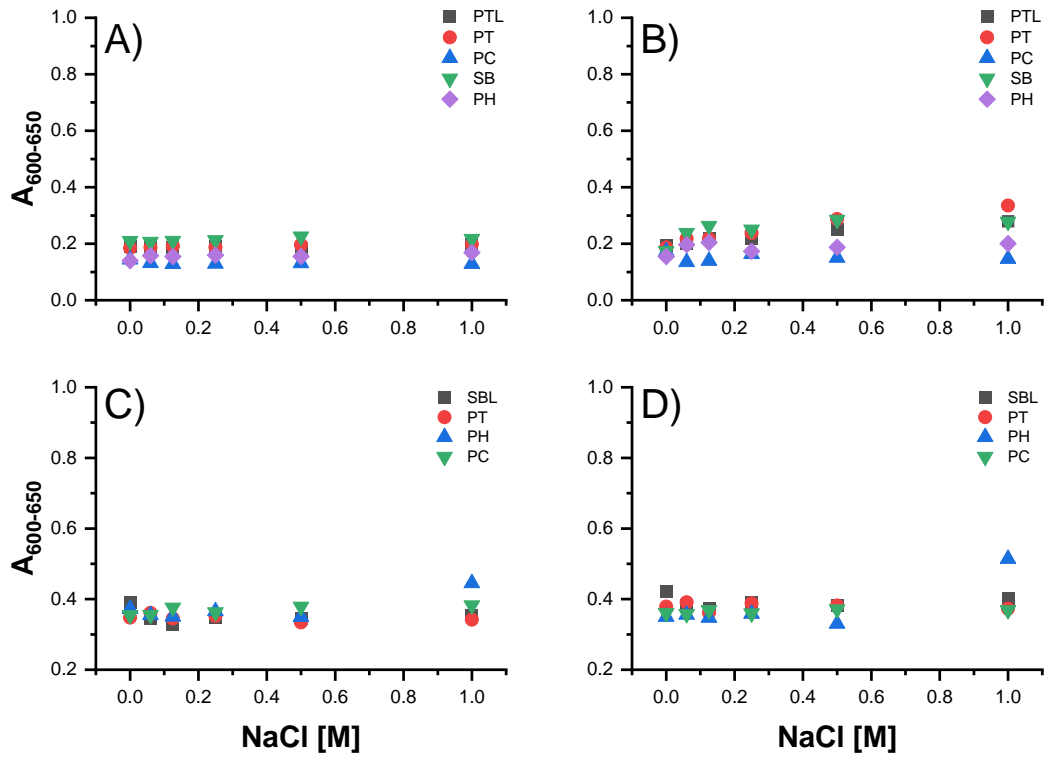


Figure 3-17 Average of absorption values (600:650 nm) of Au NPs versus NaCl concentration. A) 17 nm Au NPs at $t = 0$, B) at $t = 24h$, C) 4 nm Au NPs at $t = 0$, and D) at $t = 24h$.

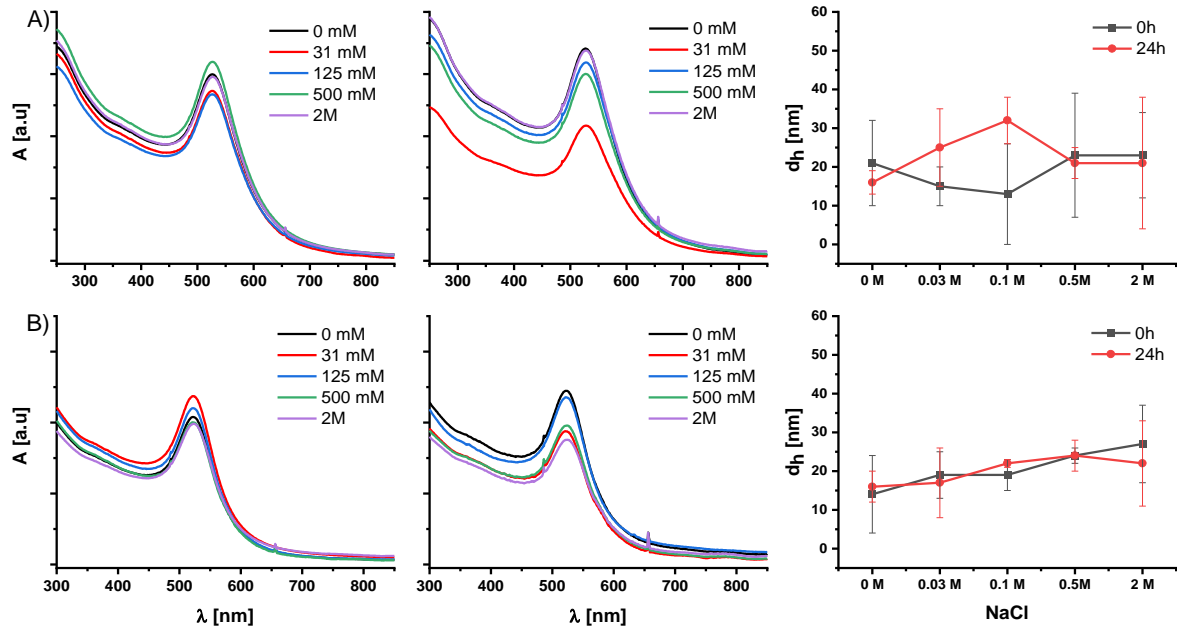


Figure 3-18 Colloidal stability of Au-PMA and Au PMAL NPs. Absorption Spectra at 0 h and 24 h (left and middle panel), and d_h results of Stability test in NaCl media for the 17 nm Au-NPs coated by A) PMA, and B) PMAL.

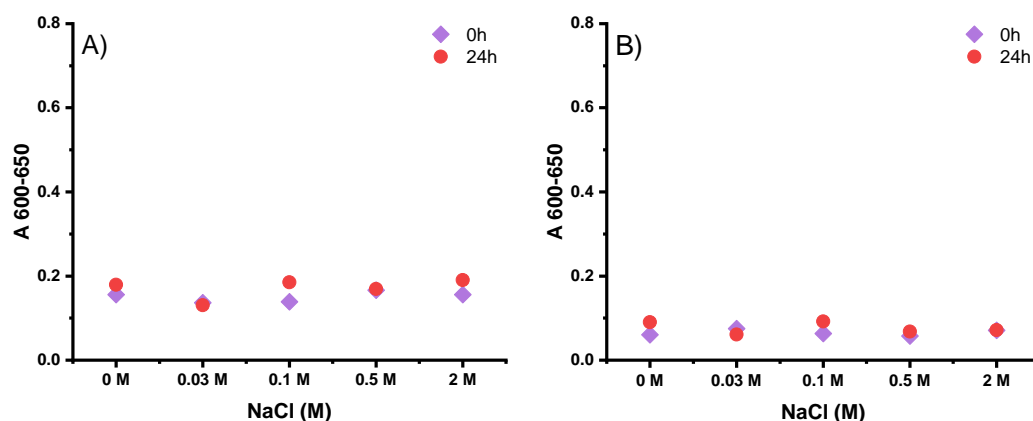


Figure 3-19 Average of absorption values (600:650 nm) of 17 nm Au NPs versus NaCl concentration. A) Coated with PMA, and B) coated with PMAL.

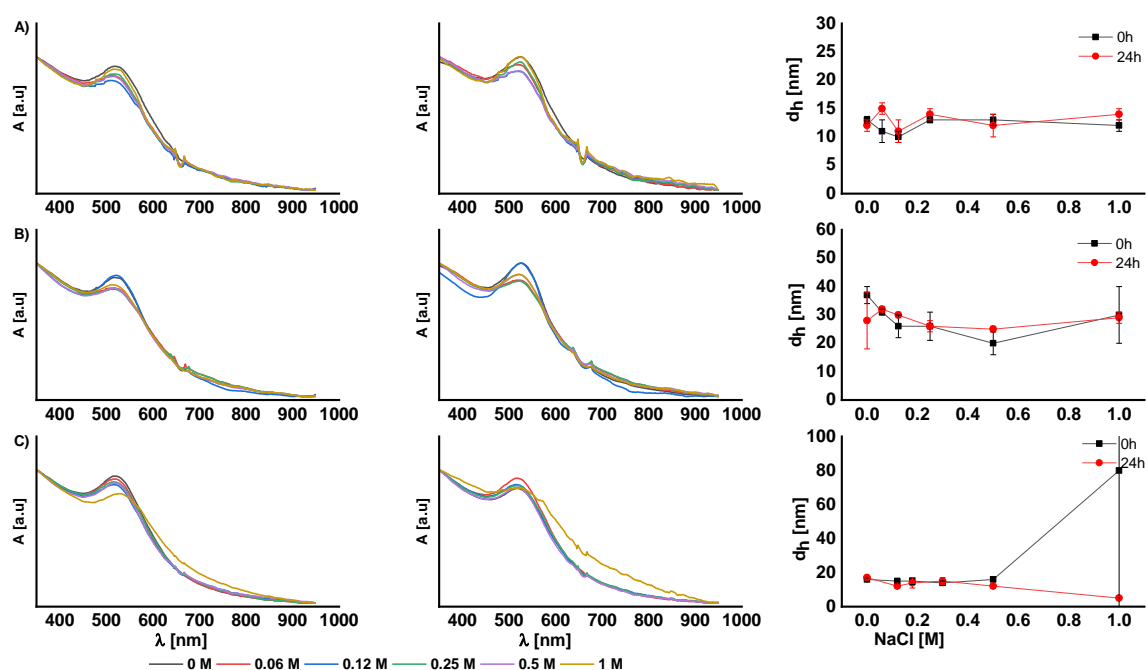


Figure 3-20 Colloidal stability of the 4 nm Au NPs. Absorption Spectra at 0 h and 24 h (left, middle panel), and DLS results of Stability test in NaCl media for 4 nm Au-NPs coated by A) SBL, B) PT, and C) PH.

UV-Vis spectroscopy and dynamic light scattering (DLS) techniques were used to evaluate the colloidal stability of the coated gold nanoparticles, as known for the metallic nanoparticles as Au, they have a characteristic surface plasmon peak, which is related to their size, shape, and local environment. Understanding the optical properties of gold nanoparticles is depending on not only the shape, composition, and size of the nanoparticles, but also we need to consider the local environment. This local environment includes the solvent effect and the interaction between the nanoparticles themselves. When two different nanoparticles come closer, their electromagnetic field interacts and results in more complex local surface plasmon resonance (LSPR). The LSPR of aggregated NPs is shifted toward lower energy, which means a longer wavelength (red-shifted). Based on that, by taking the

absorbance spectrum of the gold nanoparticles we can evaluate the aggregation degree of the sample, based on their absorbance at the longer wavelength side. (Ivanov et al., 2009, Phan, Haes, 2019, Sakura et al., 2005, Stark, 2011)

As shown in Figure 3-16, the absorption spectra of the 17 nm gold nanoparticles at 0 h and 24 h, have no significant absorption at the longer wavelength side and almost the same width of the plasmon peak, which is characteristic for Au-NPs. This is further supported as shown in Figure 3-17, where we have plotted the average of the absorption within the range of 600 to 650 nm versus different concentrations of the salt. As shown we only observe a slight increase in the absorption value after 24h incubation time, and this was clear for the PT(+), PTL(+), and SB(+/-) polymer samples. This simply indicates that no significant agglomeration or aggregation is happening for the nanoparticles. The result is further supported by measuring the hydrodynamic radius of the nanoparticles using DLS, as shown in Figure 3-16. There is no significant increase in the size of the nanoparticles after incubation with the NaCl for all the concentration series used in the present work. Overall, the coating of the 17 nm Au NPs using the current amphiphilic polymer library was successful in preserving the gold nanoparticles' dispersity and it was stable against harsh conditions as NaCl. This stability test was highly important for the nanoparticles, particularly for the next bio-applications. As reported, the nanoparticles will suffer from a complex environment, which includes macromolecules and physiological salt levels. (Hühn et al., 2016)

While, Figure 3-18 shows the absorption spectra at 0h and 24h for the 17 nm gold nanoparticles coated with PMA and PMAL polymer. The absorption spectra showed less absorption for both samples but had the same width of the plasmon peak, while their DLS results are fluctuating with no specific trend of size agglomeration. This is further supported by showing their average absorption value at a longer wavelength as shown in Figure 3-19, for both samples we observe no significant increase in their absorption at lower energy. In Figure 3-20, the colloidal stability of the 4 nm coated gold NPs is shown including both the absorption spectra and the hydrodynamic radius measured by DLS at 0h and 24h. The coated NPs showed a higher degree of stability against the different concentrations of NaCl, which is clear from their DLS and UV-Vis spectra. However, at the highest concentration point that has been used the negative Au NPs showed less stability, as the size tremendously increased at 0h point and it is clear from their significant absorption at a lower energy of their UV-Vis spectrum, which is supported by a higher increase in their absorption value as shown in Figure 3-17.

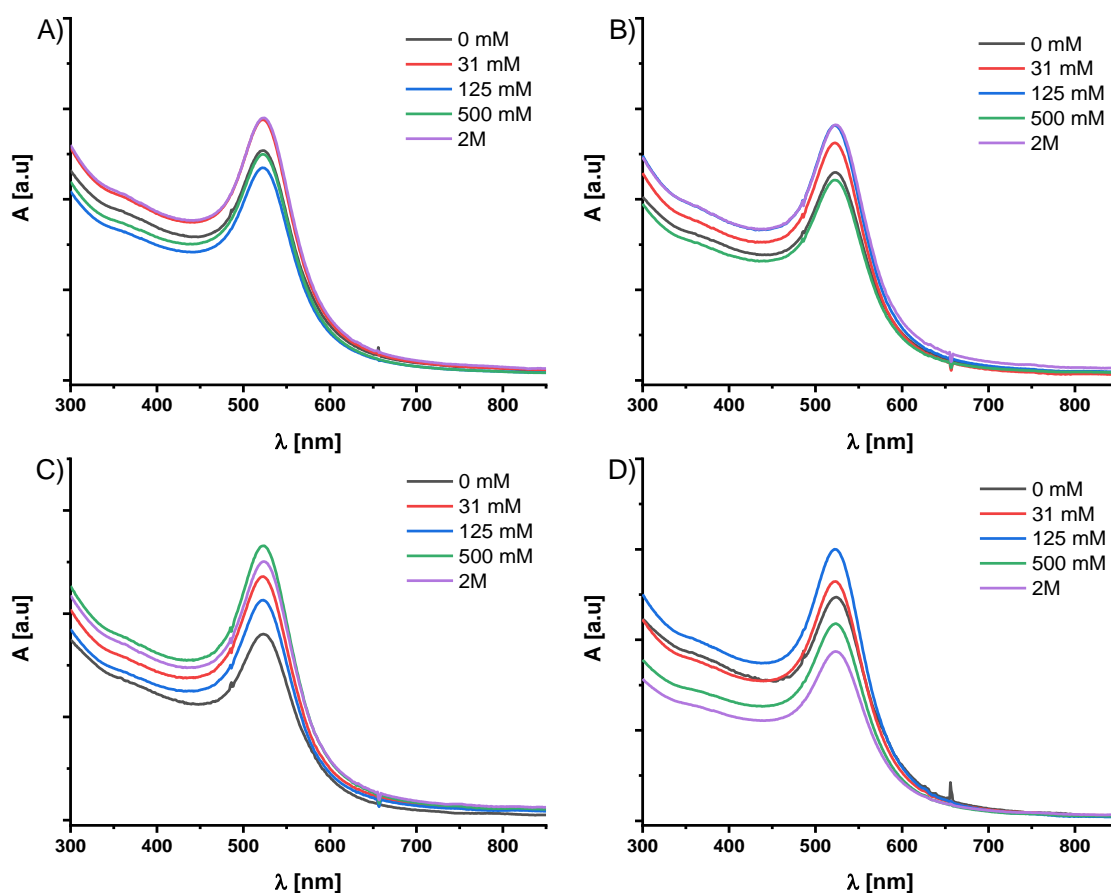


Figure 3-21 Colloidal stability of the Au-PMA as a function of time. Colloidal stability as investigated by UV-Vis spectra of the 17 nm Au-PMA against different concentrations of NaCl at A) 0 h, B) 24 h, C) 48 h, and D) 72 h.

In addition to that, we have studied the colloidal stability of the 17 nm Au-PMA NPs versus NaCl with time series. As shown in Figure 3-21 the UV-Vis spectrum of the Au-PMA NPs was measured at four different time points 0 h, 24 h, 48 h, and 72 h. The LSPR peak and the absorption at lower energy are good indicators to evaluate the stability of the gold nanoparticles. As we can see, the SPR peak position is on the same position with no significant shift with time and there is no significant absorption at the lower energy side. While the SPR peak intensity decreased with time indicating less stability of the nanoparticles at such conditions.

To conclude this part, the prepared polymer-coated nanoparticles exhibit good colloidal stability in harsh conditions such as the ionic strength media, which may indicate acceptable colloidal stability in the biological medium as well. The stability degree could vary from sample to sample, but the overall conclusion is this library of polymers showed good resistance to salt-induced aggregation. However, colloidal stability is a finite process and time is an important factor to consider when we are commenting on the stability of the nanoparticles under salt conditions. We have here tested our samples within the time window we are planning to use for further experiments.

3.5 Dynamical Interfacial Tension

The interactions between nanoparticles and proteins are one of the most important factors when we are studying potential candidates for nano-bio-applications. The process of protein adsorption onto the nanoparticles is a complex process, driven by many factors and forces, which include the nanoparticles features; like size, shape, and surface chemistry, and the thermodynamic forces; as electrostatic attraction, hydrogen bonding, van der Waal forces, and the hydrophobic interactions, among other forces. (Feliu et al., 2016, Kharazian et al., 2016, Lck et al., 1998, Mahmoudi et al., 2016, Mishra, Das, 2019)

The hydrophilicity of the nanoparticles is one of the major factors that determine the interactions of the nanoparticles with proteins and subsequently their cellular interactions. The nanoparticles with a more hydrophilic surface tend to reduce the protein adsorption and therefore inhibit their uptake by the mononuclear phagocyte system (MPS). It has also been reported that the hydrophobicity of the nanoparticles induces an immune response in both conditions, in vivo and in vitro, and the surface modification of the NPs towards a more hydrophilic surface reduces their protein adsorption and helps in improving their blood circulation. (Gao, Yang, 2014, Moyano et al., 2012, Qiao et al., 2020)

Therefore, deep understanding and full physicochemical characterization of the NPs leads us to predict or to expect their fate at the nano-bio interface. To assess the contribution of the hydrophobic forces, we have studied the hydrophilicity/hydrophobicity nature of the nanoparticles. This has been achieved by using the pendant drop methods as described elsewhere ([more details about the methods are in the method chapter](#)). (Del Pino et al., 2016, Du et al., 2019, Gao, Yang, 2014, Rana et al., 2012) We have studied the interfacial tension dynamics with time for the Au-NPs and the QDs, and the results as recorded are shown in [Figure 3-22](#) and [Figure 3-23](#).

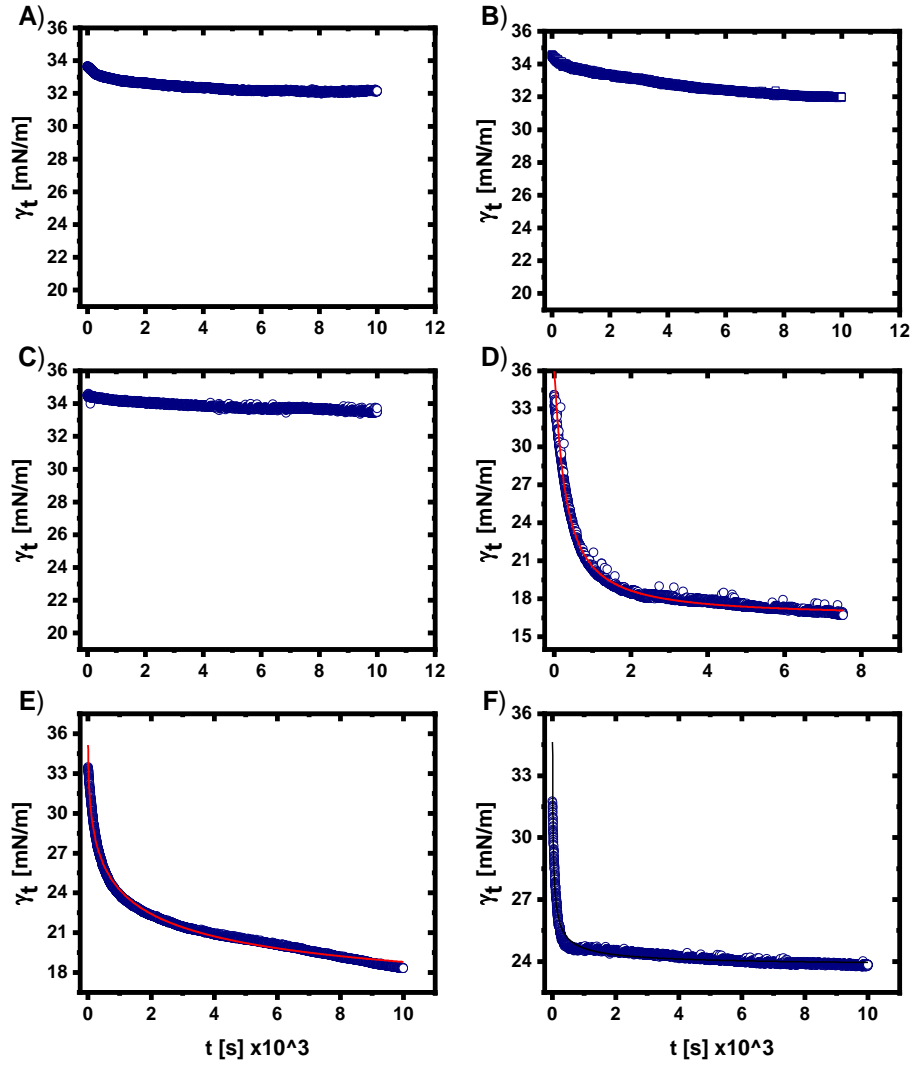


Figure 3-22 Dynamical interfacial tension of QDs. IFT of QDs coated with a) PMA (-), b) PH (-), c) PT (+), d) PC (+/-), e) PMAL (+/-), and f) SB (+/-) as measured by DSA. The red line represents the fitting by Hua and Rosen equation.

Table 3-5 Dynamic interfacial tension parameters of the QDs. Where γ_m is the meso-equilibrium interfacial tension, t_h is the half-life time to reach this value, n is a constant related to the hydrophobicity, v_{max} is the decay rate of the interfacial tension, and γ_{eq} is the equivalent value of the interfacial tension at the last time point of measurements.

Sample	γ_m [mN/m]	t_h [s]	n	v_{max} [mN/ms] *10 ⁻³	γ_{eq} [mN/m]
Q-PH (-)	----	----	----	-----	32.3±0.4
Q-PMA (-)	----	----	----	-----	32.3±0.5
Q-PT (+)	----	----	----	-----	33.6±0.1
Q-PC (+/-)	16.5±0.01	295±0.5	1.1±0.003	18	16.2±0.7
Q-PMAL (+/-)	12.2±1.5	593±182	0.5±0.03	5±1.7	16.8±1.3
Q-SB (+/-)	24±0.5	19.4±4	0.55±0.07	85.4±4	24.3±0.7

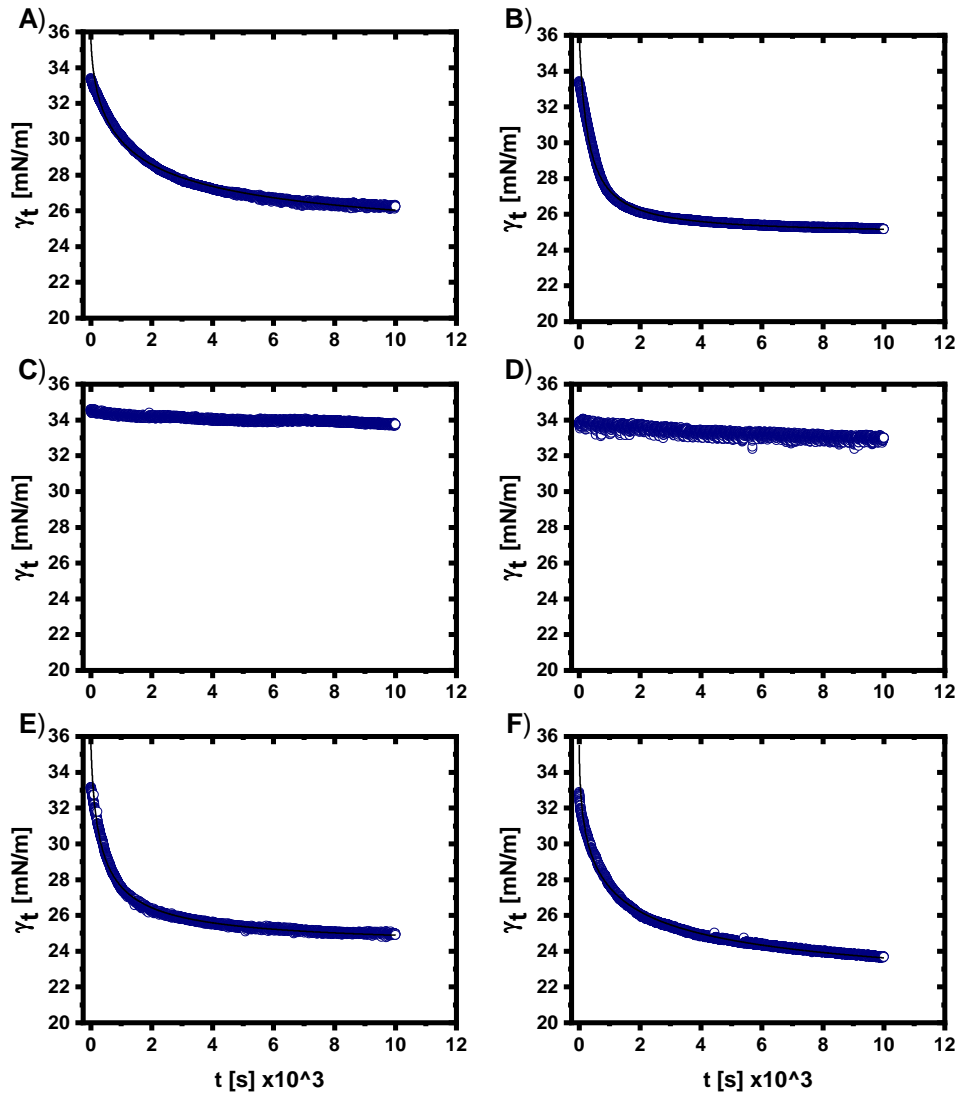


Figure 3-23 Dynamical interfacial tension of Au NPs. IFT of Au NPs coated with a) PMA (-), b) PH (-), c) PT (+), d) PTL (+), e) PC (+/-) and f) SBL (+/-) as measured by DSA. The red line represents the fitting by Hua and Rosen equation.

Table 3-6 Dynamical interfacial tension parameters of the Au NPs. Where γ_m is the meso-equilibrium interfacial tension, t_h is the half-life time to reach this value, n is a constant related to the hydrophobicity, v_{max} is the decay rate of the interfacial tension, and γ_{eq} is the equivalent value of the interfacial tension at the last time point of measurements.

Sample	γ_m [mN/m]	t_h [s]	n	v_{max} [mN/ms] * 10^{-3}	γ_{eq} [mN/m]
Au-PMA (-)	23.7±0.3	1513±599	0.6±0.01	1.3±0.5	26.8±0.8
Au-PH (-)	25±0.5	303±25	1±0.07	9.4±0.6	25±0.3
Au-PT (+)	---	---	---	---	32.8±1.3
Au-PTL (+)	---	---	---	---	32.7±0.3
Au-PC (+/-)	23.8±0.3	295±42	0.76±0.03	7.8±1	24.65±0.3
Au-SBL (+/-)	21.3±1.9	794±95	0.5±0.01	2.4±0.3	24±1.1

The results obtained have been fitted to the empirical equation developed by Hua and Rosen; in addition to that, we have calculated the decay rate of the interfacial tension as described in the method section. (Hua, Rosen, 1988, Rana et al., 2012) Out of the fitting process, we will have quantitative parameters that have been used to evaluate the hydrophilicity of the nanoparticles.

$$\gamma_t = \gamma_m + \frac{\gamma_o - \gamma_m}{1 + \left(\frac{t}{t_h}\right)^n} \quad (3-14)$$

Where, γ_m is the meso-equilibrium interfacial tension as defined by Rosen; which is below it only small change for the interfacial tension is observed, t_h is the time for the interfacial tension to reach one half of the difference between γ_o and γ_m in other words, we can say it is the half-life time to reach the meso-equilibrium value, n is a constant related to the hydrophobicity of the nanoparticles; higher n means a higher degree of hydrophobicity, v_{max} is the decay rate of the interfacial tension, and γ_{eq} is the equivalent value of the interfacial tension; the value at the last time point of acquisition. (Choi, Montemagno, 2013, Gao, Yang, 2014, Rana et al., 2012, Rotureau et al., 2004)

Table 3-5 and Table 3-6 show the fitting results of the QDs and the Au-NPs, respectively. Basically, a higher value of γ_m or γ_{eq} means higher degree of hydrophilicity and vice versa. Nevertheless, relying only on these values will not be sufficient to describe the behavior of the nanoparticles. Indeed, other factors that have been listed in the tables are also needed to describe the whole picture of the nanoparticles.

Starting from here, as shown in Table 3-5 the negative and the positive QDs have no significant decay of their interfacial tension, this means a higher degree of hydrophilicity if we compare it to the other QDs. QDs coated with zwitterionic polymers showed different kinetics, for example, Q-SB showed higher γ_m and γ_{eq} value than Q-PC and Q-PMAL. However, they showed the shortest time required to reach their equilibrium, which means less energetic barrier than Q-PC and Q-PMAL. This discrepancy makes it more difficult to conclude which QDs are more hydrophilic than the other QDs.

While for the larger size of Au-NPs, only the positive samples showed linear profiles for the interfacial tension regardless of the difference in their molecular weight. Meanwhile, the negative and the zwitterionic nanoparticles almost agreed in their γ_m and γ_{eq} , but having different dynamics as illustrated by the t_h and the v_{max} .

The charge and the molecular weight of the polymer have no effect here on their hydrophilic properties, as reported before for the linear polymer by increasing the Mw they obtain a more

hydrophobic character. While here, for example, the Au NPs coated with the same polymer (PT and PTL) but at two different sizes, both of them showed the same hydrophilic properties. (Du et al., 2019)

This in turn leads us to conclude that the zwitterionic polymers may show less degree in their hydrophilicity than the positive and the negative ones as observed by the QDs. While in the case of the Au-NPs, they share almost the same degree of hydrophilicity with the negative polymers. This fluctuation of interfacial tension could be the result of using two different cores with different sizes or the difference in their grafting density onto the nanoparticles. Concluding that the charge and the size of the polymer have no significant effect or trend on their hydrophilic properties and the difference in the hydrophilicity of these coated NPs is not significant to be considered in their further interactions. This will be discussed in the next sections.

3.6 Protein Adsorption study using Fluorescence Correlation Spectroscopy

Biomedical application of the nanoparticles faced many challenges, starting from the fabrication of the suitable nanomaterial with specific surface chemistry; which is sometimes called 'the chemical identity', to their stability in different conditions and environments, and finally their fate and interactions at the nano-bio interface. It seems a long journey from the chemistry lab to the patient's arm, well-characterized materials, and intense experiments must be executed to evaluate and to decide whether this nano-candidate is applicable and suitable for clinical studies or not. (Galdino et al., 2019, Ke et al., 2017, Mahmoudi et al., 2016)

One step in this journey, that we are trying to focus on it and discuss in this section, is the nanoparticles' interactions with proteins. It has been well reported the biomolecules in the biological milieu will decorate or adsorb on the surface of the nanoparticles, forming what is called now 'Biomolecular or Protein corona' as we have already introduced in the introduction part. This corona layer influences the efficacy of the nano-vector, by shielding its targeting agent or inducing agglomeration that facilitated the identification of the NPs by the immune system and shortens the blood circulation of the nanoparticles. On the other hand, the corona formation could be used to enhance the delivery of the nanoparticles by manipulating the corona composition, which facilitates the targeting by choosing specific proteins that occupy the corona layer. (Feliu et al., 2016, Pattipeiluhu et al., 2020, Rampado et al., 2020, Safavi-Sohi et al., 2016, Shang et al., 2014)

Because the surface of the nanoparticles is the first thing exposed to the biological media, it attracts more attention to understand how the modification of the surface chemistry of the nanoparticles could influence their protein and cell interactions. In the present work, we are trying to solve part of this question. What will happen if we use different surface chemistry, to be more precise, to decorate the surface of the nanoparticles using different surface charges while keeping the same chemistry? This we have achieved by simply encapsulating the NPs using amphiphilic polymers with different charges. This ensures the same surface chemistry has been used to coat the nanoparticles and the only factor that has been changed is the surface charge.

Yielding, differently charged nanoparticles; negative, positive, and zwitterionic nanoparticles. Studying the corona formation onto the nanoparticles has been reported elsewhere, using different techniques from DLS to proteomics techniques. (Maffre et al., 2014, Mishra, Das, 2019, Pattipeiluhu et al., 2020) Each method has its challenge and advantage over others, in our work we have tried to study the formation of protein corona onto the nanoparticles (fluorescent NPs) using fluorescence correlation spectroscopy (FCS). This technique helps in measuring the diffusion of the nanoparticles

in situ without affecting their dynamics. The formation of the protein corona on the nanoparticles physically leads to enlarging the hydrodynamic radius of it as described in [Figure 3-24](#). (Cho et al., 2011, Röcker et al., 2009)

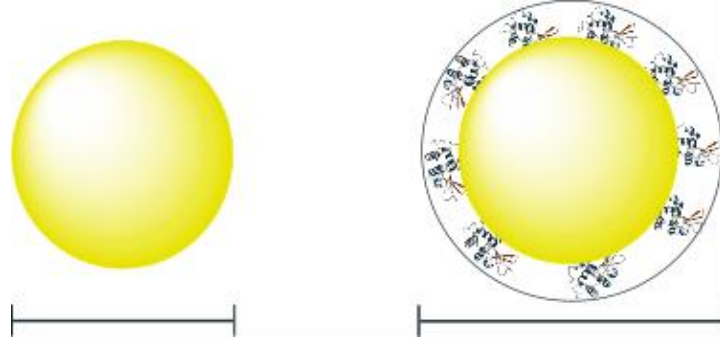


Figure 3-24 Cartoon representation for the effect of the protein corona on the hydrodynamic radius of the nanoparticles.

Thus leading to a different diffusion coefficient of the NPs before and after the corona formation. By precisely measuring the change in the diffusion coefficient of the NPs with different protein concentrations, we can deduce the change in their hydrodynamic radius ([more details are in the method section](#)). (Ashraf et al., 2016, Carril et al., 2017, Hühn et al., 2013, Maffre et al., 2014, Röcker et al., 2009)

In the following graphs, we are presenting the change of the hydrodynamic radius of the QDs that has been coated with different charged polymers upon incubation with different protein concentrations. Figure 3-25 and Figure 3-26 show the protein adsorption profile of the QDs coated with PMA, PH, PT, and PMAL polymer against HSA and Tf, respectively. While Figure 3-29 and Figure 3-30 show the protein adsorption of the Q-PC and Q-SB, respectively.

The protein adsorption profiles have been fitted according to the following equation: (Röcker et al., 2009)

$$R_h = R_{h(0)} \left(1 + c \cdot \frac{N_{max}}{1 + \left(\frac{K_D}{C_P}\right)^n} \right)^{\frac{1}{3}} \quad (3-15)$$

Where, $R_{h(0)}$ is the hydrodynamic radius of the QDs at no protein, c is the volume ratio of the protein to that of the QDs at no protein as measured by FCS; considering the QDs is a sphere, N_{max} is the maximum number of proteins adsorbed at saturation (i.e. $C_P \gg K_D$), C_P is the concentration of the protein, K_D is the dissociation coefficient, and n is the Hill coefficient.

It has been reported that the surface charge of the NPs plays a significant role in their protein interactions. (Ashraf et al., 2016, Hühn et al., 2013, Maffre et al., 2014) The negative and the positive

charged NPs have different affinity degrees toward interaction with the proteins. As shown in Figure 3-25 and Figure 3-26, the hydrodynamic radius of the negative and the positive QDs are stepwise increased when incubated with different protein concentrations, whether HSA or Tf.

The affinity toward protein adsorption is not the same between the charged QDs. The Q-PT showed the highest degree of affinity toward both proteins as shown in Table 3-7 and Table 3-8. Where its apparent dissociation coefficient (K_D) was 7.5 μM and 35.5 μM against HSA and Tf, respectively.

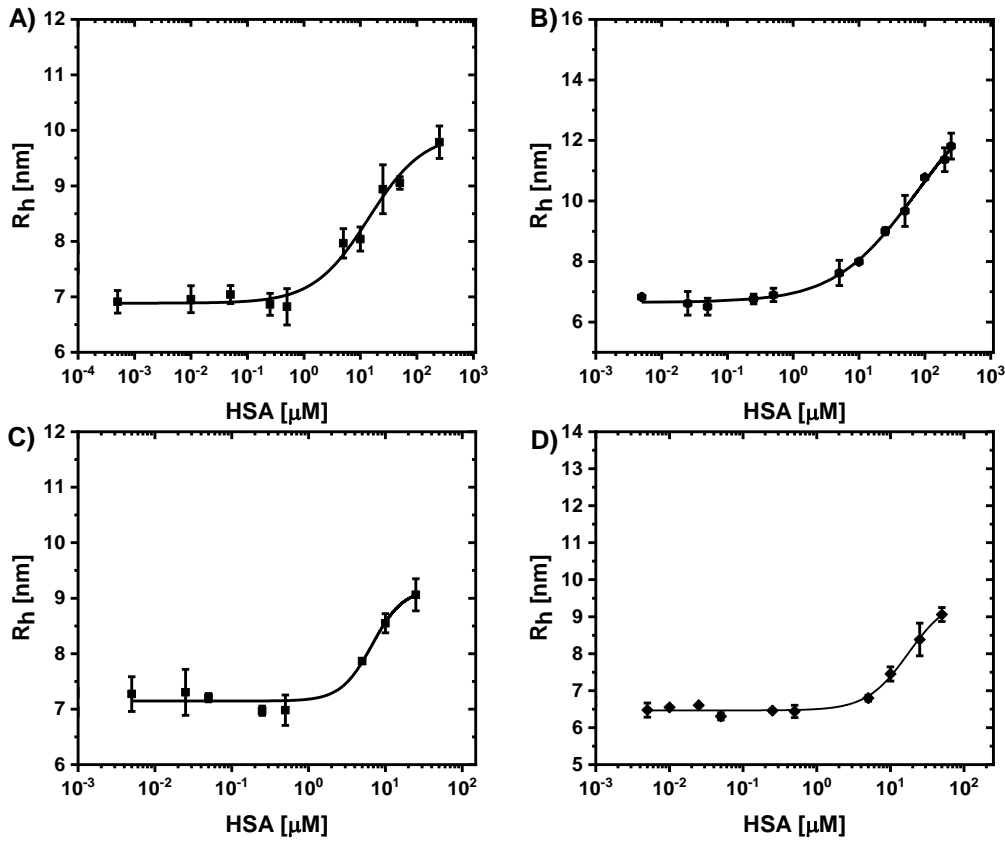


Figure 3-25 HSA protein adsorption onto QDs coated with A) PMA (-), B) PH (-), C) PT (+), and D) PMAL (+/-).

Table 3-7 Fitting parameters of the FCS results against HSA. R_0 is the hydrodynamic radius of the QDs at 0 μM of HSA, K_D is the dissociation coefficient; this measures the affinity degree between the QDs and the protein, $\frac{V_P}{V_{QDs}}$ is the volume ratio of the protein to the QDs, n is Hill coefficient, N_{max} is the maximum number of proteins adsorbed to the surface of the QDs at saturation, and ΔR is the thickness of the corona layer formed around the QDs.

Sample	R_0 [nm]	K_D [μM]	V_P/V_{QDs}	n	N_{max}	ΔR_h [nm]
Q-PMA (-)	6.88±0.09	20.8±8	0.05	0.9±0.2	40.3±7	2.9±0.1
Q-PH (-)	6.6±0.06	183±109	0.076	0.76±0.08	106±26	5±0.08
Q-PT (+)	7.14±0.07	7.5±2	0.067	2±1	16.5±3	1.9±0.07
Q-PMAL (+/-)	6.4±0.04	22±6	0.076	1.5±0.3	29±5	2.6±0.04

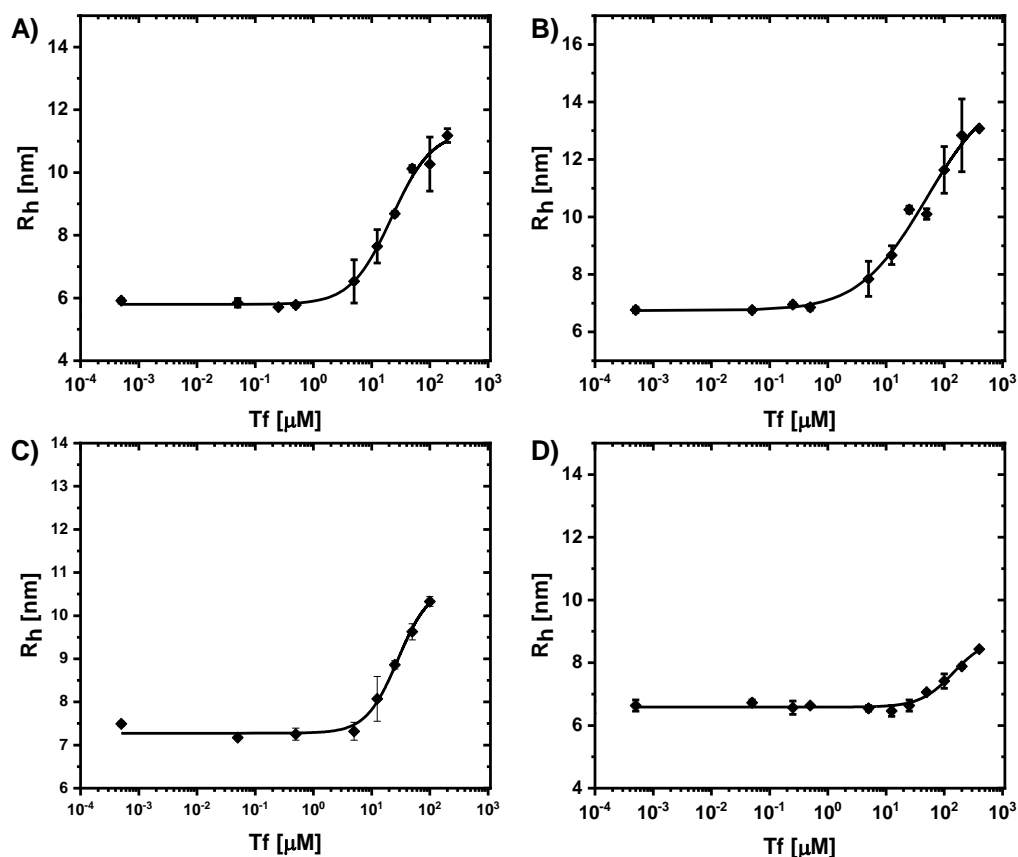


Figure 3-26 Tf protein adsorption onto QDs coated with A) PMA (-), B) PH (-), C) PT (+), and D) PMAL (+/-).

Table 3-8 Fitting parameters of the FCS results against Tf. R_0 is the hydrodynamic radius of the QDs at 0 μM of Tf, K_D is the dissociation coefficient; this measures the affinity degree between the QDs and the protein, $\frac{V_P}{V_{QDs}}$ is the volume ratio of the protein to the QDs, n is Hill coefficient, N_{max} is the maximum number of proteins adsorbed to the surface of the QDs at saturation, and ΔR is the thickness of the corona layer formed around the QDs.

Sample	R_0 [nm]	K_D [μM]	V_P/V_{QDs}	n	N_{max}	ΔR_h [nm]
Q-PMA (-)	5.79 ± 0.1	35.6 ± 7	0.38	1.33 ± 0.2	16.9 ± 2	5.2 ± 0.2
Q-PH (-)	6.7 ± 0.2	115 ± 85	0.233	0.8 ± 0.2	38 ± 12	6.5 ± 0.23
Q-PT (+)	7.27 ± 0.08	35.5 ± 9	0.197	1.6 ± 0.3	10.9 ± 2	3 ± 0.08
Q-PMAL (+/-)	6.5 ± 0.04	172 ± 66	0.248	1.5 ± 0.4	5.5 ± 1.4	1.9 ± 0.05

This higher affinity of the proteins towards the positive QDs is expected as both proteins are considered negative proteins (net charge) as illustrated from their electrostatic distribution in Figure 3-28. In both protein cases the Hill coefficient $n > 1$, indicates a cooperative binding, which means proteins that already adsorbed onto the QDs surface facilitate the further adsorption of proteins to the remaining vacant sites. Such results agree with previous work carried out on positively charged NPs, where Maffre and co-workers have studied the protein corona formation onto the QDs modified by cysteamine using FCS, which results in Hill coefficient $n = 1.5 \pm 0.4$, with the highest affinity toward

HSA in comparison to the negatively-charged QDs that have been studied in the same work. (Maffre et al., 2014) In contrast, Hühn and co-workers have studied the effect of surface charge on the protein corona formation using FCS by using polymer-coated Au NPs functionalized with a fluorophore. Based on their fitting results of the adsorption profile, the binding dynamics of the HSA to both different-charged NPs has the same adsorption cooperativity with Hill coefficient $n = 0.8 \pm 0.3$, while agreeing with our results in terms of higher affinity of the HSA to the positively-charged NPs than negatively-charged NPs. (Hühn et al., 2013) As a consequence of this higher affinity, we have observed a thinner protein layer than expected for both proteins, HSA expected to have a layer with around 3 nm in thickness while Tf expected to have a layer with 7 nm in thickness, based on an assumption with which face they are going to adsorb onto the NPs. It is worth to mention, that the presented results before we observe any significant agglomeration to the NPs upon incubation with different proteins. (Moustaoui et al., 2019)

On the other hand, the negative QDs - Q-PMA and Q-PH - have a lower affinity toward both proteins compared to Q-PT. This is clear from their K_D against both proteins, for example in the case of the HSA, the K_D of the Q-PMA is 21 μM while that of Q-PH is 183 μM . Which is less in affinity by 3-fold for the Q-PMA and by 25-fold for the Q-PH compared to the positive QDs, Q-PT. Moreover, their protein corona thickness was almost corresponding to a monolayer formation, with a slight deviation lower or higher than the expected thickness, which could be related to other factors as a different conformational change of the proteins or the existence of the protein molecules in between the polymer brushes on the surface of the NPs. As the affinity of the adsorption of protein to the QDs is a function of many variables, we can not consider these values as absolute values. That's why we can not compare the K_D and N_{max} values to previously reported results as we compare the dynamics of the adsorption represented by the Hill coefficient.

In addition to having different affinity degree between different proteins, there is also different dynamics of the adsorption process. For example, Q-PMA does not only have a different affinity towards both proteins; by having different K_D values but also it has different dynamics; by having the Hill coefficient $n > 1$ in the case of Tf and $n < 1$ in the case of the HSA. This has been supported by others who studied the HSA adsorption onto negatively-charged NPs, showing anti-cooperative binding of the HSA to the NP's surface. (Ashraf et al., 2016, Hühn et al., 2013, Maffre et al., 2011, Maffre et al., 2014, Shang, Nienhaus, 2017) It should be noted that the negative charge of the proteins is a net surface charge based on the protein batches, meanwhile, these proteins have positive batches on their surface, which are assumed to adsorb onto the negative NPs via these sites, as illustrated with the blue color in their surface electrostatic distribution in Figure 3-28.

Apart from this, we have calculated the required number of proteins to saturate the surface of the QDs based on the surface area of the protein face that is assumed to be adsorbed via it onto the QDs and the surface area of the QDs itself. Assuming the HSA will adsorb with its equilateral triangle surface of 8 nm per each side and the Tf adsorb with its approximately rectangle surface with sides 8.4 nm and 5 nm.

This finally results in around 21 HSA and 12 Tf molecules are at least required to saturate the surface of the QDs, these values are the average of each sample. We have graphically plotted these values as guidelines with the obtained results from the fitting as shown in Figure 3-27. Obviously, the formed protein corona is in good agreement with the monolayer assumption as illustrated with the blue dotted line on the graph. The number of proteins required to saturate the surface theoretically is nearly fulfilled by the negative QDs in both cases, as illustrated by the red dotted line. Conversely, this is not achieved in the case of the positive QDs for both proteins and the Q-PMAL in the case of the Tf protein. This is directly related to their protein corona thickness; a thinner layer means fewer proteins on the surface. It is worth mentioning here that the results obtained were in the window where the QDs are stable and there is no significant agglomeration observed.

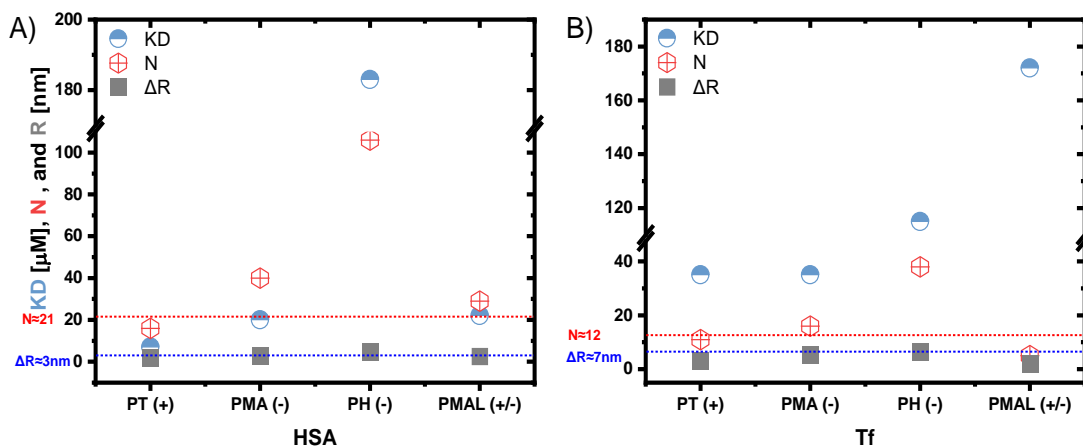


Figure 3-27 Overview of the adsorption parameters of the QDs against A) HSA, and B) Tf protein. K_D is the apparent dissociation coefficient, N is the maximum number of proteins adsorbed to the QDs, and R is the thickness of the monolayer as obtained from the fitting. The red dotted line corresponds to the calculated maximum number that saturates the surface of the QDs and the blue dotted line represents the expected thickness of the monolayer for each protein.

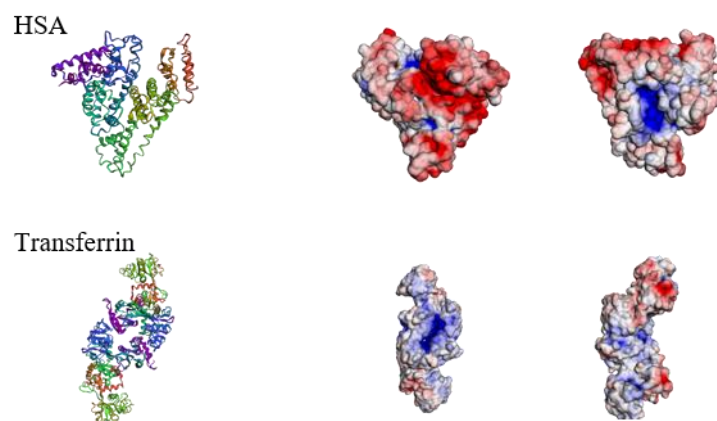


Figure 3-28 Surface electrostatic distribution of HSA and Tf proteins. Left column: cartoon representation of HSA (PDB code 1UOR), and Tf (PDB code 2HAU). Right column: surface electrostatic calculated online via (<https://server.poissonboltzmann.org/pdb2pqr>) potential range ± 5 KBT/e at pH 7.4. The potential is represented in gradual color increasing from dark blue (most positive) to light blue, white, light red to dark red (most negative).

Protein adsorption on the zwitterionic surface

The zwitterionic surfaces are well known for their anti-fouling properties, making them a good choice of surface modification for many applications; including the bio-applications. The property of having the two charges, positive and negative, on the same pendant group helps in minimizing the interactions of these moieties with the surroundings and preferred their binding interactions. In addition to the formation of a strong hydration layer that works as an energetic barrier and enhances the anti-fouling properties of the zwitterionic surface. Whereas this anti-fouling property is highly dependent on the zwitterionic structure; the position of the negative and the positive moieties on the pendant group. (Baggerman et al., 2019, Rampado et al., 2020, Schlenoff, 2014, Wu et al., 2019)

To illustrate this point, we have studied the PMAL, PC, and SB polymers; as shown in [Figure 3-1](#) they have different structures, particularly the PMAL, while the PC and SB have only different charged groups. Do we expect a difference between these structures? Can this affect their protein or cell interactions?. To have an answer to these questions, we have studied the protein adsorption using FCS and the cell interactions of these polymers as described in the following section.

[Figure 3-25d](#) and [Figure 3-26d](#) show the protein adsorption profile of the Q-PMAL against HSA and Tf, respectively. While [Figure 3-29](#) and [Figure 3-30](#) show the protein adsorption profiles of the Q-PC and Q-SB, respectively. It is clear from these protein adsorption results that the Q-PMAL has a higher affinity toward both proteins, with K_D of 22 μM in case of HSA and K_D of 172 μM in case of Tf. Showing higher affinity toward the HSA by 8-fold than that against Tf. This higher affinity could affect their cell interactions, which we will discuss in the cell uptake and biocompatibility section.

On the other hand, Q-PC and Q-SB showed a suppression of the protein corona layer against both proteins. Regardless, of the difference in their charged groups the anti-fouling property was retained and an almost linear profile of their hydrodynamic radius is observed. This indeed agrees with others who worked on zwitterionic and similar structures. (Ashraf et al., 2016, Debayle et al., 2019) Moreover, the affinity of the Q-PMAL towards proteins agrees with others, supporting our results on such polymer structures. Where Koc and coworkers have studied the protein adsorption of different polyzwitterionic materials, these zwitterionic materials have different structures; linear and non-linear (in their work they refer to the non-linear as Y-shaped). They have found that there is a significant difference in the protein suppression of the linear to the non-linear structures, revealing that not only the grafting density of the zwitterionic moieties defines their anti-fouling behavior but also the precise nature as well as the orientation of the zwitterionic moieties. (Koc et al., 2019, Laschewsky, Rosenhahn, 2019, Maffre et al., 2014) Further supporting this hypothesis, we have studied the protein adsorption of the Q-EDLF as shown in [Figure 3-31](#), where EDLF is Edelfosine, an anticancer drug.

EDLF structure is similar to that of the SB and PC, where the charge groups are located on the same pendant group. Because the EDLF is a small ligand, their hydrodynamic radius was smaller than that of the polymer-coated QDs. This in turn did not influence their anti-fouling property as shown, the Q-EDLF suppresses the protein corona formation against Tf and HSA. Concluding that the structure of the zwitterionic surface is highly crucial in their protein interactions and as a consequence their cell interactions.

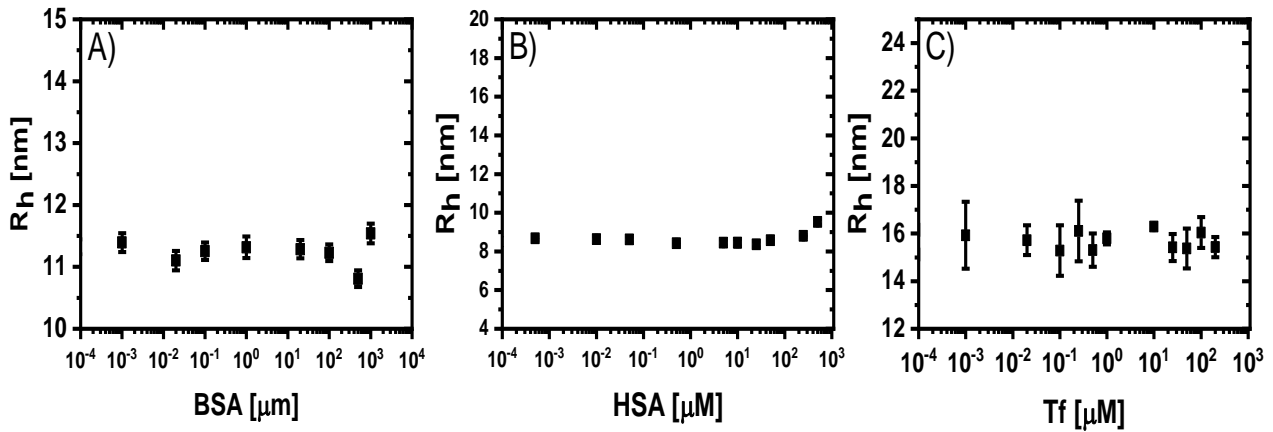


Figure 3-29 Protein adsorption profile by FCS of QDs coated with PC (+/-) against A) BSA, B) HSA, and C) Tf.

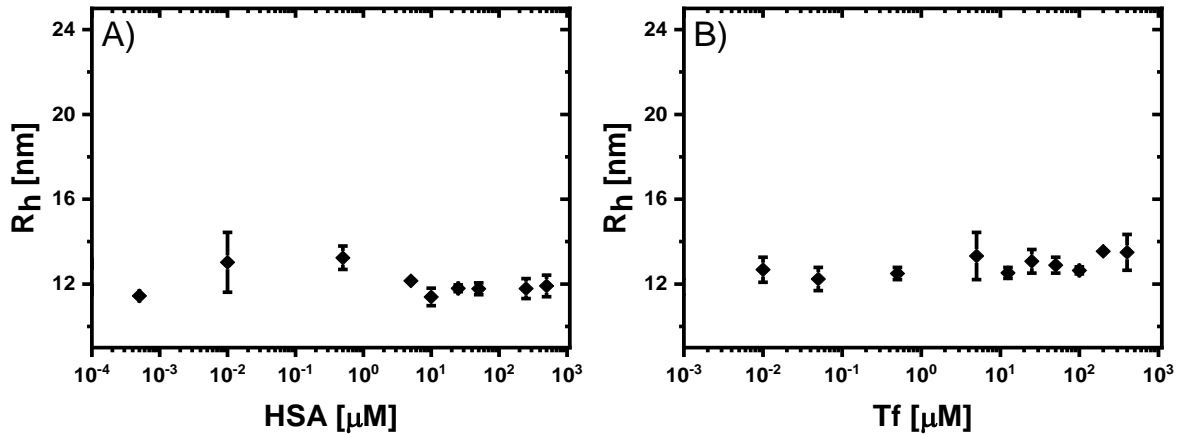


Figure 3-30 Protein adsorption profile by FCS of QDs coated with SB (+/-) against A) HSA, and B) Tf.

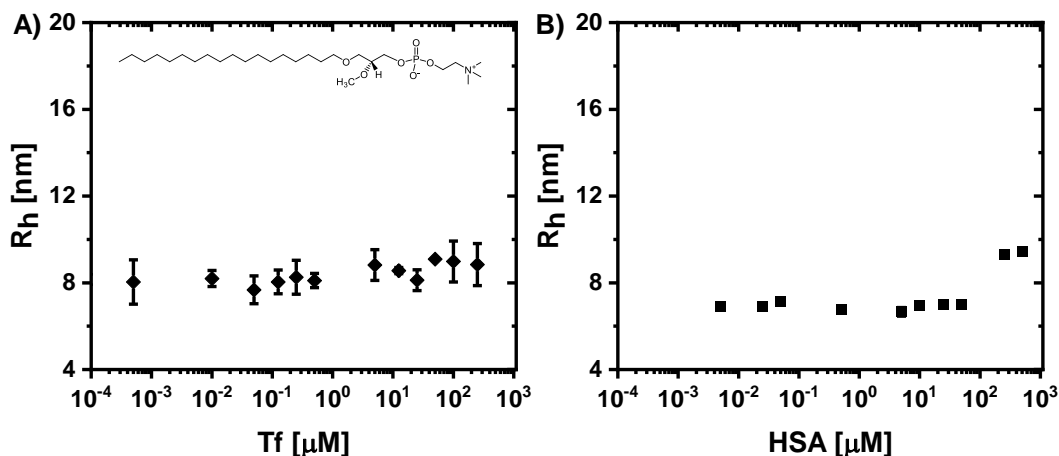


Figure 3-31 Protein adsorption profile by FCS of QDs coated with EDLf against A) Tf and B) HSA protein. EDLf structure is inserted in the Tf graph.

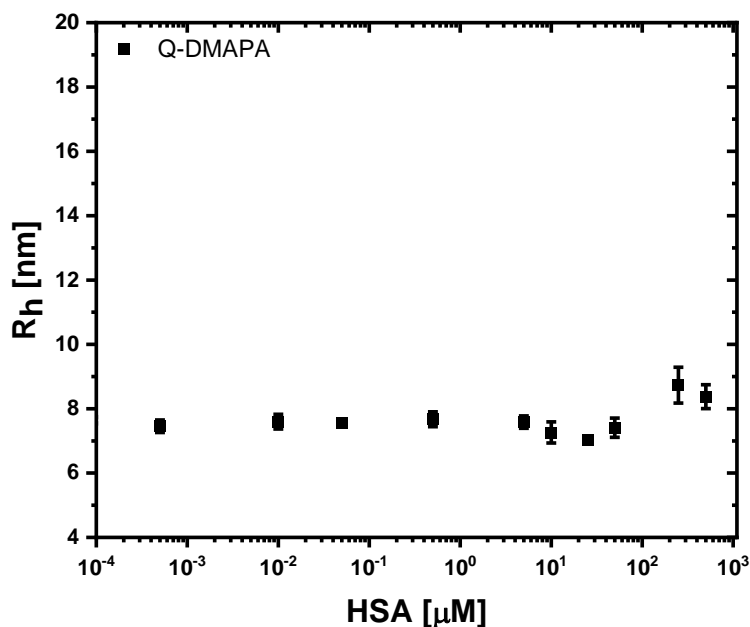


Figure 3-32 Protein adsorption profile by FCS of QDs coated with PMA-DDA-DMAPA against HSA.

At the same time to further understand the effect of the zwitterionic groups' orientation on the protein adsorption, we have tried to mimic the structure (Y-shape) of the PMAL polymer by adding DMAPA ligand to the PMA polymer. The only difference here is the charge distribution, in the case of PMAL, the positive to the negative charge is 50:50, while in PMA-DMAPA polymer this ratio is 75:25. Meaning that the negative charge distribution is much higher than the positive one.

But, this lower ratio of the positive ligand was enough to not affect the stability of the final product and to show a significant impact on their protein and cellular interactions. As shown in Figure 3-32, the protein adsorption profile of the QDs significantly changed compared to that of the PMA. This actually leads us to revise our conclusion regarding the shape or the structure of the zwitterionic

groups as a major factor to determine their anti-fouling properties. With what we have in hand now, not only their structure but the charge distribution could maintain their protein interactions and in consequence their cellular interactions.

Functionalization of the Zwitterionic polymer:

But, what if we functionalize these zwitterionic polymers with a targeting ligand? Does it influence their anti-fouling property? To evaluate that, we have modified the PC (+/-) polymer by the folic acid (FA) molecule, which is reported as a model ligand for an active targeting for most of the cancer cell lines. (Monteiro et al., 2020) Figure 3-33 shows the change in the hydrodynamic radius of the Q-PC-FA QDs against HSA as measured by FCS. As shown the QDs retain their suppression of protein corona formation, indicating that the labeling of the polymer with FA did not influence their anti-fouling property, as observed before by Debayle et al., 2019 (Debayle et al., 2019) and Loiola et al., 2019 (Loiola et al., 2019) in their double functionalization of the surface of the NPs with zwitterionic and charged ligands. Although, the zeta potential of QPC-FA was slightly positive than the Q-PC as shown in Table 3-4, and it was reported by Debayle et al., 2019 (Debayle et al., 2019) that the labeling of the polymers using charged molecules significantly influence their protein suppression, while neutral ligands will not affect their anti-fouling property. Although, the QPC-FA QDs suppressed the protein corona formation of HSA.

To conclude, whereas the IFT measurements showed that the hydrophilicity/hydrophobicity of the polymer-coated NPs is comparable between the different-charged polymers, indicating no significant difference in terms of surface property. The FCS results showed that the protein adsorption of the polymer-coated QDs is a charge-dependent process, where the positively-charged QDs showed the highest affinity toward proteins, in comparison to the negatively- and zwitterionic QDs. Indicating the electrostatic interaction between the NPs and the proteins has a major impact on the protein adsorption process. Revealing the cationic and the anionic surfaces have a significant affinity to the protein adsorption, while the neutral or zwitterionic surfaces (considering the difference in their structure; linear or non-linear) can suppress the protein corona formation, Figure 3-34. This, in turn, helps in avoiding their immunorecognition and to be screened out early from the body, resulting in a more efficient nanovector system to deliver therapeutic or diagnostic materials. In addition to that, when we have functionalized the zwitterionic polymer using active-targeting ligand as folic acid (to be more site-selective), they retain their anti-fouling properties despite being functionalized with a charged-active-targeting ligand.

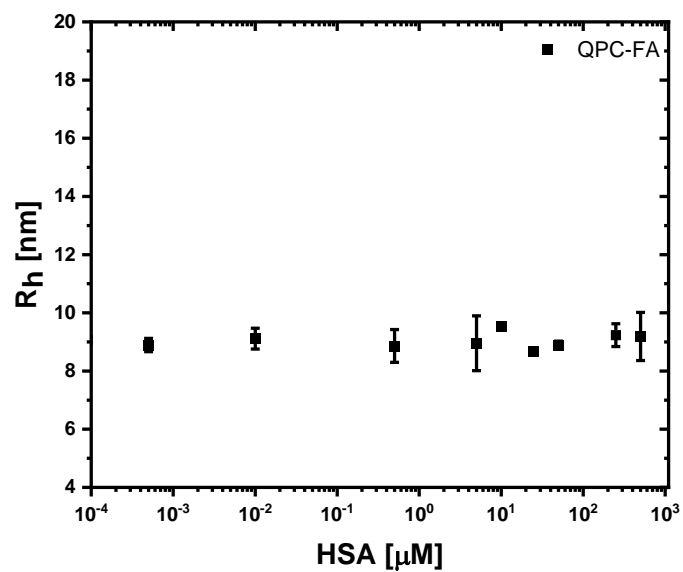


Figure 3-33 HSA adsorption on the QPC-FA QDs as obtained by FCS.

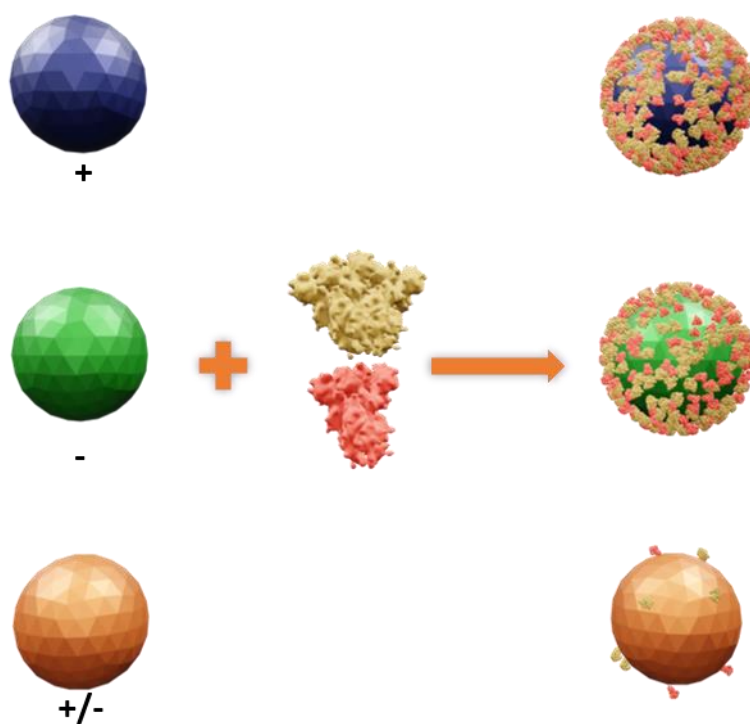


Figure 3-34 Graphic illustrations of the charge-dependent protein adsorption profiles of the NPs.

3.7 Biocompatibility of the Nanoparticles

Prior to performing any cell studies, we have to evaluate the cellular cytotoxicity of the nanoparticles. This has been done against Henrietta lacks cells (Hela), and by using resazurin assay, ([more details are in the methods section](#)). The cellular viability methods are generally categorized into four different categories based on the functionality they are detecting, this includes; the cellular mechanism, apoptotic markers, mitochondrial function, and membrane integrity. Resazurin assay measures the metabolic activity of the mitochondria, by measuring the reduction ability of the cells when the resazurin (non-fluorescent dye) is converted into resorufin (a pink fluorescent dye), Figure 3-35. Where the resazurin is reduced by nicotinamide adenine dinucleotide phosphate (NADH) into resorufin. (Abdelmonem et al., 2015, Ashraf et al., 2016, O'Brien et al., 2000, Soliman et al., 2015)

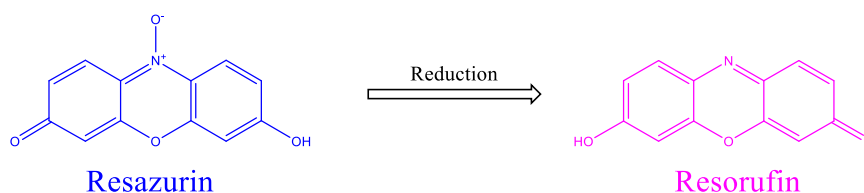


Figure 3-35 Scheme presenting the reduction of the resazurin into resorufin.

The amount of resorufin produced is directly proportional to the living cells and assessed by recording the fluorescence intensity of the resorufin.

This experiment aims to evaluate the cellular toxicity of the coated NPs and guide us to choose the safe concentration for further cellular experiments. We have studied the cytotoxicity of a series of concentrations ranging from 200 to 0.2 nM for the QDs, 40 to 0.07 $\mu\text{g}/\text{ml}$ for the 4 nm Au NPs, and 20 to 0.04 $\mu\text{g}/\text{ml}$ for the 17 nm Au NPs. The concentration of Au NPs was evaluated based on the element concentration as obtained from ICP-MS. Figure 3-36, Figure 3-37, and Figure 3-38 show the viability results of the QDs, the 4 nm Au NPs, and the 17 nm Au NPs, respectively.

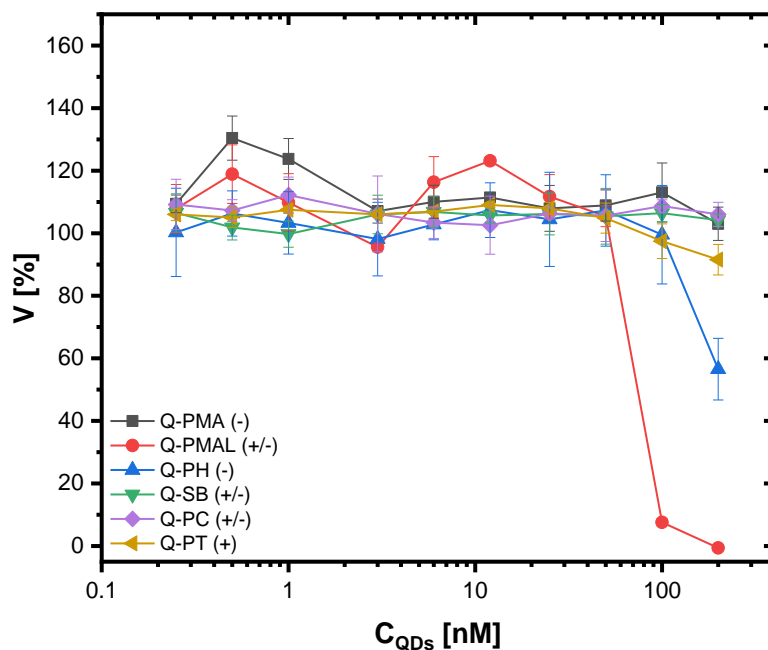


Figure 3-36 Cellular viability (V) of HeLa Cells against different concentrations of QDs, after 24 hours exposure. The data are shown from at least three different independent measurements \pm standard deviation.

As shown, the coated NPs showed a higher degree of biocompatibility over the concentration range we have used in the present work. However, in the case of the QDs, the Q-PH and the Q-PMAL showed higher toxicity levels at the highest concentration points. Thus, we chose from the QDs two different concentration points far from the toxicity range, which is 25 nM and 50 nM for cellular uptake experiments. On the other hand, in the case of the Au NPs, we chose only one concentration point, 10 μ g/ml, for further cell experiments.

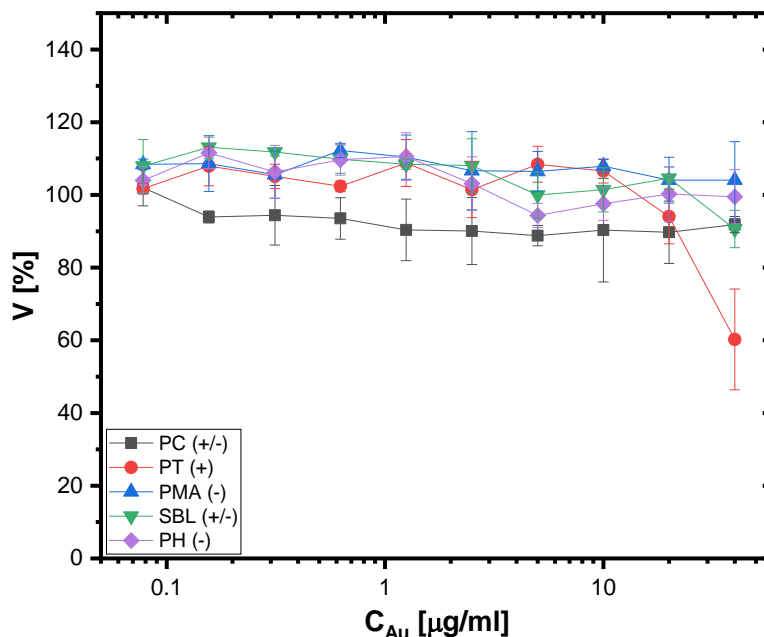


Figure 3-37 Cellular viability (V) of HeLa cells against different concentrations of the 4 nm Au NPs, after 24 h exposure. The data are shown from at least three different independent measurements \pm standard deviation.

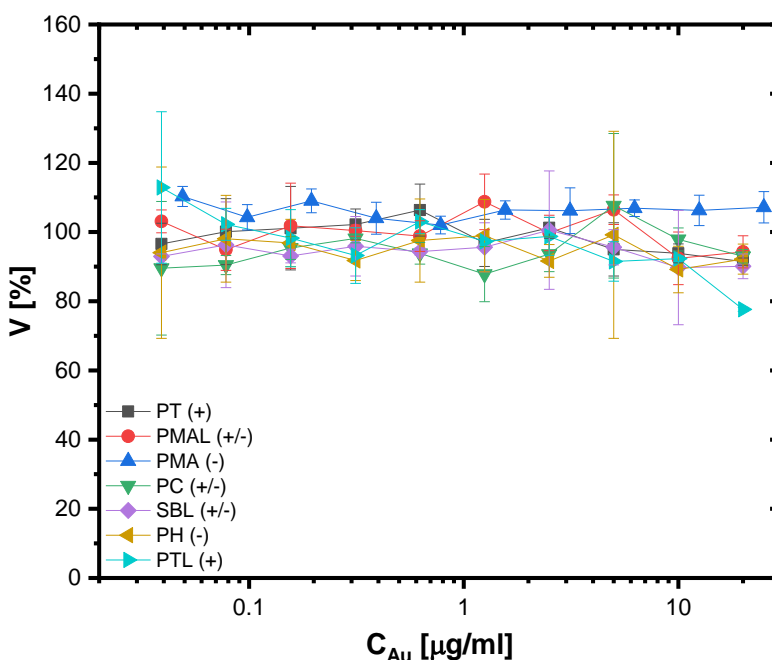


Figure 3-38 Cellular viability (V) of HeLa cells against different concentrations of 17 nm Au NPs, after 24 h exposure. The data are shown from at least three different independent measurements \pm standard deviation.

The polymer-coated Au NPs showed a higher degree of biocompatibility within the concentration range tested. Meanwhile, the positively-charged NPs showed a degree of cytotoxicity at the highest concentration point used in the present work. Such effect of the positively-charged NPs is expected for their faster uptake rate and the highest content, as will be discussed in the next section. (Abdelmonem et al., 2015, Nazarenuş et al., 2014)

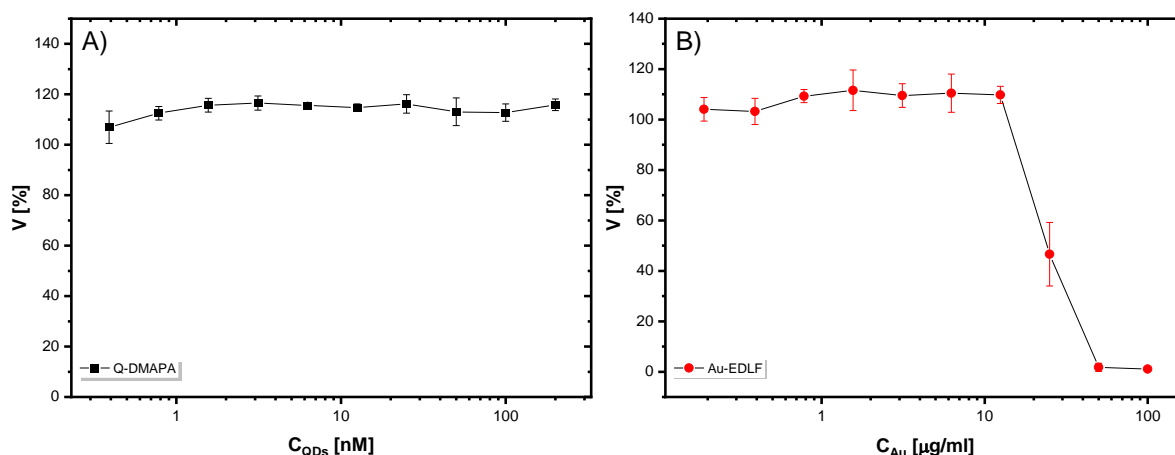


Figure 3-39 Cellular viability (V) of HeLa cells against different concentrations of 17 nm Au NPs and QDs. A) QDs coated by PMA-DMAPA, and B) Au NPs coated with EDLF. The data are shown from at least three different independent measurements \pm standard deviation.

In addition to the main polymer library we have used in the present work, we have also modified the PMA to mimic more the zwitterionic character of the commercial PMAL polymer as we mentioned before to understand more the influence of the charge distribution on the protein and cell interactions.

Therefore, Figure 3-39 shows the viability study of two different cores coated with PMA-DMAPA (QDs), and EDLF ligand (Au NPs). As shown, the conjugation of the PMA with the positive ligand did not affect their biocompatibility and the coated QDs showed almost no degree of toxicity over the concentration range that has been tested. While in the case of the Au NPs (17 nm) coated with EDLF, begins to show a significant degree of toxicity at a concentration higher than 10 µg/ml, to reach a 50% toxicity at 25 µg/ml, to fully toxic at 50 µg/ml. This toxicity profile of the EDLF-coated NPs is simply expected because of the nature of the EDLF ligand as an anticancer drug.

3.8 Cellular uptake of the Nanoparticles

To evaluate the influence of protein adsorption on the cellular interaction of the nanoparticles, we have studied the cellular uptake of Hela cells to the coated NPs. This has been done using different techniques including flow cytometry and inductive-coupled plasma mass spectrometry (ICP-MS) by exposing the cells to different concentrations, at different time points, and with different serum-supplemented mediums conditions. (Ashraf et al., 2016)

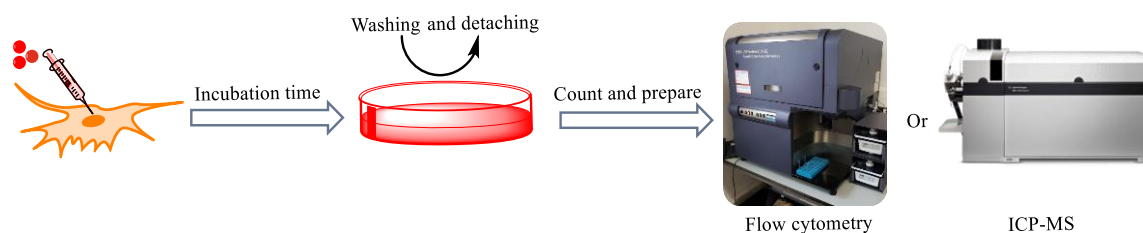


Figure 3-40 Scheme of the cellular uptake and its quantification methods.

3.8.1 Cellular Uptake using Flow Cytometry

The cellular uptake of the coated QDs by Hela cells was evaluated by using the flow cytometry for three different concentrations after 24 h exposure. As shown in Figure 3-41 the uptake was concentration-dependent for all the QDs samples regardless of the coating, which is almost doubled linearly with concentration. It has been reported that the existence of the protein corona onto the NPs transforms its surface charge into negative, regardless of the initial surface charge. (Cho et al., 2011) Herein, we have found that the cellular uptake is charge-dependent, the positive QDs are internalized in a higher amount than the negative and the zwitterionic ones, as reported by others. (Hühn et al., 2013, Mahmoudi et al., 2016, Stark, 2011) Briefly, the positive QDs are 2-fold higher in uptake than the negative QDs, and from 20x to 100x higher than the zwitterionic QDs depending on the concentration. Where, at the lowest concentration the ratio was 20x higher, at 25 nM was 100x higher, and at 50 nM dropped to 70x times higher. This agrees with previous work carried out on different charged NPs and is highly correlated to their corona profile as measured by FCS. The positive QDs, which have the highest affinity to the protein, have the highest uptake, followed by the negative and the zwitterionic QDs. (Ashraf et al., 2016) As it can be seen, the Q-PMAL has a higher uptake profile than the zwitterionic QDs, which is agreed with their protein corona profile as measured by FCS. (Abdelmonem et al., 2015, Hühn et al., 2013, Mahmoudi et al., 2016, Stark, 2011)

To conclude, we have found that there is a relation between the formation of protein corona and the internalization of the NPs by cells. Higher affinity towards the formation of the protein corona, means higher uptake into the cells, regardless of the initial surface charge of the NPs. Although, it has been

reported that the formation of protein corona results in transforming the surface charge of the NPs into negatively charged. (Cho et al., 2011)

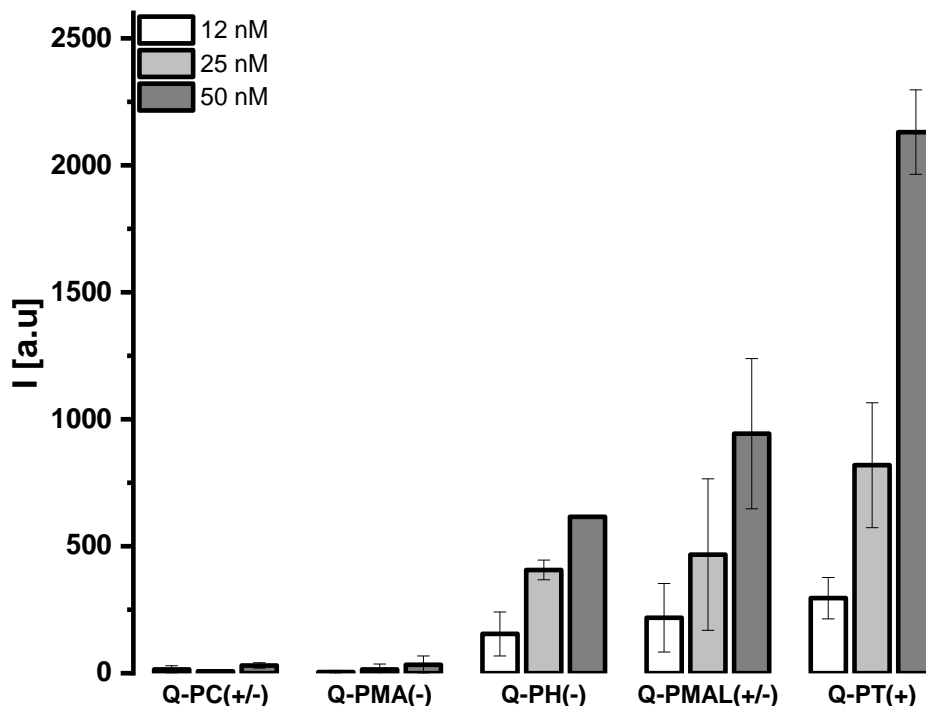


Figure 3-41 Cellular uptake of the QDs as measured by Flow cytometry. Mean fluorescence intensity (background corrected) of the internalized QDs in 10% FBS measured by flow cytometry after 24 h exposure. The data are shown from at least three different independent measurements \pm standard deviation.

3.8.2 Cellular Uptake using ICP-MS

Further supporting the results obtained by the flow cytometry, we have also quantified the cellular uptake of the coated NPs by the ICP-MS. The experiment, according to the protocol described in the method section, was carried out for different cores and sizes. The exposure of the QDs was for two different concentration points, 25 and 50 nM, while for the Au-NPs the exposed concentration was only, 10 $\mu\text{g/ml}$. The exposure time varies among different time points for different serum-supplemented medium conditions.

Figure 3-42 and Figure 3-44 show the uptake results of the 25 and 50 nM of the QDs, respectively as exposed for 6 h and with two different serum conditions. While Figure 3-43 and Figure 3-45 show their QDs content (represented by Cd content) in media after the exposure time. We have worked at this

time point because the QDs were highly toxic in serum-free supplemented medium condition (- FBS) for a longer exposure time.

It can be seen, the internalization amount as determined by ICP-MS shows the same uptake trend that has been observed by flow cytometry, where $QDs_{+ve} > QDs_{-ve} > QDs_{zwitter}$, with the same exception for the Q-PMAL, which is further supporting the results obtained by flow cytometry. The serum condition has also a significant role in the uptake value. In non-serum conditions, the QDs were internalized with a higher amount than in serum-condition. It is worth here mentioning that at the non-serum condition the Q-PT was toxic for the 50 nM concentration point. This is highly related to their higher uptake content, even at this short time point. This agreed with previous studies carried out on different charged NPs. Such faster incorporation kinetics of the positively-charged NPs is already reported elsewhere, and this is based on the fact that the net charge of the outer cell membrane is negative. This, in turn, facilitates the association between the positively-charged NPs with the cell membrane making their internalization process faster than other charged or non-charged NPs. (Abdelmonem et al., 2015, Ashraf et al., 2016, Hühn et al., 2013)

Furthermore, the uptake ratio between the two different conditions (serum or serum-free medium) is varied, meaning that the surface charge has a significant impact on the uptake profile. For instance, the uptake ratio of the Q-SB was almost 2x higher in non-serum to serum-supplemented medium, while for the Q-PT and Q-PH was 13x times and 15x times higher, respectively. This ratio was doubled for the Q-PH but still the same for the Q-SB at the highest concentration point. Revealing, the effect of protein corona on the cellular uptake of the charged QDs. As the current study did not focus more on studying the mechanism of uptake into cells, there is already plenty of research studies that deeply discussed it. So, to briefly discuss what could be the reasons for the higher uptake of the charged NPs and its relation to the protein corona formation, we can simply here refer to two different things. Firstly, the net charge of the cell membrane is reported to be negative, which facilitates the internalization of the positively charged NPs. Secondly, the uptake process of the NPs involved different endocytotic pathways that could vary from one sample to another, and one of these is the clathrin-mediated endocytosis which is facilitated by the Transferrin receptor. According to the FCS results, the coated-NPs have a higher degree of affinity toward the Tf, this, in turn, makes their internalization much faster than NPs that suppress the corona formation. (Chithrani, Chan, 2007, Rennick et al., 2021)

On the other hand, the uptake content of the different charged QDs was also different and vary from one sample to another. For example, the cellular uptake of the Q-PT was on average 40x times higher than that of the zwitterionic QDs, and 15x times higher than the negative QDs at the 25 nM. This ratio

decreased by half in the case of the zwitterionic QDs and by 3x times for the negative QDs at the 50 nM condition. Indicating, the uptake is a charge, concentration, and serum-dependent. Which is related to the different corona profiles of these QDs. The uptake was directly proportional to the affinity towards the protein corona formation. (Ashraf et al., 2016, Behzadi et al., 2017, Fu et al., 2021, Hühn et al., 2013, Safavi-Sohi et al., 2016, Shang et al., 2014, Verma, Stellacci, 2010)

Meanwhile, we have measured the QDs content in the media after the exposure time, as shown in [Figure 3-43](#) and [Figure 3-45](#). Which is clearly correlated to the uptake trend, where $QD_{S+ve} > QD_{S-ve} > QD_{S_{zwi}}$, their media content is $QD_{S_{zwi}} > QD_{S-ve} > QD_{S+ve}$.

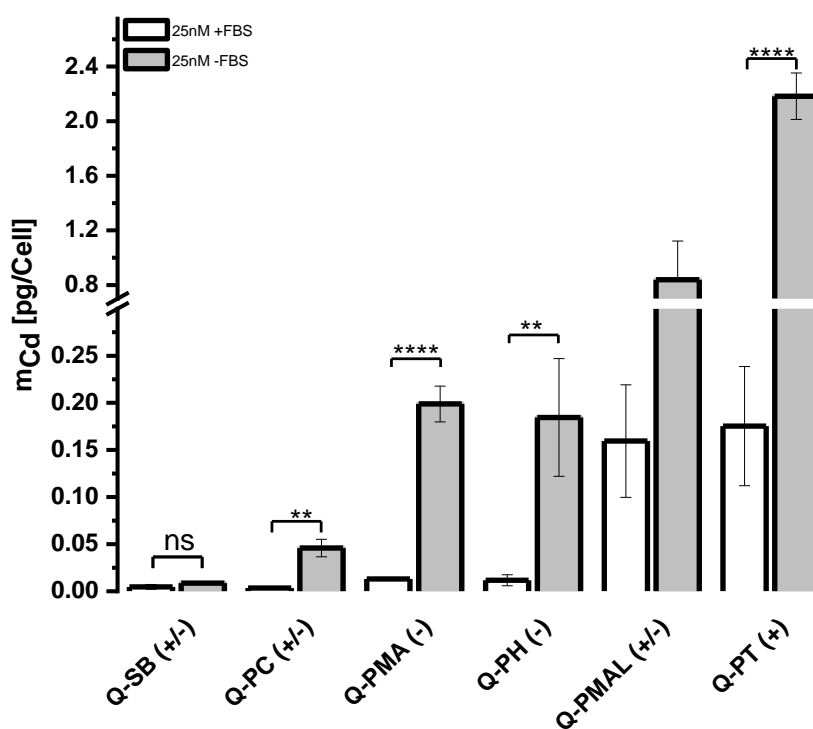


Figure 3-42 Cellular uptake of 25nM QDs by HeLa cells at 6h exposure time at two different serum conditions. The data are shown from at least three different independent measurements \pm standard deviation, statistical followed the student's t-test, * represent $P < 0.05$, ** $P < 0.01$, and *** $P < 0.001$.

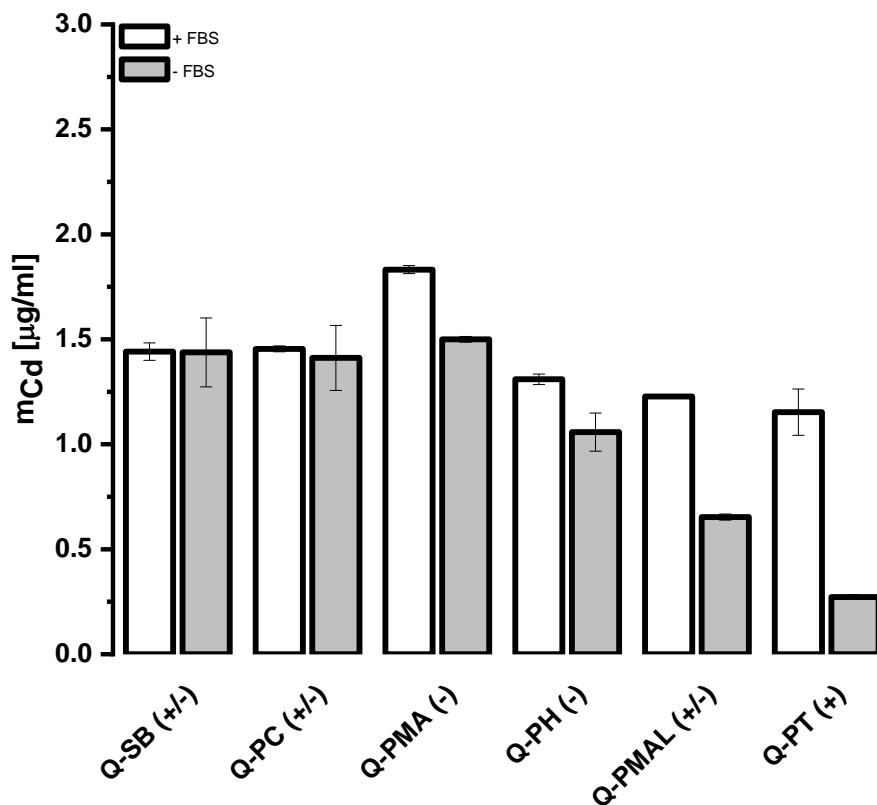


Figure 3-43 QDs content in the media after 6 h exposure time of the 25 nM QDs. The data are shown from at least three different independent measurements \pm standard deviation.

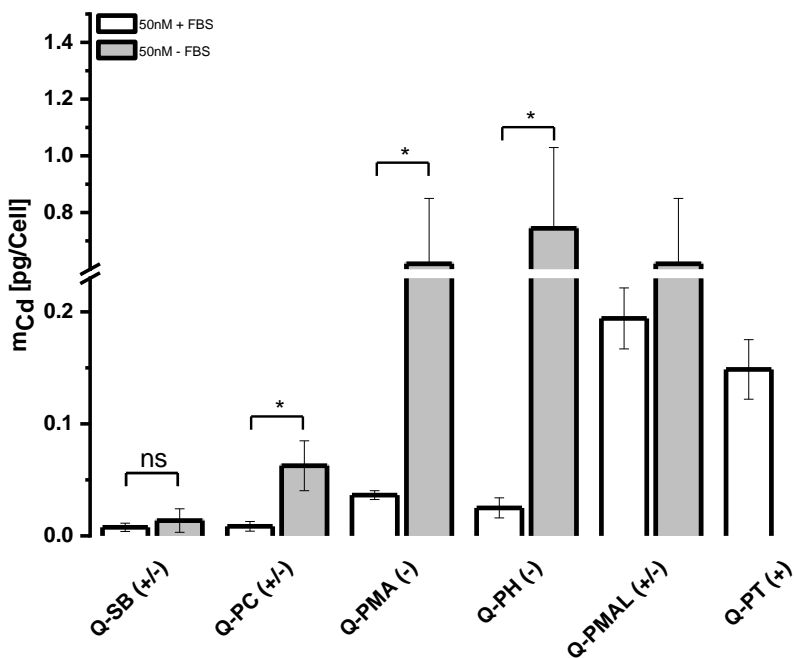


Figure 3-44 Cellular uptake of 50nM QDs by HeLa cells at 6h exposure time at two different serum conditions. The data are shown from at least three different independent measurements \pm standard deviation, statistical followed the student's t-test, * represent $P < 0.05$, ** $P < 0.01$, and *** $P < 0.001$.

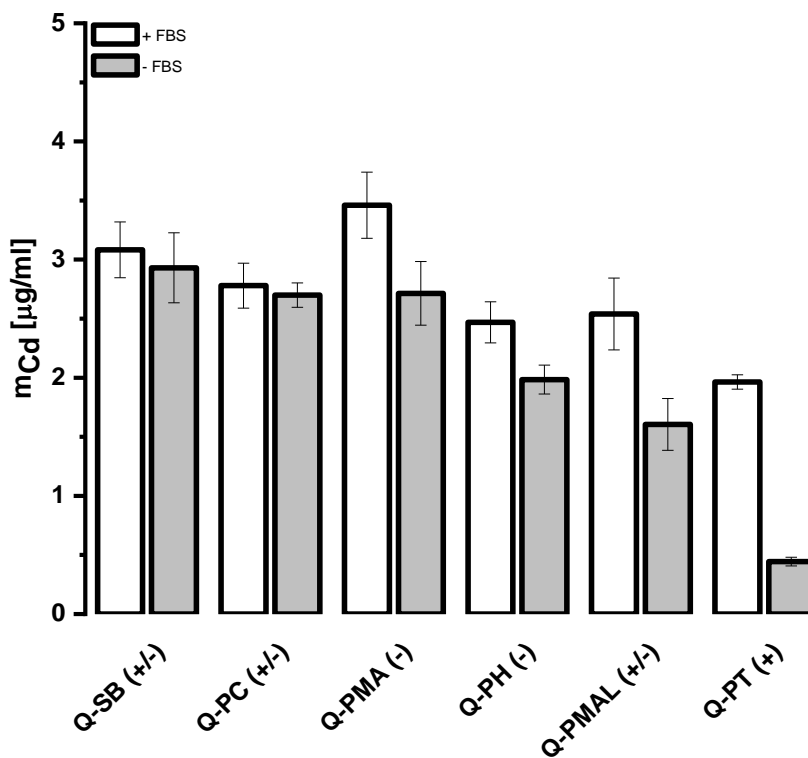


Figure 3-45 QDs content in the media after 6 h exposure time of the 50 nM QDs. The data are shown from at least three different independent measurements \pm standard deviation.

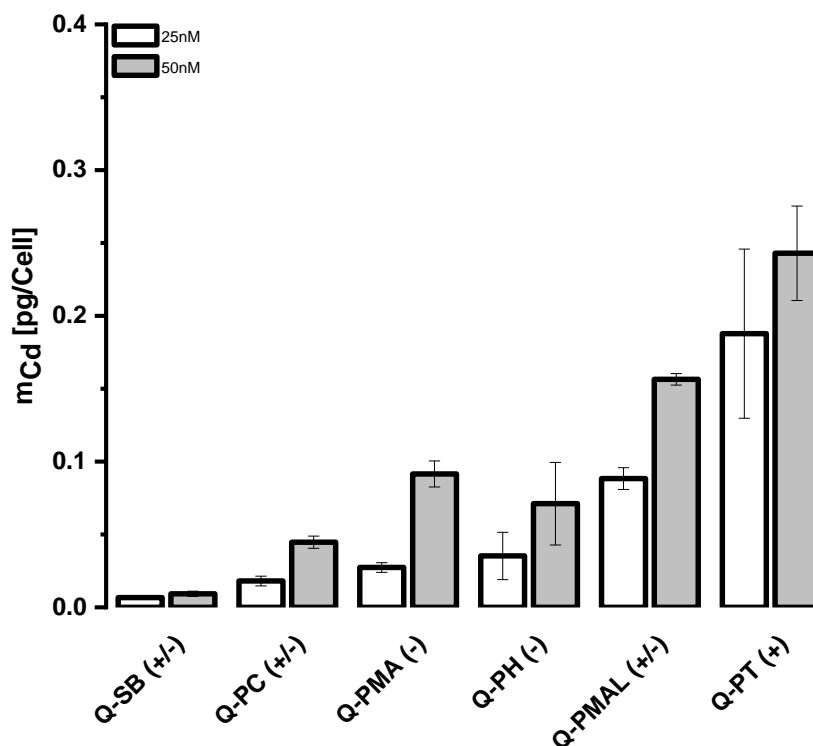


Figure 3-46 Cellular uptake of Hela cells of QDs at two different concentrations for 24h exposure time with 10% FBS. The data are shown from at least three different independent measurements \pm standard deviation.

Figure 3-46 shows the cellular uptake of the QDs at 25 and 50 nM after 24 h exposure time in a serum-supplemented medium. As shown, the uptake is concentration-dependent and by comparing the uptake content with the 6 h exposure time for the two concentration points, we found that the uptake is also time-dependent. The uptake of the 50 nM after 24 h was on average 2-fold higher than that of the 25 nM. While, the uptake ratio between the 24 h to the 6 h exposure time is varied, for instance, the uptake content of the Q-PH increased almost 10-fold than at 6 h, while for Q-PMA this ratio was only 2-fold higher, Q-SB was 1.5-fold higher, and for Q-PT was almost no change.

This indicates the fast kinetics of the uptake of the positive QDs than other samples, consequently overwhelming the cells. That's why we have observed a higher toxicity profile for the Q-PT when we incubate it in non-serum conditions even for a shorter exposure time, 6 h.

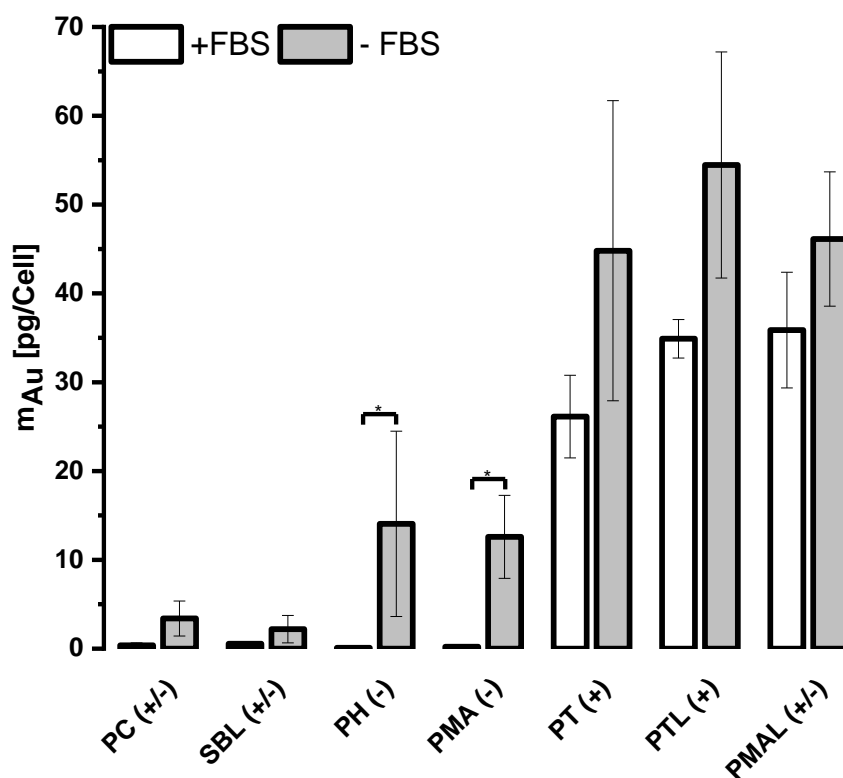


Figure 3-47 Cellular uptake of 17 nm Au NPs by HeLa cells after 24 h exposure time at two different serum conditions. The data are shown from at least three different independent measurements \pm standard deviation, statistical followed the student's t-test, * represent $P < 0.05$, ** $P < 0.01$, and *** $P < 0.001$.

In Figure 3-47, we are presenting the cellular uptake of the 17 nm Au NPs by HeLa cells after 24 h exposure time and at two different serum conditions. In good agreement with the uptake profile of the QDs, the Au NPs showed the same trend, with charge and serum-dependent uptake. The $Au_{+ve} > Au_{-ve} > Au_{zwi}$, following the same charge-dependent profile of the QDs. In addition to the higher uptake content of the Au NPs in non-serum condition than serum condition as shown before for the QDs.

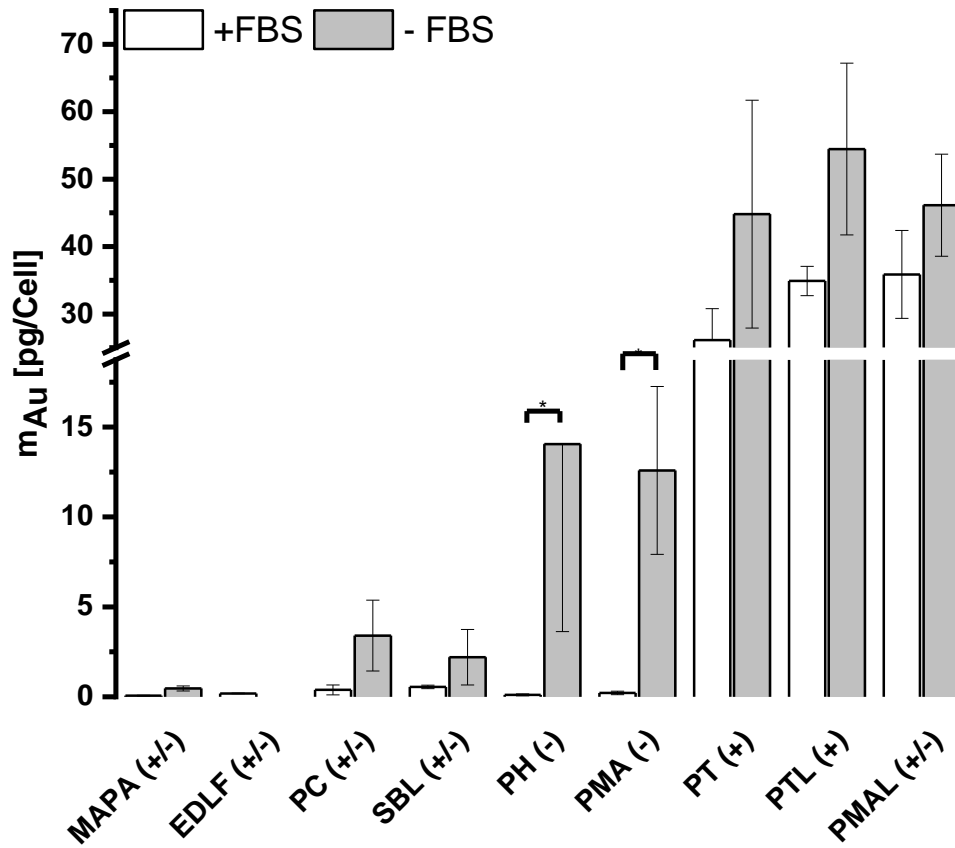


Figure 3-48 Cellular uptake of 17 nm Au NPs coated with MAPA and ELDF. The uptake results are shown versus of different samples after 24 h exposure time at two different serum conditions. The data are shown from at least three different independent measurements \pm standard deviation, statistical followed the student's t-test, * represent $P < 0.05$, ** $P < 0.01$, and *** $P < 0.001$.

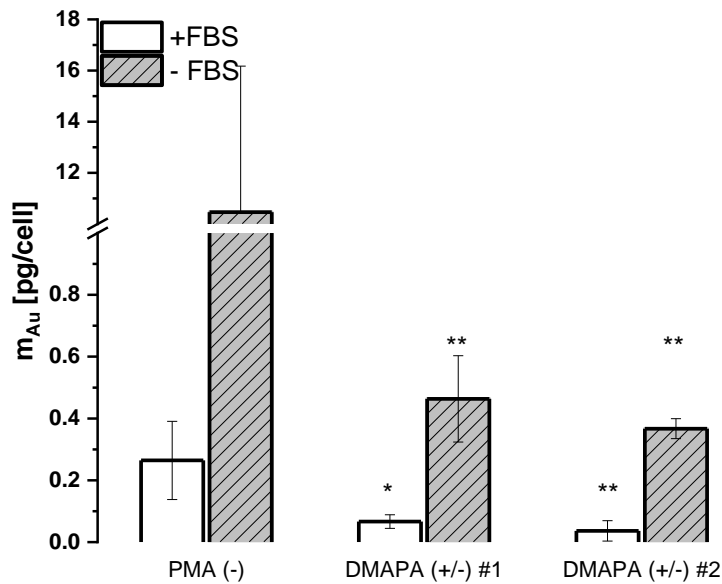


Figure 3-49 Cellular uptake by Hela cells of 17 nm Au NPs coated with DMAPA vs PMA after 24 h incubation time. The incubation was at two different conditions (+FBS/-FBS).

This means the charge-dependent uptake is independent of the core itself, and also the size, as shown in Figure 3-50 the uptake profile of the 4 nm Au NPs is also a charge-dependent process. In addition to that, the quantification of the uptake results of the Au NPs, for both cores, prove not only the faster dynamics in uptake for the positively-charged NPs among others but also show the number of NPs is higher for smaller NPs in comparison to the larger ones. This has been shown before from previous studies for different sizes of NPs, showing how the smaller NPs internalized in higher numbers than the bigger size. The faster aggregate formation of the smaller NPs could be one of the reasons, why they have been internalized in higher numbers than bigger ones, which have a slower aggregate formation rate. This results in serum-free conditions the smaller NPs showed a higher degree of toxicity for a longer exposure time that has been used in the current study. (Cho et al., 2011, Nazarenus et al., 2014, Shang et al., 2014, Stark, 2011)

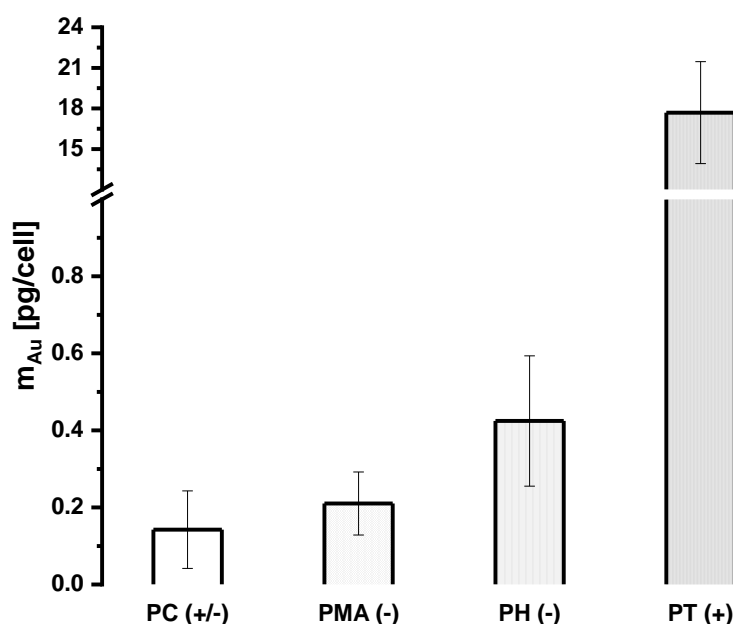


Figure 3-50 Cellular uptake of the 4 nm Au NPs by HeLa cells at 24h exposure time. The data are shown from at least three different independent measurements \pm standard deviation.

We did not only observe a toxicity profile for the smaller NPs at the serum-free condition at a longer incubation time as 24 h, but we have also observed the same for the Au NPs (large size) coated with EDLF ligand, Figure 3-48. Such toxicity at non-serum condition even though they showed a lower content of uptake (based on their zwitterionic character) in serum-supplemented medium. We believe that this high degree of toxicity came from their nature as an anticancer drug, which is somehow predicted from their viability profile discussed in the previous section.

To further support our finding of the FCS and protein corona profile of the NPs, the PMA-DMAPA polymer showed anti-fouling properties compared to the PMA. Their uptake profile also was lower than that of the PMA significantly at two different incubation condition and using two different batches of the NPs, indicating that their protein corona profile has a significant effect on their cellular interactions, Figure 3-48 and Figure 3-49. Concluding that higher affinity to proteins results in higher internalization rate by cells.

Cellular uptake of the PC-FA polymer.

The functionalization of the PC (+/-) polymer with FA has no significant effect on their protein interaction as we have observed by FCS. We have studied also their cell interaction to investigate how the functionalization contributes to their uptake, and at which conditions. Figure 3-51 and Figure 3-52 show the uptake of the Q-PC and Q-PC-FA after 6h as measured by ICP-MS for two different cell lines, Hela; overexpress folate receptor and MCF7; lower expression of folate receptors. (Monteiro et al., 2020)

The cellular uptake of Hela cells for the Q-PC at 25 nM was 14x higher in non-serum conditions than in serum conditions. While the uptake of the Q-PC-FA was 92x higher than serum conditions, this ratio decreased for the higher concentration 50nM to 30x and decreased the half for the Q-PC QDs. The same ratio for the Q-PC was observed for the MCF7 cell line, while for the Q-PC-FA this ratio dropped by 10 fold for the 25 nM and by half for the 50 nM. This higher internalization is related to the presence of the FA onto the QDs, which facilitate their internalization by Hela cells; where the folate receptor is highly expressed on its surface as reported before by others. Where the zwitterionic modification help in suppressing the formation of protein corona and at the same time keeping the targeting ability of the active-targeting ligand. (De et al., 2008, Loiola et al., 2019, Monteiro et al., 2020, Rampado et al., 2020, Safavi-Sohi et al., 2016) It is worth here to mention this behavior was not observed when we did the same for the 4 nm Au NPs, at 24h incubation time Figure 3-54 and also at 6h exposure Figure 3-55 and Figure 3-56. In addition to that, when we have worked using younger passage of the cell line, the uptake ratio of the Q-PC-FA dropped to be 20x (-FBS/+FBS) at 25 nM, Figure 3-53.

This could be due to the lower ratio of labelling of the FA to the polymer backbone and the lower uptake content of the PC-coated NPs themselves. In addition to that, the monovalent NPs are less likely to increase the targeting ability of the NPs compared to the multivalent design. Moreover, the anti-fouling properties of the PC polymer and its hydration shell may affect the direct interaction of the ligand with its receptor. This could explain why we have observed higher uptake content of the PC-FA QDs only at the free-serum condition. (Woythe et al., 2021)

These fluctuations in results lead us to rethink the active uptake of the Q-PC-FA samples, therefore we have carried out a **blocking experiment**. In which we have used a cell medium supplemented with a higher concentration of the folic acid (250 µg/ml), for both conditions (+FBS and -FBS). As shown in Figure 3-57 and Figure 3-58, there is no significant difference in the cellular uptake in presence of the FA at serum-supplemented medium. While in serum-free medium, we have observed not a blocking condition in presence of FA but a facilitating effect. Where the NPs coated with Q-PC-FA have been internalized in a higher amount than in the absence of FA. This could be due to the stress exerted on the cells in the serum-free condition making them look more for nutrition, which could be a reason for the higher uptake.

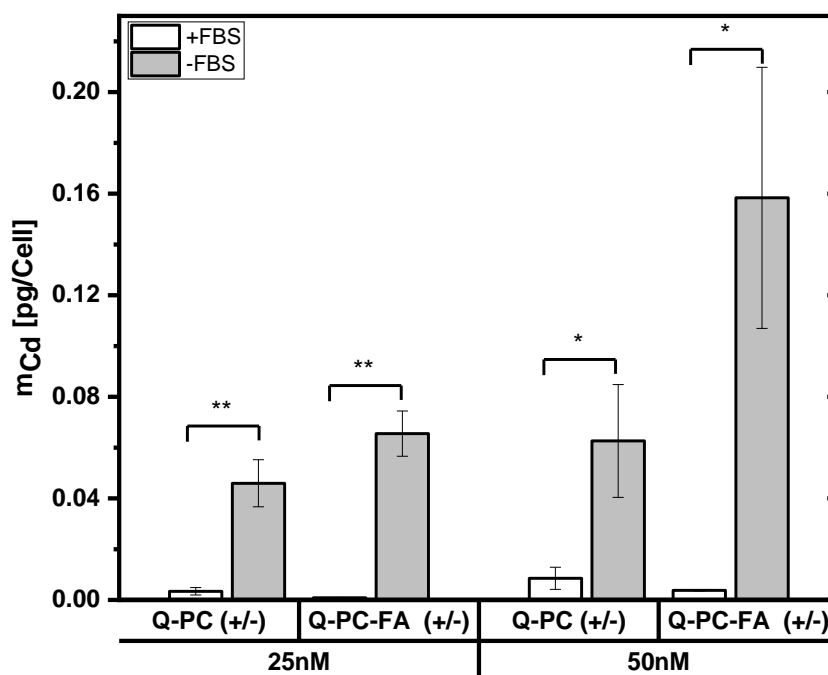


Figure 3-51 Cellular uptake of Q-PC and Q-PC-FA by Hela cells at 6h exposure. The data are shown from at least three different independent measurements \pm standard deviation, statistical followed the student's t-test, * represent $P < 0.05$, ** $P < 0.01$, and *** $P < 0.001$.

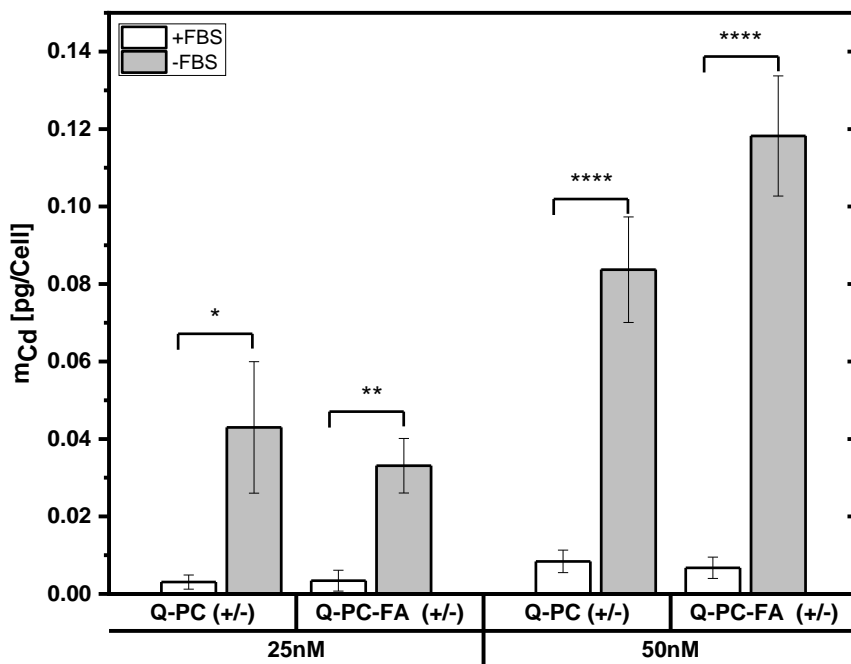


Figure 3-52 Cellular uptake of Q-PC and Q-PC-FA QDs by MCF7 cell line after 6h exposure. The data are shown from at least three different independent measurements \pm standard deviation, statistical followed the student's t-test, * represent $P < 0.05$, ** $P < 0.01$, and *** $P < 0.001$.

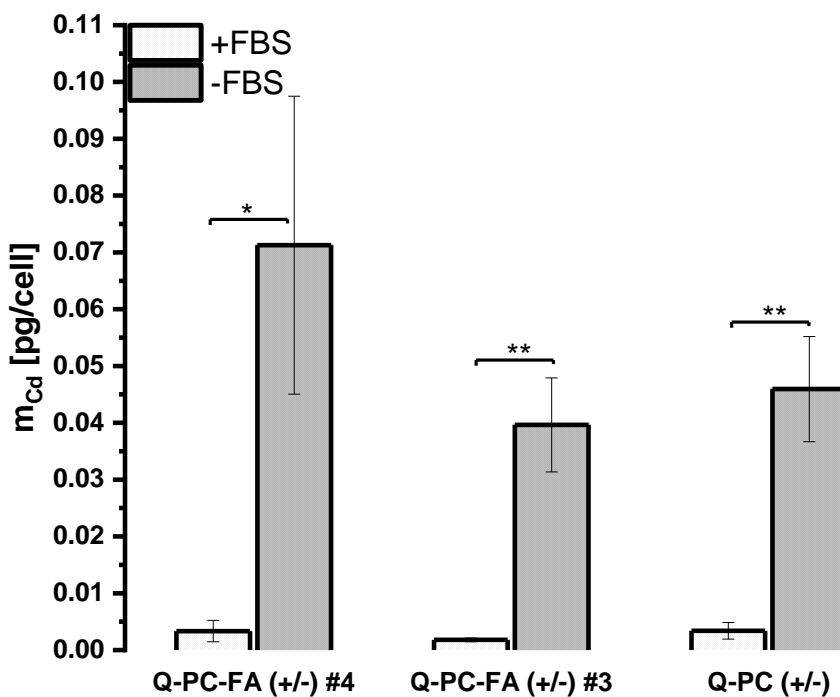


Figure 3-53 Cellular uptake of different batches of Q-PC-FA by HeLa cells for 6h incubation time. The obtained results here for different batches of QPC-FA 25 nM and against younger cell passage. The data are shown from at least three different independent measurements \pm standard deviation, statistical followed the student's t-test, * represent $P < 0.05$, ** $P < 0.01$, and *** $P < 0.001$.

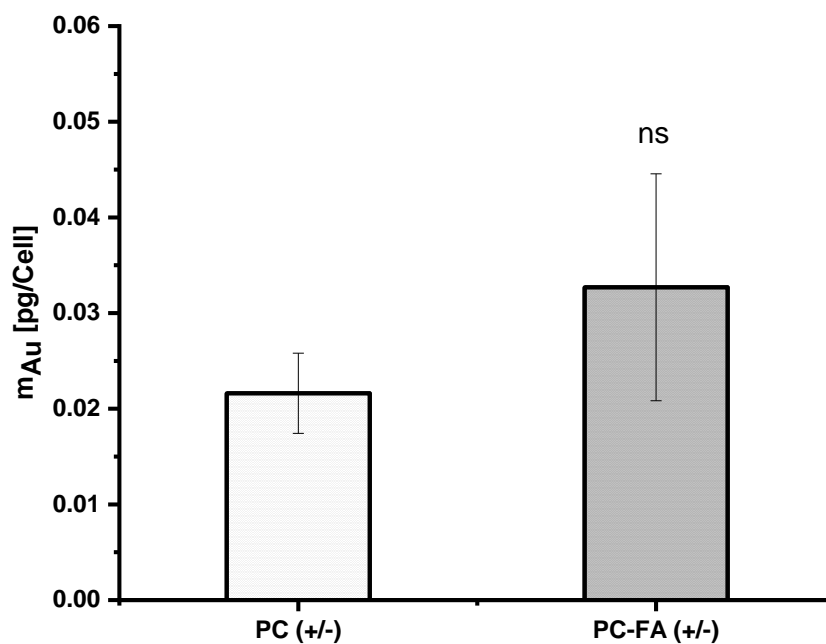


Figure 3-54 Cellular uptake of the 4 nm Au NPs (PC and PC-FA) by HeLa cells after 24 h.

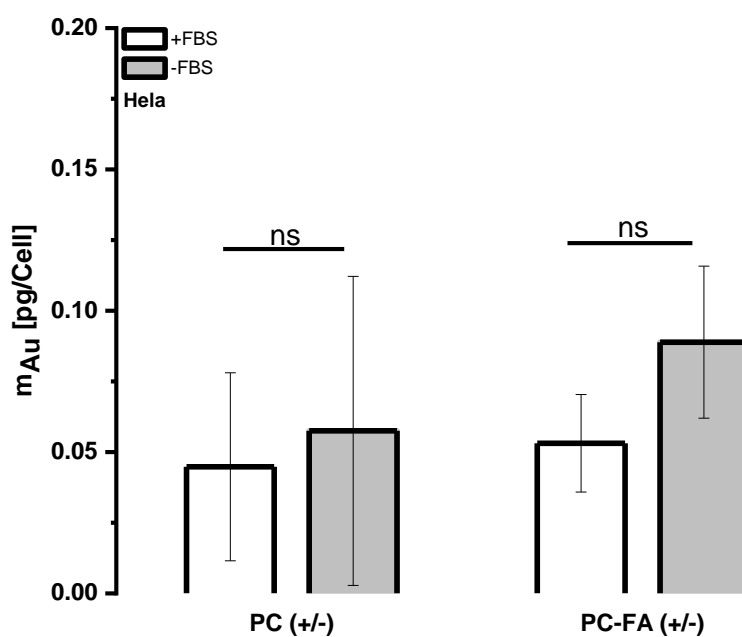


Figure 3-55 Cellular uptake of the 4 nm Au NPs (PC and PC-FA) by HeLa cells after 6h incubation. The incubation was in two different serum conditions (+FBS/-FBS). The data are shown from at least three different independent measurements \pm standard deviation, statistical followed the student's t-test, * represent $P < 0.05$, ** $P < 0.01$, and *** $P < 0.001$.

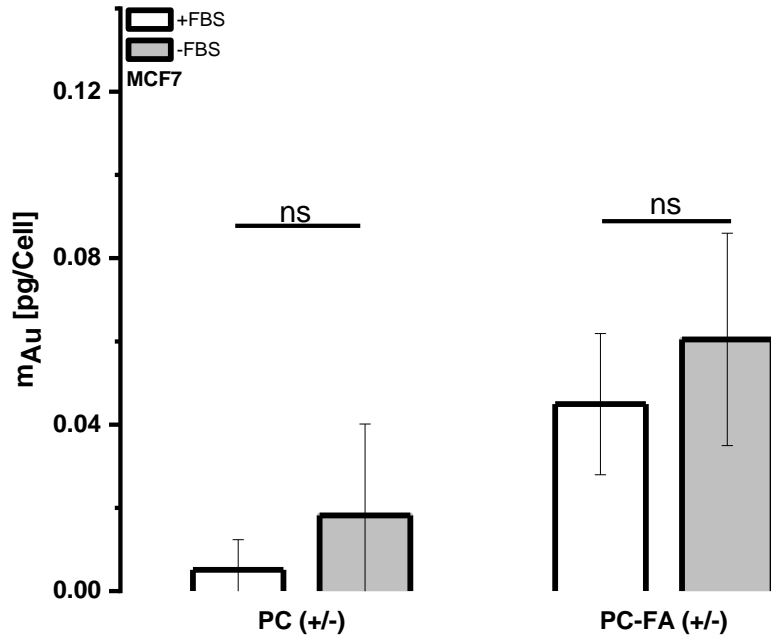


Figure 3-56 Cellular uptake of the 4 nm Au NPs (PC and PC-FA) by MCF7 cells after 6h incubation. The incubation was in two different serum conditions (+FBS/-FBS). The data are shown from at least three different independent measurements \pm standard deviation, statistical followed the student's t-test, * represent $P < 0.05$, ** $P < 0.01$, and *** $P < 0.001$.

Blocking experiment results:

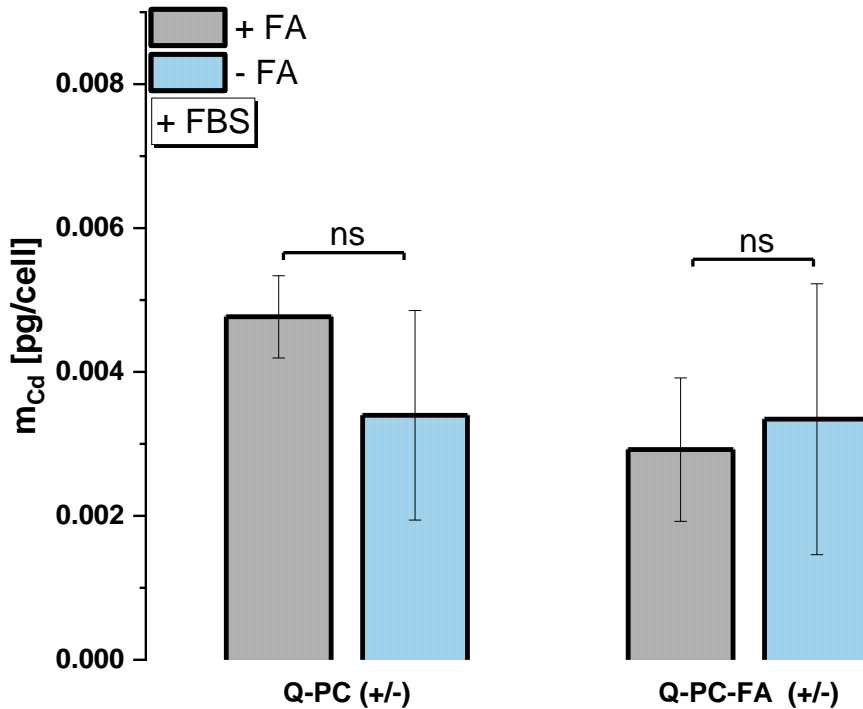


Figure 3-57 Blocking experiment of the QDs at 25 nM in a serum-supplemented medium for 6h incubation time. The data are shown from at least three different independent measurements \pm standard deviation, statistical followed the student's t-test, * represent $P < 0.05$, ** $P < 0.01$, and *** $P < 0.001$.

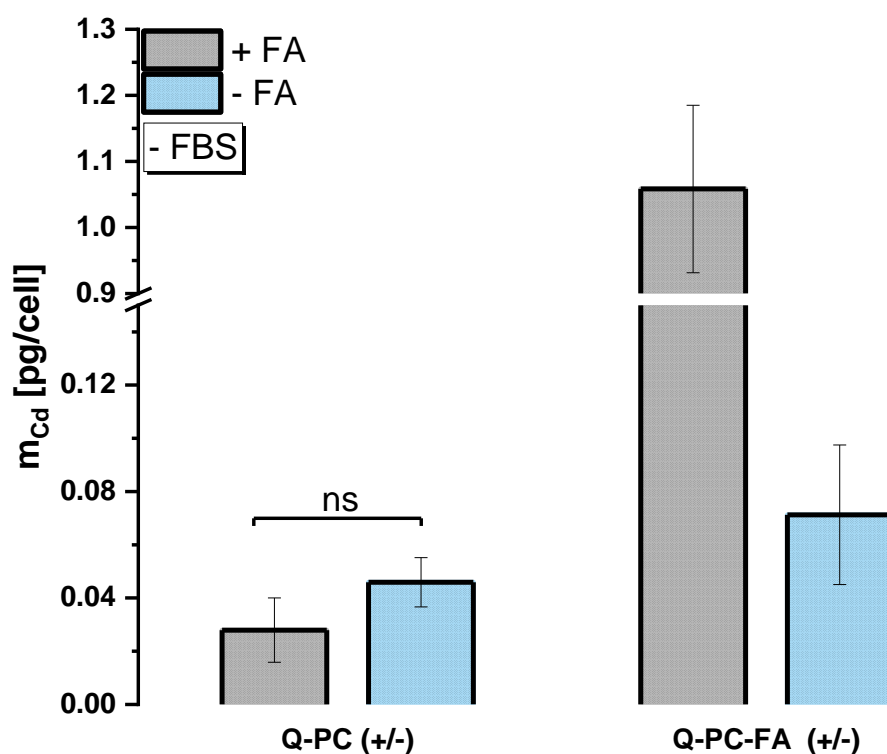


Figure 3-58 Blocking experiment of the QDs at 25 nM in serum-free medium for 6h incubation time. The data are shown from at least three different independent measurements \pm standard deviation, statistical followed the student's t-test, * represent $P < 0.05$, ** $P < 0.01$, and *** $P < 0.001$.

To conclude, the cellular uptake of the polymer-coated NPs showed a charge-, size-, time-, and dose-dependent trend. Where the positively-charged NPs showed the highest degree of internalization by the cells, and the zwitterionic ones showed the less uptake value. This is highly correlated with their protein adsorption profile, where the positively-charged NPs have the highest affinity degree toward protein adsorption as shown by FCS. While the different polymer-coated NPs almost showed the same degree of hydrophilicity, the uptake and the protein adsorption process is assumed to be mainly a charge-dependent process. In addition to being the highest incorporated by cells, the positively-charged NPs also showed a faster rate to be internalized by the cells. Where, at short exposure time that has been used in this study- 6 h - the elemental content of the positively-charged NPs were almost the same after 24 h. In contrast, this ratio was higher than that for the negative and zwitterionic NPs. Besides that, the cellular uptake of the NPs was dose-, and size-dependent. The smaller NPs have been incorporated by the cells in higher numbers than the bigger ones and for larger doses more uptake than the lower dose. Whereas the linear-zwitterionic coating reduces the uptake of the QDs, the dual-functionalization of this structure using folic acid as an active-targeting ligand result in a substantial increase in the uptake, only at serum-free conditions (for our labeling ratio) while retaining their anti-fouling properties.

4 Conclusion and Outlook

In the present study, we have introduced a universal approach for the surface modification of the nanoparticles using amphiphilic polymers, retaining the physicochemical properties of the nanoparticles, and stabilizing them whether due to the electrostatic repulsion or via steric hindrance. We have successfully coated different cores and sizes of the Au NPs and QDs with different charged amphiphilic polymers including, negative, positive, and zwitterionic-charged polymers. The coated NPs showed a higher degree of colloidal stability, in terms of size, as exposed to harsh conditions by incubating them with high ionic strength media.

In addition to that, these NPs showed a comparable degree of hydrophilicity indicating the same surface properties. The in situ formation of protein corona was evaluated using fluorescence correlation spectroscopy revealing the protein adsorption is charge-dependent, where the negative and the positive NPs showed higher affinity toward the protein adsorption, while the zwitterionic ones suppress the formation of it. Moreover, this study highlighted the impact of the zwitterionic ligand structure, the position of the ionic groups on the zwitterionic moieties that govern their protein interactions. We have found that the linear structure and position of the ionic groups are efficiently suppressing the formation of the protein corona, while the non-linear structure has more affinity toward protein adsorption.

Further supporting these findings, the cellular interactions of the NPs were correlating with their protein interactions, higher affinity towards protein adsorption leads to higher internalization rate and vice versa. Where we have found the cellular internalization of the NPs is the highest for the positive NPs, and the lowest was for the linear-structured zwitterionic NPs. These results were supported with two different techniques for three different cores of the NPs.

Moreover, the targeting ability of the zwitterionic NPs was studied by introducing folic acid as an active targeting ligand on the surface of the NPs. The protein adsorption of such a system reveals that the zwitterionic surface retains its anti-fouling properties over a broad range of protein concentrations. Interestingly, their cellular uptake dramatically increased upon the existence of the targeting ligand, indicating the ability to introduce active targeting nanomedicine via the utilization of the zwitterionic properties.

In view of what has been achieved so far, and the current barriers that prevent many of NPs, particularly, those with active-targeting design to being clinically translated. For instance, the protein corona, the extracellular matrix formation that limits their diffusion, and the blood vessel structure limiting the delivery of the NPs to its target. The current study focused on studying the first barrier

and how to overcome it. Therefore, we can not describe the recipe for the magic bullet that can solve everything in one shot. This could be further illustrated not only because of the above-mentioned barriers but also for the heterogeneity and complexity of the overall system. For example, in terms of the NPs design, the density and distribution of ligands on the surface of the NPs are not highly homogenous, and most of the available methods to quantify these ligands are ensemble methods. Therefore, it lacks the resolution of the individual NP. The flexibility of the NPs, greater the flexibility greater the chance to make more simultaneous interactions. In this regard, solid NPs are limited. Add to that, it's more preferred to have a multivalent design for the NPs rather than a monovalent design, which is mimicking nature. This, in turn, makes the exact design of the NPs more complex.

On the other hand, in terms of the target itself, knowing the receptor expression is not only enough, but also we need to know their dynamics. Additionally, their internalization upon interaction with their ligands, due to some of them do not internalize upon interaction. The heterogeneity of these receptors is not only from one person to another but in the same person and even in the same cell type. Therefore, personalized nanomedicine is now more promising.

One of the possible solutions for that is the super-resolution methods and the single-molecule techniques, thank their super-resolution, individual, and quantitative characterization. The multivalent design of the NPs is of utmost importance while having the ability to overcome the stated barrier as protein corona, also retain their functionality, and the ability to bond with different cell receptors. By using the super-resolution techniques, could help in improving the design of the NPs, characterizing their functionality, and understanding the dynamics on an individual basis.

This may solve part of the puzzle but not all, each technique has its limitation. Therefore, the integration of different techniques is highly recommended to move a step forward. Through understanding and overcoming the biological barriers (protein corona and cell barriers), developing more quantitative methodologies for the analysis of the NPs before, and after interactions with cells, agreeing on a standardization approach, a guideline named MIRIBEL (Minimum Information Reporting in Bio-Nano Experimental Literature) was recently suggested and it could be considered as a first step to improve the overall reproducibility, clinical translation, and the nano-bio applications.

5 Materials and experimental protocols

In this chapter, we are presenting the materials and the experimental protocols we have followed to perform our experiments. Starting with the materials that have been used in the current work, followed by the protocols for each experiment.

5.1 Materials

Tetrachloroauric acid (HAuCl_4), trisodium citrate, Dodecylamine, tetraoctylammonium bromide (TOAB), NaOH, dodecanethiol (DDT), poly(isobutylene-alt-maleic anhydride), Nitric acid, Resazurin sodium salt, Rhodamine 6G dye (Rh6G) are provided from Sigma Aldrich group, while Tetrahydrofuran (THF), Chloroform, and Hydrochloric acid (HCl) are provided by Carl Roth. Methoxy-mercapto-PEG ($\text{CH}_3\text{O-PEG-SH}$) is supplied from Rapp polymer. Dulbecco's modified eagle medium (DMEM), and trypsin-EDTA are provided from Thermo Fisher. PT, PC, and SB polymers are provided by our collaborators at Max Planck Institute for Polymer Research, Mainz, Germany. While the QDs (Core/shell/shell) CdSe/CdS/ZnS QDs Lot No. SAB-0-365-6 are provided by Fraunhofer-Zentrum für Angewandte Nanotechnologie CAN, Hamburg, Germany.

5.2 Gold Nanoparticles synthesis

5.2.1 Synthesis of ≈ 17 nm Au NPs

To synthesize the 17 nm Au NPs, we have followed the protocol of Bastus (Bastús et al., 2011) with some modifications. Briefly, we prepared 1.32 mM (in 150 ml) sodium citrate solution in a three-neck flask. Then, we heated the solution till boiling and left it for 5 minutes after boiling. After that, we injected 1.5 ml of 25 mM tetrachloroauric acid (HAuCl_4), the color of the mixture changed from pale yellow, light blue until soft red. At this stage, we left the solution to boil for another 10 minutes and then cooled it down to room temperature while stirring. The obtained product is a ≈ 15 nm Au NPs with citrate as a capping agent.

5.2.2 Phase Transfer

For purpose of polymer coating, it is essential to ensure a high yield of coated nanoparticles, we have to transfer the NPs from water into hydrophobic solvent decorated with different surface chemistry. Normally, this capping agent is a hydrophobic one with a long hydrocarbon chain. This is simply achieved by functionalizing the surface of the NPs with Polyethylene glycol (PEG) that helps in transferring the NPs into chloroform this process is called PEGylation.

For PEGylation, we used PEG-SH (2 KDa, Rapp polymer) with $C_{\text{NP}}/C_{\text{PEG}} = 3 \times 10^4$. The mixture was left under stirring overnight and then was centrifuged to obtain purified PEG-Au NPs. For transferring the

PEG-Au NPs into chloroform, we added Dodecyl amine (DDA) 0.4 M in chloroform to the PEG-Au NPs with a volume ratio of 1:3. The mixture was left under vigorous stirring till transferring the Au NPs into chloroform. The transferred NPs were purified by centrifugation (12000 rpm / 20 min) and the collected pellets were dissolved in chloroform and kept at 4 °C for further experiments. (Hühn et al., 2016)

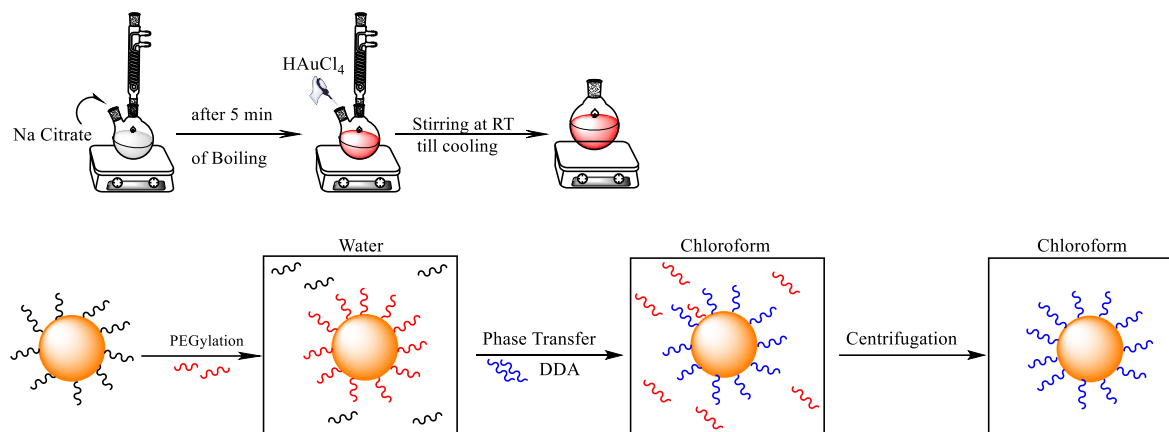


Figure 5-1 Schematic of the Au NPs synthesis and phase transfer steps.

5.2.3 Synthesis of the 4 nm Au NPs

To synthesize the 4 nm Au NPs, we followed the Brust-Schiffrin method with some modifications (Brust et al., 1994, Hühn et al., 2016). Typically, 300 mg of tetrachloroauric acid dissolved in 25 ml Milli-Q water (aqueous phase) and 2.170 g tetraoctylammonium bromide (TOAB) dissolved in 80 ml of Toluene (organic phase).

Both solutions were mixed in a separation funnel and shaken vigorously till transferring the Au salts into the organic phase (this is known by the colorless of the aqueous phase after shaking). Then, this solution was transferred into a 250 ml round flask.

A freshly prepared solution of strong reducing agent - 334 mg of sodium borohydride in 25 ml Milli-Q water- was added within 1 min to the organic phase under vigorous stirring. The solution color changed from deep orange to red-violet (indicating the formation of TOAB capped Au NPs, TOAB-Au NPs), this solution was kept stirring for 1 h to reduce the remaining gold ions.

After that, the aqueous phase was discarded using a separation funnel and the remaining solution was washed by 10 mM HCl, 10 mM NaOH, and Milli-Q water, each solution is 25 ml and has been used sequentially. The final solution (ca. 80 ml) was transferred to a 250 ml round flask and was kept stirring overnight to get a narrow size distribution.

Ligand Exchange

The ligand of TOAB-Au NPs was exchanged by a stronger ligand, alkanethiols ligand. For this, we used dodecanethiol (DDT). In brief, 10 ml of DDT was added to the TOAB-Au NPs and the mixture was heated to 65 °C and was kept for 2 h stirring, then cooled down to RT. During this process, the mercapto group of DDT displaces the TOAB and leads to the formation of DDT-Au NPs.

The obtained DDT-Au NPs were purified by centrifugation at 900 rcf for 5 min, to remove the bigger agglomerates, by discarding the pellets. The supernatant was purified more by using an anti-solvent (MeOH) and the collected pellets were dissolved in chloroform. The precipitation process was repeated two times. Finally, the pellets were resuspended in chloroform to have purified DDT-Au NPs.

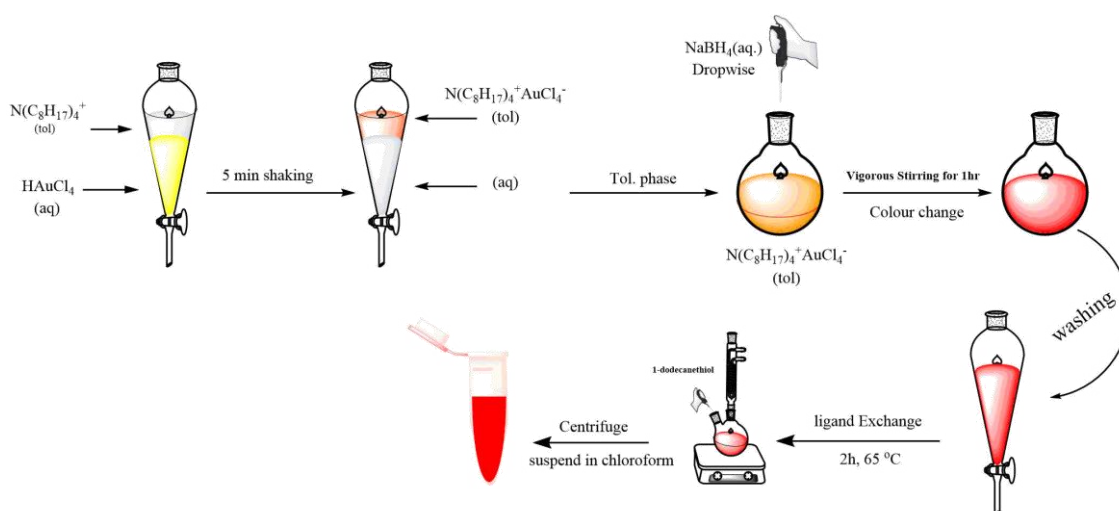


Figure 5-2 Schematic of the 4nm Au NPs synthesis and ligand exchange steps.

5.3 Polymer Synthesis

5.3.1 Synthesis of the PMA-grafted dodecylamine

The synthesis of the poly(isobutylene-alt-maleic anhydride) – grafted – dodecylamine (PAM-g-DDA) was reported before (Hühn et al., 2016, Lin et al., 2008, Zhang et al., 2011). Typically, 2.7 g of DDA dissolved in THF was added to 3.084 g of PMA in 250 ml round-bottom flask and sonicated for ca. 20 s, followed by heating to 55 – 60 °C for 3 h under stirring. The cloudiness of the mixture turned transparent after a while, which indicates the coupling of the DDA to the PMA rings.

Then, the solution concentrated to 30 – 40 ml by evaporating the THF using the rotary evaporator and kept overnight stirring under reflux. The next day, all the THF evaporated and the dried film was dissolved in 40 ml of anhydrous chloroform to have a 0.5 M monomer concentration.

5.3.2 Synthesis of the PMA-DDA-DMAPA polymer

Synthesis of poly (isobutylene-alt-maleic anhydride) – grafted – dodecylamine – grafted – 3-(dimethylamino)-1-propylamine (PMA-DDA-DMAPA) has been prepared following the same protocol for the synthesis of the PMA-g-DDA, with slight modification in the molar ratio of the grafted ligands. Herein, we have added DDA with only a 50% molar ratio. In brief, 1.542 g of PMA has been added to 50 ml of THF (mixture is cloudy), then 630 µl of DMAPA has been added under reflux, which in seconds formed white precipitated. The mixture was then sonicated and 1.7 ml of DDA has been added under reflux, and the mixture was left overnight at 90 °C. The next day, the mixture turned clear, and the THF dried to have a white film, dissolved in 20 ml of chloroform.

5.4 Polymer Coating

The polymer coating process was achieved by following the previous protocols (Geidel et al., 2011, Lin et al., 2008). The concentration of the hydrophobic monomer units has been calculated as following.

Lets first define these parameters, M_w is the molecular weight of the polymer, M_{wM1} is the molecular weight of the monomer unit, R_M is the monomer ratio, g is the weight amount of the polymer, V is the solvent volume and C_p is the concentration of the polymer.

First, we need to know the number of units per chain and the number of polymer chains.

$$\text{Average monomer units per chain (unists/chain)} = \frac{M_w}{(R_{M1} \cdot M_{wM1} + R_{M2} \cdot M_{wM2})}$$

$$\text{Monomers per chain (M2/chain)} = \text{Average monomer units per chain} \left(\frac{\text{unists}}{\text{chain}} \right) * R_{M2}$$

$$\text{Number of polymer chains (mol)} = \frac{g}{M_w}$$

$$\text{Number of M2 monomers} = \text{Number of polymer chains (mol)} * \text{Monomers per chain (M2/chain)}$$

$$C_p = \frac{\text{Number of M2 monomers}}{V}$$

The amphiphilic polymers were dissolved in chloroform where the concentration of the hydrophobic chain is 0.5 M. The amount of polymer needed V_p was calculated according to the following equation.

$$V_p = \frac{R \cdot A_{eff} \cdot C_{NP} \cdot V_{NP}}{C_p} \quad (5-1)$$

Where, R is the ratio of the hydrophobic monomer units per unit area – which was between 50 for smaller NPs and 2000 for the 15 nm Au NPs, A_{eff} is the effective surface area, C_{NP} and V_{NP} are the concentration and the volume of the NPs, respectively and C_P is the concentration of the hydrophobic monomers.

Then, the mixture was stirred using the rotary evaporator set up for around 10 minutes, followed by evaporation of the solvent under reduced pressure till we obtain a dried film. The film was hydrated using basic buffer (sodium borate 50 mM, 12pH or 0.1 M NaOH) for the zwitterionic and anionic polymers, and acidic buffer (0.1 M NaCl at pH 3.3, adjusted by HCl) for the cationic polymers. Firstly, the collected NPs were purified by pushing them through a 0.2 μm syringe filter (except the cationic NPs), followed by centrifugation. For the 4-5 nm NPs we have used the ultracentrifugation (250000 g for 30 min.) and for the \approx 15 nm Au NPs we have used the normal centrifugation (12000 rpm for 20 min.).

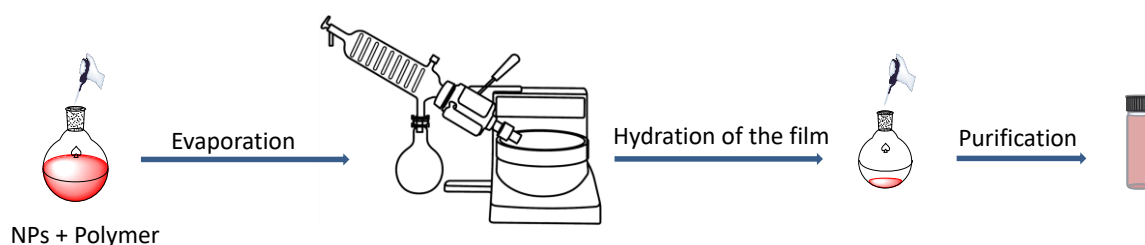


Figure 5-3 scheme of the main coating steps of the NPs by the amphiphilic polymers.

5.5 UV-Vis spectroscopy Measurements

The UV-Vis absorption spectra of the synthesized nanoparticles were measured by Agilent 8453 UV-Vis spectrophotometer, the spectra were collected between 200 to 1000 nm at room temperature using 10 mm quartz cuvettes. All the data were presented using the Origin software (Origin 2018).

5.6 Photoluminescence Measurements

The fluorescence spectra of the QDs were recorded by Fluorolog fluorescence spectrophotometer equipped with a 450 W Xe-lamp (FL3-22, Horiba Jobin Yvon) with excitation at 400 nm and the emission window between 500 to 750 nm at room temperature. All the data were presented using Origin software (Origin 2018).

5.7 Dynamic light scattering and ζ -potential measurements

The hydrodynamic size and the ζ - potential of the nanoparticles were carried out using a Malvern Zetasizer Zs series, all the measurements were carried out in MQ water.

5.8 Interfacial Tension measurements

The dynamical interfacial tension (IFT) of the coated nanoparticles was evaluated by the pendant drop method (Del Pino et al., 2016, Rana et al., 2012). To do that, we produce 50 μl drop (by stainless steel needle - 1.85 mm diameter - plugged into the syringe) of the Nanoparticles solution in a glass cup filled with toluene and the shape of the drop was recorded (using a high-frame-rate camera implemented with the Drop Shape Analyzer (DSA30, Krüss, Germany)) with time. The IFT was calculated according to Young-Laplace fitting as shown in the following formula (Du et al., 2019, Rana et al., 2012).

$$\gamma = \frac{\Delta\rho g d_e}{H} \quad (5-2)$$

Where $\Delta\rho$ is the density difference between the liquid drop and its surrounding medium (toluene), g is the gravitational acceleration, d_e is the largest horizontal diameter of the drop, and H is a function of $S_n (d_n/d_e)$, where d_n is the horizontal diameter at a distance equal to $d_e (n/10)$ from the bottom of the drop.

The obtained drop profile for each sample was fitted by the empirical Hua and Rosen equation (Del Pino et al., 2016, Hua, Rosen, 1988, Rana et al., 2012).

$$\gamma_t = \gamma_m + \frac{\gamma_0 - \gamma_m}{1 + \left(\frac{t}{t_h}\right)^n} \quad (5-3)$$

Where, γ_t is the interfacial tension at any time t , γ_0 is the interfacial tension of the pure solvent used (water-toluene) (Joseph J. Jasper, 2009), γ_m is the interfacial tension at the meso-equilibrium, n is a dimensionless exponent, and t_h is the half-life time to reach meso-equilibrium state.

In addition to knowing these parameters which help in evaluating the differences in hydrophobicity/hydrophilicity of the examined nanoparticles. We have also tried another way of interpreting such results by calculating the decay rate of the interfacial tension v_{max} , in an attempt to fully understand the behavior of the nanoparticles (Rana et al., 2012).

$$v_{max} = \frac{n (\gamma_0 - \gamma_m)}{4 t_h} \quad (5-4)$$

So, by combining the results obtained from both equations we were able to drive a clear understanding of the hydrophobicity/hydrophilicity of the nanoparticles, as shown in the discussion section.

5.9 Fluorescence Correlation Spectroscopy Measurements (FCS)

To assess the differences in protein adsorption, we have used fluorescence correlation spectroscopy (FCS) to help in determining the change in the hydrodynamic radius (Thomaz et al., 2015) of the QDs which is related to the formation of the protein layer around the QDs. We have followed previously reported protocols (Hühn et al., 2013, Röcker et al., 2009, Shang, Nienhaus, 2017). The measurements were carried out in a Zeiss Spectral Confocal Microscopy LSM 880 (Carl-Zeiss, Germany) upright with a Zeiss plan-Apochromat 40x/1.0 water DIC (WD: 2.5 mm) objective. The measurement environment temperature was controlled at 25 °C using the incubator of the LSM 880.

The focal volume was calibrated using Rhodamine 6G dye (Rh6G) at a 488 nm excitation laser line. A fixed concentration of the QDs was incubated with a series of concentrations of the protein with the same volume ratio, all were in PBS. The mixture was kept for \approx 15 min before measurements. The measurements were performed for five different cycles, each for 10 runs/10 s, and the outlier runs were excluded from further processing. Keep in mind to help in obtaining good quality data, the QDs were purified by sucrose gradient centrifugation.

We used the Zen software (Zen 2.3 SP1) for calculating the correlation curves and performing the fitting according to the following equation (Liedl et al., 2005, Röcker et al., 2009, Thomaz et al., 2015).

$$G_{\tau} = \frac{1}{N} \left(1 + \frac{T}{1-T} e^{-\frac{\tau}{\tau_T}} \right) \sum_{i=1}^M \frac{f_i}{1 + \frac{\tau}{\tau_{Di}}} \frac{1}{\sqrt{1 + \frac{\tau}{\tau_{Di}} S^2}} \quad (5-5)$$

Where N is the average number of fluorophores within the effective detection volume, M is the number of the different fluorescent components (in our case M=1), f_i determines the contribution of the different fluorescent components to the autocorrelation function, T is the fraction of the fluorescence decay from the triplet state and τ_T is the lifetime of the triplet state.

In the case of the QDs, we have excluded the triplet part from the fitting equation, as we were working with very low excitation power and the QDs we have is a core/shell/shell that should be expected to have no or less blinking.

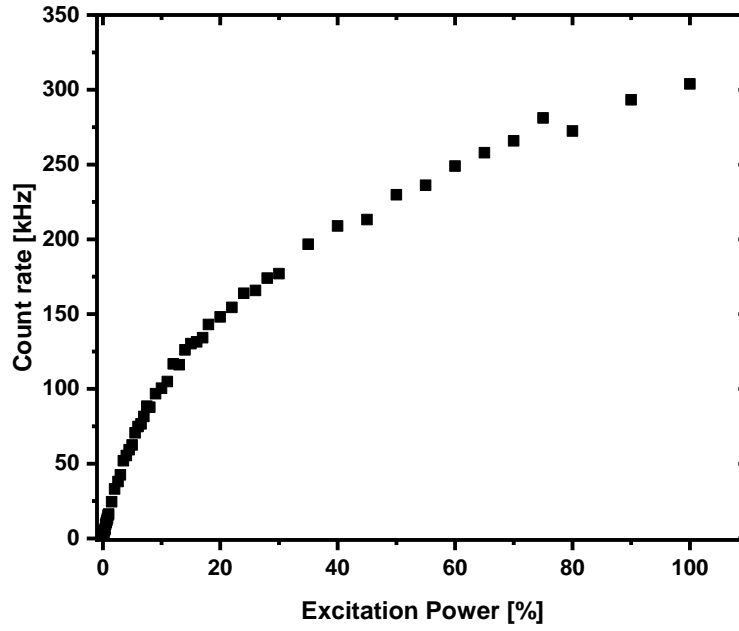


Figure 5-4 Intensity of the QDs as a function of the excitation power.

The confocal volume was calibrated based on the assumption of Gaussian ellipsoid for the volume, therefore the lateral radius ω_0 was calibrated according to the following formula.

$$\tau_D = \frac{\omega_0^2}{4D} \quad (5-6)$$

Where D is the diffusion coefficient, and τ_D is the diffusion time of the fluorophore.

After performing the fitting for the acquired results of the QDs, we were able to derive the diffusion coefficient of the QDs. By assuming the sphere shape and using the Stokes-Einstein formula, we were able to calculate the corresponding hydrodynamic radius R_h .

$$R_h = \frac{K_B T}{6 \pi \eta D} \quad (5-7)$$

Where K_B is Boltzmann constant, T is the temperature in kelvin, η is the solvent viscosity, and D is the diffusion coefficient as obtained from the fitting.

To get more quantification about the protein adsorption onto the QDs, we have fitted the results to the isotherm model, Hill model, by assuming the change in the size of the QDs is related to the number of protein molecules adsorbed onto the surface. This can be illustrated with the following formula (Ashraf et al., 2016, Hühn et al., 2013, Maffre et al., 2011, Maffre et al., 2014, Röcker et al., 2009, Shang, Nienhaus, 2017).

$$R_h = R_h(0) \cdot \sqrt[3]{1 + c \frac{N_{max}}{1 + \left(\frac{K_D}{C_p}\right)^n}} \quad (5-8)$$

Where, $R_h(0)$ is the hydrodynamic radius of the QDs without the presence of protein, $c = V_p/V_{QD}$ is the volume ratio of the protein to the volume of the QDs, calculated based on $R_h(0)$, C_p is the concentration of the protein, N_{max} is the maximum number of the protein adsorbed at the saturation, K_D is the apparent dissociation coefficient, and n is the Hill coefficient.

All the measurements were carried out at 25 °C and for three independent replicates.

5.10 Cellular Viability Study

The cytotoxicity of the NPs was carried out against Hela cells according to a previously reported protocol (Abdelmonem et al., 2015, Ashraf et al., 2016, Chakraborty et al., 2018, O'Brien et al., 2000, Soliman et al., 2015). Briefly, Hela cells were plated in a 96-well plate with a cell density of 7500 cells/well for 24 h at 37°C and 5 % CO₂. Then, the cells were incubated with different series concentrations of NPs for 24 h. After incubation, the cells were washed with PBS three times and then incubated with resazurin solution (0.02 mg/ml, 100 µl) for 4 h. The fluorescence intensity of the wells was determined using a fluorescence spectrophotometer with excitation at 560 nm and emission range between 580 and 590 nm. The processing of the viability percent was calculated according to the following formula.

$$V(\%) = \frac{I_s - I_b}{I_c - I_b} \times 100 \quad (5-9)$$

Where, I_s , I_c and I_b are the intensity of the wells incubated with NPs, control wells, and blank wells, respectively.

All the measurements were carried out at least three times and presented as the mean value \pm SD.

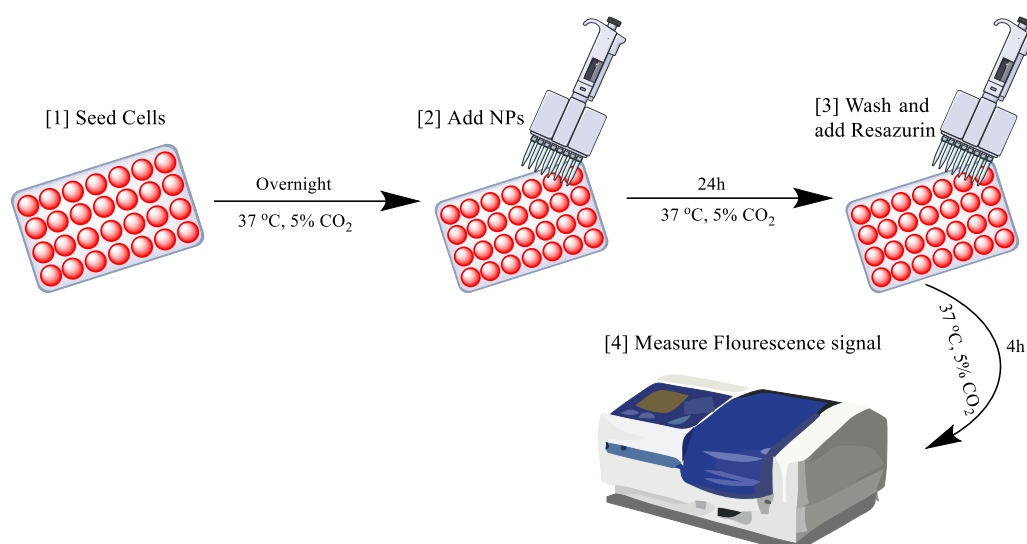


Figure 5-5 Scheme of the biocompatibility study.

5.11 Cellular Uptake Study

The cellular uptake of the nanoparticle was evaluated by two different methods using Flow Cytometry and Inductive Coupled Plasma Mass Spectrometry (ICP-MS) instruments.

5.11.1 Cellular Uptake using Flow Cytometry

To quantify the cellular uptake of the coated NPs, we have followed the standard protocols reported elsewhere (Ashraf et al., 2016). In brief, HeLa cells were seeded in a 24-well plate at a density of 40,000 cells/well in a 10% FBS supplemented DMEM medium. On the next day, the medium was removed, and the cells were incubated with the desired concentration of the QDs for a specific time point at 37 °C and 5 % CO₂.

After incubation, the cells were washed three times by PBS, detached using 0.05 % trypsin-EDTA, collected by centrifugation at 300 g for 5 min, and finally resuspended in 300 µl of cold PBS for flow cytometer analysis (BD LSRFortessa™, BD Bioscience, US). The fluorescence signal was collected with 610/20 nm a bandpass filter at 405 nm excitation for ≈ 10,000 gated cells and the results were analyzed using Flowjo software. The measurements were carried out for three different passages and presented as mean value ± SD.

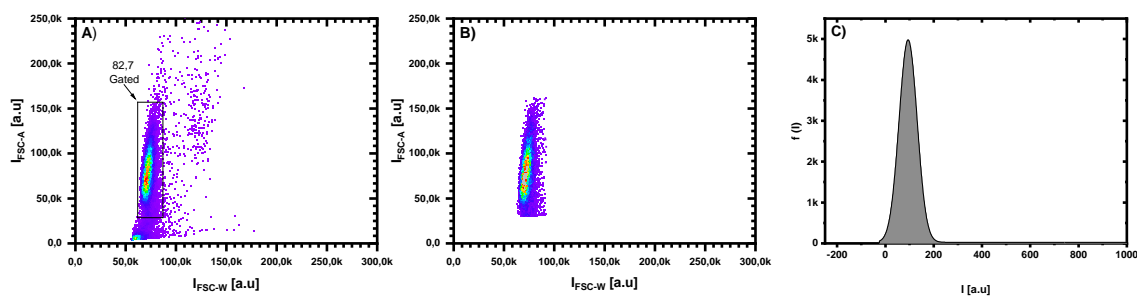


Figure 5-6 Gating strategy for HeLa cells. A) Density plot of the forward scattering area intensity I_{FSC-A} versus the forward scattering width intensity I_{FSC-W} . B) Density plot of the gated single cells displayed as I_{FSC-A} versus I_{FSC-W} . C) fluorescence distribution as measured by flow cytometry for HeLa cells.

5.11.2 Cellular uptake using ICP-MS

Alongside the uptake evaluation of the nanoparticles using the flow cytometer, we have also used the ICP-MS for quantifying the cellular content of the elemental Cd or Au. To do that, HeLa cells were seeded in a 6-well plate at a density of 200,000 cells/well in 2 ml of medium supplemented by 10% FBS. On the next day, the medium was removed, and the cells were incubated with the desired concentration of the nanoparticles for a specific time point at 37 °C and 5 % CO₂.

After incubation, the cells were washed three times using PBS, detached by 0.05 % trypsin-EDTA, and the cells were counted using the counting chamber. Then, the cell pellets were collected by centrifugation at 4000 rpm for 10 min.

The cell lysates containing the internalized nanoparticles were digested by 75 μ l of HNO₃ (67 wt%, Fisher Chemical, USA) for 24 h, then 150 μ l of HCl (37%, Fisher Chemical, USA) was added for another 24 h and finally the whole mixture was transferred into perfluoroalkoxy alkane tubes (PFA) prefilled with 2,275 μ l of 2% HCl. All the measurements were carried out for three different cell passages and the results were presented as mean value \pm SD.

6 Appendix

6.1 Gel Electrophoresis of the Au NPs

Gel electrophoresis is one of the methods that can be used to purify the NPs or separate them based on size or surface charge density. As the NPs are migrating into the gel under the applied electric field, therefore based on the charge, charge density, and size we can separate the NPs or identify the different surface charges. This helps in our case to visually prove the surface modification of the NPs by different charged amphiphilic polymers. As expected the positive, and the zwitterionic NPs will not migrate in the gel matrix, while the negative NPs will migrate under the effect of the electric force towards the positive pole of the gel apparatus.

For gel preparation, we have followed previously published protocol (Hühn et al., 2016). In brief, for 2% agarose gel preparation, 3 g of agarose powder was dissolved in 150 mL of 0.5x trisborate buffer (TBE) (44.5 mM Tris-borate and 1 mM ethylenediaminetetraacetic acid (EDTA)), pH 8.3 in a 500 mL Erlenmeyer flask. The solution was heated in a microwave oven for 8 min till boiling and till full dissolving of the agarose powder. The agarose solution was poured in a 10 x 15 cm gel tray, with a specific comb and left to cool down and solidify the gel. The NPs were loaded by mixing them first with a loading buffer (30% glycerol with 0.3% Orange G) and run the gel at a constant voltage of 100 V for 30-100 min.

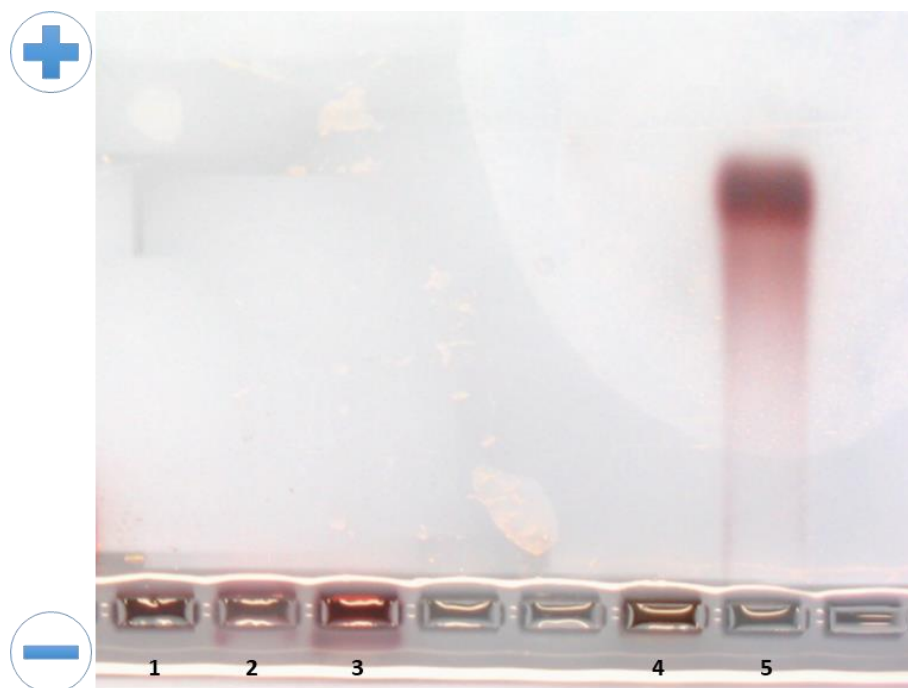


Figure 6-1 Au NPs migration in agarose gel electrophoresis. The migration of 1) Au-PT (+), 2) Au-SB (+/-), 3) Au-PC (+/-), 4) 4nm Au-PT (+), and 5) 4nm Au-PMA (-) in agarose gel upon electric force pushing the negatively charged NPs toward the positive pole.

Figure 6-1 shows the obtained results after running the gel with the Au NPs, it can be seen that only the negative charged NPs were able to migrate towards the positive pole, while the positive and the zwitterionic NPs did not. This visually proves the successful coating of the different sizes of the Au NPs and shows clearly (even in some cases the zeta potential of the SB zwitterionic NPs gave negative results) the zwitterionic and the positive character of the NPs.

6.2 Quantification of the adsorbed protein

The amount of protein adsorbed onto the NPs could be quantified using different techniques. In the present work, we have used two different methods to quantify the amount of BSA protein adsorbed onto the 15 nm Au-PMA NPs, the Coomassie Bradford assay (CBA) and by using SDS-PAGE gel electrophoresis, the procedures of the experiment were carried out according to the manufacture protocols and according to previous standard protocols here (Hühn et al., 2016). Briefly, the Au NPs were incubated with different concentrations of BSA protein at 37 °C for 1h, followed by the purification by using centrifugation for 3x times, and the pellets were split, one for CBA quantification and the other one for the SDS-PAGE gel.

Figure 6-2 and Figure 6-3 show the amount of protein adsorbed onto the NPs as measured by CBA and SDS-PAGE gel, respectively. As expected for the negative NPs and supporting for the results obtained by the FCS, they showed a stepwise degree of protein adsorption as a function of protein concentration. This has been proved by the CBA and by quantifying the gel bands in the SDS-PAGE gel, the later we have calibrated the gel by using known concentrations of the protein and the image has been processed by Fiji (Schindelin et al., 2012).

It has been observed from both methods, the amount of the protein adsorbed onto the surface of the NPs is less than 3% of the initial protein at the highest concentration point. This supports our assumption in performing the Hill model for the protein adsorption by FCS, as the model rely on neglecting the amount of the adsorbed protein onto the surface of the NPs.

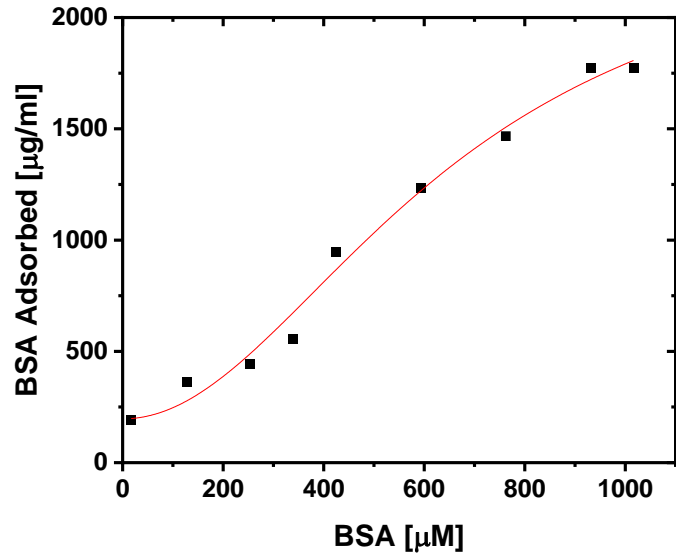


Figure 6-2 BSA protein adsorption as measured by Coomassie Bradford assay. The BSA adsorption onto the 15 nm Au-PMA NPs quantified by CBA, showing a stepwise increase in the adsorbed BSA.

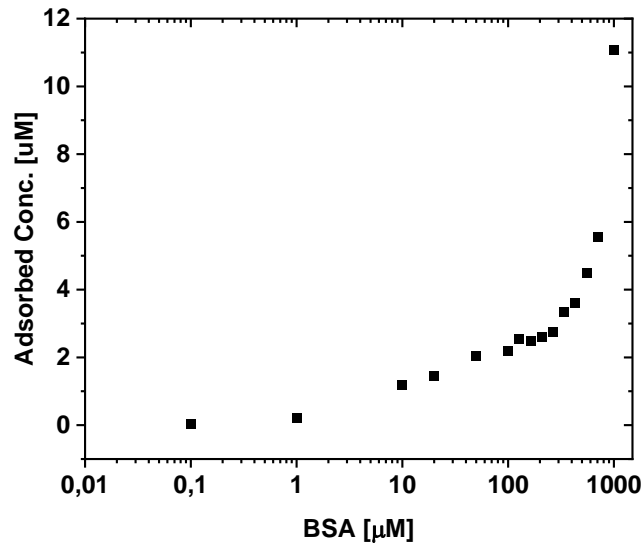


Figure 6-3 BSA adsorption as measured by SDS-PAGE gel electrophoresis. The BSA adsorption onto the 15 nm Au-PMA NPs quantified by the SDS-PAGE gel method, showing stepwise increases in the BSA as a function of the initial concentration.

6.3 List of hazardous substances

Chemical	CAS-No.	GHS Pictogram	H-Statements	P-Statements
HAuCl ₄	27988-77-8		H-314, H-317, H-318	P260, P303+P361+P353 P305+P351+P338 P301+P330+P331
Nitric acid	7697-37-2		H272 H290 H314 EUH071	P280 P304+ P305+ P310 P303 P220
Dodecylamine	124-22-1		H304 H314 H335 H373 H410	P260 P264 P271 P273 P280 P301+ P303 P304 P305
Chloroform	67-66-3		H302 H315 H319 H331 H336 H351 H372	P201 P202 P260 P264 P270 P271 P273 P280 P301 P302
tetraoctylammoniumbromide (TOAB)	14866-33-2			
HCl	7647-01-0		H314 H335	P260 P303+ P305+ P301+ P405 P501
NaOH	1310-73-2			
dodecanethiol (DDT)	112-55-0		H314 H318 H317 H400 H410	P261 P264 P272 P273 P280 P301 P303 P304 P305
THF	109-99-9		H225 H319 H351 H335	P210 P261 P303+ P305+ P405 P501
HSA	70027-90-7		No hazard statements	
Tf	11096-37-0		No hazard statements	
Rhodamine 6G dye (Rh6G)	989-38-8		No hazard statements	
trisodium citrate	6132-04-3		No hazard statements	
Resazurin	62758-13-8		No hazard statements	
poly(isobutylene-alt-maleic anhydride)	26426-80-2		No hazard statements	

7 References

- Abdelmonem, A. M.; Pelaz, B.; Kantner, K.; Bigall, N. C.; Del Pino, P.; Parak, W. J. Charge and agglomeration dependent in vitro uptake and cytotoxicity of zinc oxide nanoparticles. *Journal of Inorganic Biochemistry* **2015**, *153*, 334–338.
- Alfrey, T.; Morawetz, H.; Fitzgerald, E. B.; Fuoss, R. M. SYNTHETIC ELECTRICAL ANALOG OF PROTEINS 1. *J. Am. Chem. Soc.* **1950**, *72* (4), 1864. DOI: 10.1021/ja01160a532.
- Anselmo, A. C.; Mitragotri, S. Nanoparticles in the clinic: An update post COVID -19 vaccines. *Bioeng Transl Med* **2021**, e10246. DOI: 10.1002/btm2.10246.
- Ashraf, S.; Park, J.; Bichelberger, M. A.; Kantner, K.; Hartmann, R.; Maffre, P.; Said, A. H.; Feliu, N.; Lee, J.; Lee, D.; Nienhaus, G. U.; Kim, S.; Parak, W. J. Zwitterionic surface coating of quantum dots reduces protein adsorption and cellular uptake. *Nanoscale* **2016**, *8* (41), 17794–17800. DOI: 10.1039/c6nr05805a.
- Baggerman, J.; Smulders, M. M. J.; Zuilhof, H. Romantic Surfaces: A Systematic Overview of Stable, Biospecific, and Antifouling Zwitterionic Surfaces. *Langmuir : the ACS journal of surfaces and colloids* **2019**, *35* (5), 1072–1084. DOI: 10.1021/acs.langmuir.8b03360.
- Balog, S.; Rodriguez-Lorenzo, L.; Monnier, C. A.; Obiols-Rabasa, M.; Rothen-Rutishauser, B.; Schurtenberger, P.; Petri-Fink, A. Characterizing nanoparticles in complex biological media and physiological fluids with depolarized dynamic light scattering. *Nanoscale* [Online] **2015**, *7* (14), 5991–5997. <https://pubs.rsc.org/en/content/articlelanding/2015/NR/C4NR06538G>.
- Barrán-Berdón, A. L.; Pozzi, D.; Caracciolo, G.; Capriotti, A. L.; Caruso, G.; Cavaliere, C.; Riccioli, A.; Palchetti, S.; Laganà, A. Time evolution of nanoparticle-protein corona in human plasma: relevance for targeted drug delivery. *Langmuir : the ACS journal of surfaces and colloids* **2013**, *29* (21), 6485–6494. DOI: 10.1021/la401192x.
- Bastús, N. G.; Comenge, J.; Puentes, V. Kinetically controlled seeded growth synthesis of citrate-stabilized gold nanoparticles of up to 200 nm: size focusing versus Ostwald ripening. *Langmuir : the ACS journal of surfaces and colloids* **2011**, *27* (17), 11098–11105. DOI: 10.1021/la201938u.
- Behzadi, S.; Serpooshan, V.; Tao, W.; Hamaly, M. A.; Alkawareek, M. Y.; Dreaden, E. C.; Brown, D.; Alkilany, A. M.; Farokhzad, O. C.; Mahmoudi, M. Cellular uptake of nanoparticles: journey inside the cell. *Chemical Society reviews* **2017**, *46* (14), 4218–4244. DOI: 10.1039/c6cs00636a.

References

- Bevilacqua, P.; Nuzzo, S.; Torino, E.; Condorelli, G.; Salvatore, M.; Grimaldi, A. M. Antifouling Strategies of Nanoparticles for Diagnostic and Therapeutic Application: A Systematic Review of the Literature. *Nanomaterials (Basel, Switzerland)* [Online] **2021**, *11* (3), 780. <https://www.mdpi.com/2079-4991/11/3/780>.
- Bonvin, D.; Aschauer, U.; Alexander, D. T. L.; Chiappe, D.; Moniatte, M.; Hofmann, H.; Mionić Ebersold, M. Protein Corona: Impact of Lymph Versus Blood in a Complex In Vitro Environment. *Small (Weinheim an der Bergstrasse, Germany)* [Online] **2017**, *13* (29), 1700409. <https://onlinelibrary.wiley.com/doi/10.1002/sml.201700409>.
- Brust, M.; Walker, M.; Bethell, D.; Schiffrin, D. J.; Whyman, R. Synthesis of thiol-derivatised gold nanoparticles in a two-phase Liquid–Liquid system. *Journal of the Chemical Society, Chemical Communications* [Online] **1994**, No. 7, 801–802.
- Cao, Z.; Jiang, S. Super-hydrophilic zwitterionic poly(carboxybetaine) and amphiphilic non-ionic poly(ethylene glycol) for stealth nanoparticles. *Nano Today* [Online] **2012**, *7* (5), 404–413. <https://www.sciencedirect.com/science/article/pii/S1748013212000813>.
- Carril, M.; Padro, D.; Del Pino, P.; Carrillo-Carrion, C.; Gallego, M.; Parak, W. J. In situ detection of the protein corona in complex environments. *Nature communications* **2017**, *8* (1), 1542. DOI: 10.1038/s41467-017-01826-4.
- Carrillo-Carrion, C.; Carril, M.; Parak, W. J. Techniques for the experimental investigation of the protein corona. *Current Opinion in Biotechnology* [Online] **2017**, *46*, 106–113. <https://www.sciencedirect.com/science/article/pii/S0958166916302701>.
- Casals, E.; Pfaller, T.; Duschl, A.; Oostingh, G. J.; Puntès, V. Time evolution of the nanoparticle protein corona. *ACS nano* **2010**, *4* (7), 3623–3632. DOI: 10.1021/nn901372t.
- Cedervall, T.; Lynch, I.; Lindman, S.; Berggård, T.; Thulin, E.; Nilsson, H.; Dawson, K. A.; Linse, S. Understanding the nanoparticle-protein corona using methods to quantify exchange rates and affinities of proteins for nanoparticles. *Proceedings of the National Academy of Sciences of the United States of America* **2007**, *104* (7), 2050–2055. DOI: 10.1073/pnas.0608582104.
- Chakraborty, I.; Feliu, N.; Roy, S.; Dawson, K.; Parak, W. J. Protein-Mediated Shape Control of Silver Nanoparticles. *Bioconjugate Chemistry* **2018**, *29* (4), 1261–1265. DOI: 10.1021/acs.bioconjchem.8b00034.

References

- Chen, B.-M.; Cheng, T.-L.; Roffler, S. R. Polyethylene Glycol Immunogenicity: Theoretical, Clinical, and Practical Aspects of Anti-Polyethylene Glycol Antibodies. *ACS nano* **2021**, *15* (9), 14022–14048. DOI: 10.1021/acsnano.1c05922.
- Chithrani, B. D.; Chan, W. C. W. Elucidating the mechanism of cellular uptake and removal of protein-coated gold nanoparticles of different sizes and shapes. *Nano letters* **2007**, *7* (6), 1542–1550. DOI: 10.1021/nl070363y.
- Cho, E. C.; Zhang, Q.; Xia, Y. The effect of sedimentation and diffusion on cellular uptake of gold nanoparticles. *Nature Nanotech* [Online] **2011**, *6* (6), 385–391. <https://www.nature.com/articles/nnano.2011.58>.
- Choi, H.-J.; Montemagno, C. D. Recent Progress in Advanced Nanobiological Materials for Energy and Environmental Applications. *Materials (Basel, Switzerland)* [Online] **2013**, *6* (12), 5821–5856. <https://www.mdpi.com/1996-1944/6/12/5821/htm>.
- Da Huang; Wang, Y.; Yang, F.; Shen, H.; Weng, Z.; Wu, D. Charge-reversible and pH-responsive biodegradable micelles and vesicles from linear-dendritic supramolecular amphiphiles for anticancer drug delivery. *Polym. Chem.* [Online] **2017**, *8* (43), 6675–6687. <https://pubs.rsc.org/en/content/articlelanding/2017/PY/C7PY01556A>.
- Da Huang; Yang, F.; Wang, X.; Shen, H.; You, Y.; Wu, D. Facile synthesis and self-assembly behaviour of pH-responsive degradable polyacetal dendrimers. *Polym. Chem.* [Online] **2016**, *7* (40), 6154–6158. <https://pubs.rsc.org/en/content/articlelanding/2016/PY/C6PY01511E>.
- Dai, S.; Ravi, P.; Tam, K. C. pH-Responsive polymers: synthesis, properties and applications. *Soft Matter* [Online] **2008**, *4* (3), 435–449. <https://pubs.rsc.org/en/content/articlelanding/2008/SM/B714741D>.
- Dawson, K. A.; Yan, Y. Current understanding of biological identity at the nanoscale and future prospects. *Nature nanotechnology* [Online] **2021**.
- De, M.; Ghosh, P. S.; Rotello, V. M. Applications of Nanoparticles in Biology. *Adv. Mater.* [Online] **2008**, *20* (22), 4225–4241. <https://onlinelibrary.wiley.com/doi/10.1002/adma.200703183>.
- Debayle, M.; Balloul, E.; Dembele, F.; Xu, X.; Hanafi, M.; Ribot, F.; Monzel, C.; Coppey, M.; Fragola, A.; Dahan, M.; Pons, T.; Lequeux, N. Zwitterionic polymer ligands: an ideal surface coating to totally suppress protein-nanoparticle corona formation? *Biomaterials* **2019**, *219*, 119357. DOI: 10.1016/j.biomaterials.2019.119357.

References

- Del Pino, P.; Pelaz, B.; Zhang, Q.; Maffre, P.; Nienhaus, G. U.; Parak, W. J. Protein corona formation around nanoparticles – from the past to the future. *Mater. Horiz.* **2014**, *1* (3), 301–313. DOI: 10.1039/C3MH00106G.
- Del Pino, P.; Yang, F.; Pelaz, B.; Zhang, Q.; Kantner, K.; Hartmann, R.; Martinez de Baroja, N.; Gallego, M.; Möller, M.; Manshian, B. B.; Soenen, S. J.; Riedel, R.; Hampp, N.; Parak, W. J. Basic Physicochemical Properties of Polyethylene Glycol Coated Gold Nanoparticles that Determine Their Interaction with Cells. *Angewandte Chemie (International ed. in English)* **2016**, *55* (18), 5483–5487. DOI: 10.1002/anie.201511733.
- Ding, L.; Yao, C.; Yin, X.; Li, C.; Huang, Y.; Wu, M.; Wang, B.; Guo, X.; Wang, Y.; Wu, M. Size, Shape, and Protein Corona Determine Cellular Uptake and Removal Mechanisms of Gold Nanoparticles. *Small (Weinheim an der Bergstrasse, Germany)* **2018**, *14* (42), e1801451. DOI: 10.1002/smll.201801451.
- Dobrovolskaia, M. A.; Patri, A. K.; Zheng, J.; Clogston, J. D.; Ayub, N.; Aggarwal, P.; Neun, B. W.; Hall, J. B.; McNeil, S. E. Interaction of colloidal gold nanoparticles with human blood: effects on particle size and analysis of plasma protein binding profiles. *Nanomedicine : nanotechnology, biology, and medicine* [Online] **2009**, *5* (2), 106–117. <https://www.sciencedirect.com/science/article/pii/S1549963408001445>.
- Du, J.-Z.; Li, H.-J.; Wang, J. Tumor-Acidity-Cleavable Maleic Acid Amide (TACMAA): A Powerful Tool for Designing Smart Nanoparticles To Overcome Delivery Barriers in Cancer Nanomedicine. *Accounts of chemical research* **2018**, *51* (11), 2848–2856. DOI: 10.1021/acs.accounts.8b00195.
- Du, J.-Z.; Sun, T.-M.; Song, W.-J.; Wu, J.; Wang, J. A tumor-acidity-activated charge-conversional nanogel as an intelligent vehicle for promoted tumoral-cell uptake and drug delivery. *Angewandte Chemie International Edition* [Online] **2010**, *49* (21), 3621–3626. https://onlinelibrary.wiley.com/doi/10.1002/anie.200907210?__cf_chl_jschl_tk__=pmd_ce8Fd.GWWjZJFrb6g1g6zhzqjSwJ_XCY3xij_l39ons-1635860954-0-gqNtZGzNAiWjcnBszQz9.
- Du, Y.; Jin, J.; Liang, H.; Jiang, W. Structural and Physicochemical Properties and Biocompatibility of Linear and Looped Polymer-Capped Gold Nanoparticles. *Langmuir : the ACS journal of surfaces and colloids* **2019**, *35* (25), 8316–8324. DOI: 10.1021/acs.langmuir.9b00045.
- Eagle, F. W.; Park, N.; Cash, M.; Cossairt, B. M. Surface Chemistry and Quantum Dot Luminescence: Shell Growth, Atomistic Modification, and Beyond. *ACS Energy Lett.* **2021**, *6* (3), 977–984. DOI: 10.1021/acsenergylett.0c02697.

References

- Faria, M.; Björnmalm, M.; Thurecht, K. J.; Kent, S. J.; Parton, R. G.; Kavallaris, M.; Johnston, A. P. R.; Gooding, J. J.; Corrie, S. R.; Boyd, B. J.; Thordarson, P.; Whittaker, A. K.; Stevens, M. M.; Prestidge, C. A.; Porter, C. J. H.; Parak, W. J.; Davis, T. P.; Crampin, E. J.; Caruso, F. Minimum information reporting in bio-nano experimental literature. *Nature nanotechnology* **2018**, *13* (9), 777–785. DOI: 10.1038/s41565-018-0246-4.
- Feliu, N.; Docter, D.; Heine, M.; Del Pino, P.; Ashraf, S.; Kolosnjaj-Tabi, J.; Macchiarini, P.; Nielsen, P.; Alloyeau, D.; Gazeau, F.; Stauber, R. H.; Parak, W. J. In vivo degeneration and the fate of inorganic nanoparticles. *Chemical Society reviews* **2016**, *45* (9), 2440–2457. DOI: 10.1039/C5CS00699F.
- Ferrand, P.; Wenger, J.; Rigneault, H. Fluorescence correlation spectroscopy. *Methods in molecular biology (Clifton, N.J.)* **2011**, *783*, 181–195. DOI: 10.1007/978-1-61779-282-3_10.
- Florence, A. T. Trajectories in nanotechnology: embracing complexity, seeking analogies. *Drug delivery and translational research* **2021**, 1–7. DOI: 10.1007/s13346-020-00877-3.
- Fu, K.; Wang, X.; Yuan, X.; Wang, D.; Mi, X.; Tan, X.; Zhang, Y. Size-Dependent Penetration of Gold Nanoprobes into Fixed Cells. *ACS omega* **2021**, *6* (5), 3791–3799. DOI: 10.1021/acsomega.0c05458.
- Galdino, F. E.; Picco, A. S.; Sforca, M. L.; Cardoso, M. B.; Loh, W. Effect of particle functionalization and solution properties on the adsorption of bovine serum albumin and lysozyme onto silica nanoparticles. *Colloids and surfaces. B, Biointerfaces* **2019**, *186*, 110677. DOI: 10.1016/j.colsurfb.2019.110677.
- Gao, Y.; Yang, X. Equilibrium and Dynamic Surface Properties of Sulfosuccinate Surfactants. *J Surfact Deterg* [Online] **2014**, *17* (6), 1117–1123. <https://aocs.onlinelibrary.wiley.com/doi/full/10.1007/s11743-014-1612-3>.
- García-Álvarez, R.; Vallet-Regí, M. Hard and Soft Protein Corona of Nanomaterials: Analysis and Relevance. *Nanomaterials (Basel, Switzerland)* [Online] **2021**, *11* (4), 888. <https://www.mdpi.com/2079-4991/11/4/888>.
- Geidel, C.; Schmachtel, S.; Riedinger, A.; Pfeiffer, C.; Müllen, K.; Klapper, M.; Parak, W. J. A general synthetic approach for obtaining cationic and anionic inorganic nanoparticles via encapsulation in amphiphilic copolymers. *Small (Weinheim an der Bergstrasse, Germany)* **2011**, *7* (20), 2929–2934. DOI: 10.1002/smll.201100509.
- Grenier, P.; Viana, Iara Maíra de Oliveira; Lima, E. M.; Bertrand, N. Anti-polyethylene glycol antibodies alter the protein corona deposited on nanoparticles and the physiological pathways

References

- regulating their fate in vivo. *Journal of controlled release : official journal of the Controlled Release Society* [Online] **2018**, *287*, 121–131. <https://www.sciencedirect.com/science/article/pii/S0168365918304887>.
- Hadjidemetriou, M.; McAdam, S.; Garner, G.; Thackeray, C.; Knight, D.; Smith, D.; Al-Ahmady, Z.; Mazza, M.; Rogan, J.; Clamp, A.; Kostarelos, K. The Human In Vivo Biomolecule Corona onto PEGylated Liposomes: A Proof-of-Concept Clinical Study. *Advanced Materials* [Online] **2019**, *31* (4), e1803335. <https://onlinelibrary.wiley.com/doi/10.1002/adma.201803335>.
- HILL, A. The possible effects of the aggregation of the molecules of haemoglobin on its dissociation curves. *The Journal of Physiology* [Online] **1910**, *40* (suppl), 4–7. <https://ci.nii.ac.jp/naid/10008305829/en/>.
- Ho, Y. T.; Azman, N. '.; Loh, F. W. Y.; Ong, G. K. T.; Engudar, G.; Kriz, S. A.; Kah, J. C. Y. Protein Corona Formed from Different Blood Plasma Proteins Affects the Colloidal Stability of Nanoparticles Differently. *Bioconjugate Chemistry* **2018**, *29* (11), 3923–3934. DOI: 10.1021/acs.bioconjchem.8b00743.
- Hua, X. Y.; Rosen, M. J. Dynamic surface tension of aqueous surfactant solutions. *Journal of Colloid and Interface Science* [Online] **1988**, *124* (2), 652–659. <http://www.sciencedirect.com/science/article/pii/0021979788902032>.
- Hühn, D.; Kantner, K.; Geidel, C.; Brandholt, S.; Cock, I. de; Soenen, S. J. H.; Rivera_Gil, P.; Montenegro, J.-M.; Braeckmans, K.; Müllen, K.; Nienhaus, G. U.; Klapper, M.; Parak, W. J. Polymer-Coated Nanoparticles Interacting with Proteins and Cells: Focusing on the Sign of the Net Charge. *ACS nano* **2013**, *7* (4), 3253–3263. DOI: 10.1021/nn3059295.
- Hühn, J.; Carrillo-Carrion, C.; Soliman, M. G.; Pfeiffer, C.; Valdeperez, D.; Masood, A.; Chakraborty, I.; Zhu, L.; Gallego, M.; Yue, Z.; Carril, M.; Feliu, N.; Escudero, A.; Alkilany, A. M.; Pelaz, B.; Del Pino, P.; Parak, W. J. Selected Standard Protocols for the Synthesis, Phase Transfer, and Characterization of Inorganic Colloidal Nanoparticles. *Chemistry of Materials* **2016**, *29* (1), 399–461. DOI: 10.1021/acs.chemmater.6b04738.
- Ivanov, M. R.; Bednar, H. R.; Haes, A. J. Investigations of the mechanism of gold nanoparticle stability and surface functionalization in capillary electrophoresis. *ACS nano* **2009**, *3* (2), 386–394. DOI: 10.1021/nn8005619.

References

- John Turkevich; Peter Cooper Stevenson; James Hillier. A study of the nucleation and growth processes in the synthesis of colloidal gold. *Discuss. Faraday Soc.* **1951**, *11* (0), 55–75. DOI: 10.1039/DF9511100055.
- Joseph J. Jasper. The Surface Tension of Pure Liquid Compounds. *Journal of Physical and Chemical Reference Data* [Online] **2009**, *1* (4), 841. <https://aip.scitation.org/doi/10.1063/1.3253106>.
- Ke, P. C.; Lin, S.; Parak, W. J.; Davis, T. P.; Caruso, F. A Decade of the Protein Corona. *ACS nano* **2017**, *11* (12), 11773–11776. DOI: 10.1021/acsnano.7b08008.
- Kharazian, B.; Hadipour, N. L.; Ejtehadi, M. R. Understanding the nanoparticle-protein corona complexes using computational and experimental methods. *The international journal of biochemistry & cell biology* **2016**, *75*, 162–174. DOI: 10.1016/j.biocel.2016.02.008.
- Koc, J.; Schönemann, E.; Amuthalingam, A.; Clarke, J.; Finlay, J. A.; Clare, A. S.; Laschewsky, A.; Rosenhahn, A. Low-Fouling Thin Hydrogel Coatings Made of Photo-Cross-Linked Polyzwitterions. *Langmuir : the ACS journal of surfaces and colloids* **2019**, *35* (5), 1552–1562.
- Koll, R.; Fruhner, L. S.; Heller, H.; Allgaier, J.; Pyckhout-Hintzen, W.; Kruteva, M.; Feoktystov, A.; Biehl, R.; Förster, S.; Weller, H. Creating a synthetic platform for the encapsulation of nanocrystals with covalently bound polymer shells. *Nanoscale* [Online] **2019**.
- Krieger, J. W.; Singh, A. P.; Bag, N.; Garbe, C. S.; Saunders, T. E.; Langowski, J.; Wohland, T. Imaging fluorescence (cross-) correlation spectroscopy in live cells and organisms. *Nature protocols* **2015**, *10* (12), 1948–1974. DOI: 10.1038/nprot.2015.100.
- Laschewsky, A.; Rosenhahn, A. Molecular Design of Zwitterionic Polymer Interfaces: Searching for the Difference. *Langmuir : the ACS journal of surfaces and colloids* **2019**, *35* (5), 1056–1071. DOI: 10.1021/acs.langmuir.8b01789.
- Lck, M.; Paulke, B.-R.; Schröder, W.; Blunk, T.; Müller, R. H. Analysis of plasma protein adsorption on polymeric nanoparticles with different surface characteristics. *J. Biomed. Mater. Res.* **1998**, *39* (3), 478–485. DOI: 10.1002/(SICI)1097-4636(19980305)39:3<478:AID-JBM19>3.0.CO;2-6.
- Liedl, T.; Keller, S.; Simmel, F. C.; Rädler, J. O.; Parak, W. J. Fluorescent nanocrystals as colloidal probes in complex fluids measured by fluorescence correlation spectroscopy. *Small (Weinheim an der Bergstrasse, Germany)* **2005**, *1* (10), 997–1003. DOI: 10.1002/sml.200500108.
- Lin, C.-A. J.; Sperling, R. A.; Li, J. K.; Yang, T.-Y.; Li, P.-Y.; Zanella, M.; Chang, W. H.; Parak, W. J. Design of an amphiphilic polymer for nanoparticle coating and functionalization. *Small (Weinheim an der Bergstrasse, Germany)* **2008**, *4* (3), 334–341. DOI: 10.1002/sml.200700654.

References

- Link, S.; El-Sayed, M. A. Optical properties and ultrafast dynamics of metallic nanocrystals. *Annual review of physical chemistry* **2003**, *54*, 331–366. DOI: 10.1146/annurev.physchem.54.011002.103759.
- Loiola, L. M. D.; Batista, M.; Capeletti, L. B.; Mondo, G. B.; Rosa, R. S. M.; Marques, R. E.; Bajgelman, M. C.; Cardoso, M. B. Shielding and stealth effects of zwitterion moieties in double-functionalized silica nanoparticles. *Journal of Colloid and Interface Science* **2019**, *553*, 540–548.
- Lundqvist, M.; Cedervall, T. Three Decades of Research about the Corona Around Nanoparticles: Lessons Learned and Where to Go Now. *Small (Weinheim an der Bergstrasse, Germany)* [Online] **2020**, e2000892.
- Maffre, P.; Brandholt, S.; Nienhaus, K.; Shang, L.; Parak, W. J.; Nienhaus, G. U. Effects of surface functionalization on the adsorption of human serum albumin onto nanoparticles - a fluorescence correlation spectroscopy study. *Beilstein journal of nanotechnology* **2014**, *5*, 2036–2047. DOI: 10.3762/bjnano.5.212.
- Maffre, P.; Nienhaus, K.; Amin, F.; Parak, W. J.; Nienhaus, G. U. Characterization of protein adsorption onto FePt nanoparticles using dual-focus fluorescence correlation spectroscopy. *Beilstein journal of nanotechnology* **2011**, *2*, 374–383. DOI: 10.3762/bjnano.2.43.
- Mahmoudi, M.; Bertrand, N.; Zope, H.; Farokhzad, O. C. Emerging understanding of the protein corona at the nano-bio interfaces. *Nano Today* **2016**, *11* (6), 817–832. DOI: 10.1016/j.nantod.2016.10.005.
- Mirshafiee, V.; Mahmoudi, M.; Lou, K.; Cheng, J.; Kraft, M. L. Protein corona significantly reduces active targeting yield. *Chem. Commun.* [Online] **2013**, *49* (25), 2557–2559. <https://pubs.rsc.org/en/content/articlelanding/2013/CC/c3cc37307j>.
- Mishra, K.; Das, P. K. Thermodynamics of adsorption of lysozyme on gold nanoparticles from second harmonic light scattering. *Physical chemistry chemical physics : PCCP* **2019**, *21* (14), 7675–7684. DOI: 10.1039/c8cp07299j.
- Monteiro, C. A. P.; Oliveira, A. D. P. R.; Silva, R. C.; Lima, R. R. M.; Souto, F. O.; Baratti, M. O.; Carvalho, H. F.; Santos, B. S.; Cabral Filho, P. E.; Fontes, A. Evaluating internalization and recycling of folate receptors in breast cancer cells using quantum dots. *Journal of photochemistry and photobiology. B, Biology* [Online] **2020**, *209*, 111918. <https://reader.elsevier.com/reader/sd/pii/S1011134420303687?token=E236C9678661E48CA44C71BA1CCACD42B766F5DBFD444C9F78B4F>

References

- EBB6D986E0CC3C5CCAD5F084C5ED58AC78C7346D3FC&originRegion=eu-west-1&originCreation=20210724134612.
- Morgese, G.; Shirmardi Shaghasemi, B.; Causin, V.; Zenobi-Wong, M.; Ramakrishna, S. N.; Reimhult, E.; Benetti, E. M. Next-Generation Polymer Shells for Inorganic Nanoparticles are Highly Compact, Ultra-Dense, and Long-Lasting Cyclic Brushes. *Angewandte Chemie International Edition* [Online] **2017**, *56* (16), 4507–4511. <https://onlinelibrary.wiley.com/doi/10.1002/anie.201700196>.
- Moustaoui, H.; Saber, J.; Djeddi, I.; Liu, Q.; Movia, D.; Prina-Mello, A.; Spadavecchia, J.; La Lamy de Chapelle, M.; Djaker, N. A protein corona study by scattering correlation spectroscopy: a comparative study between spherical and urchin-shaped gold nanoparticles. *Nanoscale* **2019**, *11* (8), 3665–3673. DOI: 10.1039/c8nr09891c.
- Moyano, D. F.; Goldsmith, M.; Solfiell, D. J.; Landesman-Milo, D.; Miranda, O. R.; Peer, D.; Rotello, V. M. Nanoparticle hydrophobicity dictates immune response. *Journal of the American Chemical Society* **2012**, *134* (9), 3965–3967. DOI: 10.1021/ja2108905.
- Moyano, D. F.; Saha, K.; Prakash, G.; Yan, B.; Kong, H.; Yazdani, M.; Rotello, V. M. Fabrication of corona-free nanoparticles with tunable hydrophobicity. *ACS nano* **2014**, *8* (7), 6748–6755. DOI: 10.1021/nn5006478.
- Müller, J.; Bauer, K. N.; Prozeller, D.; Simon, J.; Mailänder, V.; Wurm, F. R.; Winzen, S.; Landfester, K. Coating nanoparticles with tunable surfactants facilitates control over the protein corona. *Biomaterials* **2017**, *115*, 1–8. DOI: 10.1016/j.biomaterials.2016.11.015.
- Nanotechnology Timeline | National Nanotechnology Initiative. <https://www.nano.gov/timeline> (accessed August 25, 2021).
- Nazareus, M.; Zhang, Q.; Soliman, M. G.; Del Pino, P.; Pelaz, B.; Carregal-Romero, S.; Rejman, J.; Rothen-Rutishauser, B.; Clift, M. J. D.; Zellner, R.; Nienhaus, G. U.; Delehanty, J. B.; Medintz, I. L.; Parak, W. J. In vitro interaction of colloidal nanoparticles with mammalian cells: What have we learned thus far? *Beilstein journal of nanotechnology* **2014**, *5*, 1477–1490. DOI: 10.3762/bjnano.5.161.
- Nsubuga, A.; Sgarzi, M.; Zarschler, K.; Kubeil, M.; Hübner, R.; Steudtner, R.; Graham, B.; Joshi, T.; Stephan, H. Facile preparation of multifunctionalisable 'stealth' upconverting nanoparticles for biomedical applications. *Dalton transactions (Cambridge, England : 2003)* **2018**, *47* (26), 8595–8604. DOI: 10.1039/c8dt00241j.

References

- O'Brien, J.; Wilson, I.; Orton, T.; Pognan, F. Investigation of the Alamar Blue (resazurin) fluorescent dye for the assessment of mammalian cell cytotoxicity. *European Journal of Biochemistry* [Online] **2000**, *267* (17), 5421–5426. <https://febs.onlinelibrary.wiley.com/doi/full/10.1046/j.1432-1327.2000.01606.x?sid=nlm%3Apubmed>.
- Ouyang, B.; Poon, W.; Zhang, Y.-N.; Lin, Z. P.; Kingston, B. R.; Tavares, A. J.; Zhang, Y.; Chen, J.; Valic, M. S.; Syed, A. M.; MacMillan, P.; Couture-Senécal, J.; Zheng, G.; Chan, W. C. W. The dose threshold for nanoparticle tumour delivery. *Nature materials* **2020**, *12* (19), 1362–1371. DOI: 10.1038/s41563-020-0755-z.
- Pang, X.; Jiang, Y.; Xiao, Q.; Leung, A. W.; Hua, H.; Xu, C. pH-responsive polymer-drug conjugates: Design and progress. *Journal of controlled release : official journal of the Controlled Release Society* [Online] **2016**, *222*, 116–129. <https://www.sciencedirect.com/science/article/pii/S0168365915302765>.
- Pattipeiluhu, R.; Crielard, S.; Klein-Schiphorst, I.; Florea, B. I.; Kros, A.; Campbell, F. Unbiased Identification of the Liposome Protein Corona using Photoaffinity-based Chemoproteomics. *ACS central science* **2020**, *6* (4), 535–545. DOI: 10.1021/acscentsci.9b01222.
- Pellegrino, T.; Kudera, S.; Liedl, T.; Muñoz Javier, A.; Manna, L.; Parak, W. J. On the development of colloidal nanoparticles towards multifunctional structures and their possible use for biological applications. *Small (Weinheim an der Bergstrasse, Germany)* **2005**, *1* (1), 48–63. DOI: 10.1002/smll.200400071.
- Pellegrino, T.; Manna, L.; Kudera, S.; Liedl, T.; Koktysh, D.; Rogach, A. L.; Keller, S.; Rädler, J.; Natile, G.; Parak, W. J. Hydrophobic Nanocrystals Coated with an Amphiphilic Polymer Shell: A General Route to Water Soluble Nanocrystals. *Nano Lett.* **2004**, *4* (4), 703–707. DOI: 10.1021/nl035172j.
- Petrášek, Z.; Schwill, P. Fluctuations as a source of information in fluorescence microscopy. *J. R. Soc. Interface* **2009**, *6* (suppl_1). DOI: 10.1098/rsif.2008.0200.focus.
- Phan, H. T.; Haes, A. J. What Does Nanoparticle Stability Mean? *The journal of physical chemistry. C, Nanomaterials and interfaces* **2019**, *123* (27), 16495–16507. DOI: 10.1021/acs.jpcc.9b00913.
- Qiao, R.; Fu, C.; Li, Y.; Qi, X.; Ni, D.; Nandakumar, A.; Siddiqui, G.; Wang, H.; Zhang, Z.; Wu, T.; Zhong, J.; Tang, S.-Y.; Pan, S.; Zhang, C.; Whittaker, M. R.; Engle, J. W.; Creek, D. J.; Caruso, F.; Ke, P. C.; Cai, W.; Whittaker, A. K.; Davis, T. P. Sulfoxide-Containing Polymer-Coated Nanoparticles Demonstrate Minimal Protein Fouling and Improved Blood Circulation. *Adv. Sci.* **2020**, *7* (13), 2000406. DOI: 10.1002/adv.202000406.

References

- Rampado, R.; Crotti, S.; Caliceti, P.; Pucciarelli, S.; Agostini, M. Recent Advances in Understanding the Protein Corona of Nanoparticles and in the Formulation of "Stealthy" Nanomaterials. *Frontiers in bioengineering and biotechnology* **2020**, *8*, 166. DOI: 10.3389/fbioe.2020.00166.
- Rana, S.; Yu, X.; Patra, D.; Moyano, D. F.; Miranda, O. R.; Hussain, I.; Rotello, V. M. Control of surface tension at liquid-liquid interfaces using nanoparticles and nanoparticle-protein complexes. *Langmuir : the ACS journal of surfaces and colloids* **2012**, *28* (4), 2023–2027. DOI: 10.1021/la204017z.
- Rennick, J. J.; Johnston, A. P. R.; Parton, R. G. Key principles and methods for studying the endocytosis of biological and nanoparticle therapeutics. *Nature nanotechnology* **2021**. DOI: 10.1038/s41565-021-00858-8.
- Röcker, C.; Pötzl, M.; Zhang, F.; Parak, W. J.; Nienhaus, G. U. A quantitative fluorescence study of protein monolayer formation on colloidal nanoparticles. *Nature nanotechnology* **2009**, *4* (9), 577–580. DOI: 10.1038/nnano.2009.195.
- Rossner, C.; König, T. A. F.; Fery, A. Plasmonic Properties of Colloidal Assemblies. *Adv. Optical Mater.* **2021**, *9* (8), 2001869. DOI: 10.1002/adom.202001869.
- Rotureau, E.; Leonard, M.; Dellacherie, E.; Durand, A. Amphiphilic derivatives of dextran: adsorption at air/water and oil/water interfaces. *Journal of Colloid and Interface Science* **2004**, *279* (1), 68–77. DOI: 10.1016/j.jcis.2004.06.040.
- Roy, S.; Liu, Z.; Sun, X.; Gharib, M.; Yan, H.; Huang, Y.; Megahed, S.; Schnabel, M.; Zhu, D.; Feliu, N.; Chakraborty, I.; Sanchez-Cano, C.; Alkilany, A. M.; Parak, W. J. Assembly and Degradation of Inorganic Nanoparticles in Biological Environments. *Bioconjugate Chemistry* **2019**, *30* (11), 2751–2762. DOI: 10.1021/acs.bioconjchem.9b00645.
- Safavi-Sohi, R.; Maghari, S.; Raoufi, M.; Jalali, S. A.; Hajipour, M. J.; Ghassempour, A.; Mahmoudi, M. Bypassing Protein Corona Issue on Active Targeting: Zwitterionic Coatings Dictate Specific Interactions of Targeting Moieties and Cell Receptors. *ACS applied materials & interfaces* **2016**, *8* (35), 22808–22818. DOI: 10.1021/acsami.6b05099.
- Sakura, T.; Takahashi, T.; Kataoka, K.; Nagasaki, Y. One-pot preparation of mono-dispersed and physiologically stabilized gold colloid. *Colloid Polym Sci [Online]* **2005**, *284* (1), 97–101. <https://link.springer.com/article/10.1007/s00396-005-1339-9>.

References

- Sanchez-Cano, C.; Carril, M. Recent Developments in the Design of Non-Biofouling Coatings for Nanoparticles and Surfaces. *International Journal of Molecular Sciences* [Online] **2020**, *21* (3), 1007. <https://www.mdpi.com/1422-0067/21/3/1007>.
- Schindelin, J.; Arganda-Carreras, I.; Frise, E.; Kaynig, V.; Longair, M.; Pietzsch, T.; Preibisch, S.; Rueden, C.; Saalfeld, S.; Schmid, B.; Tinevez, J.-Y.; White, D. J.; Hartenstein, V.; Eliceiri, K.; Tomancak, P.; Cardona, A. Fiji: an open-source platform for biological-image analysis. *Nat Methods* [Online] **2012**, *9* (7), 676–682. <https://www.nature.com/articles/nmeth.2019>.
- Schlenoff, J. B. Zwitteration: coating surfaces with zwitterionic functionality to reduce nonspecific adsorption. *Langmuir : the ACS journal of surfaces and colloids* **2014**, *30* (32), 9625–9636. DOI: 10.1021/la500057j.
- Schroffenegger, M.; Leitner, N. S.; Morgese, G.; Ramakrishna, S. N.; Willinger, M.; Benetti, E. M.; Reimhult, E. Polymer Topology Determines the Formation of Protein Corona on Core-Shell Nanoparticles. *ACS nano* [Online] **2020**, *14* (10), 12708–12718. <https://pubs.acs.org/doi/pdf/10.1021/acsnano.0c02358>.
- Shang, L.; Nienhaus, G. U. In Situ Characterization of Protein Adsorption onto Nanoparticles by Fluorescence Correlation Spectroscopy. *Accounts of chemical research* **2017**, *50* (2), 387–395. DOI: 10.1021/acs.accounts.6b00579.
- Shang, L.; Nienhaus, K.; Nienhaus, G. U. Engineered nanoparticles interacting with cells: size matters. *Journal of nanobiotechnology* **2014**, *12*, 1–11. DOI: 10.1186/1477-3155-12-5.
- Slenders, E.; Castello, M.; Buttafava, M.; Villa, F.; Tosi, A.; Lanzanò, L.; Koho, S. V.; Vicidomini, G. Confocal-based fluorescence fluctuation spectroscopy with a SPAD array detector. *Light, science & applications* **2021**, *10* (1), 31. DOI: 10.1038/s41377-021-00475-z.
- Soliman, M. G.; Pelaz, B.; Parak, W. J.; Del Pino, P. Phase Transfer and Polymer Coating Methods toward Improving the Stability of Metallic Nanoparticles for Biological Applications. *Chem. Mater.* **2015**, *27* (3), 990–997. DOI: 10.1021/cm5043167.
- Sperling, R. A.; Parak, W. J. Surface modification, functionalization and bioconjugation of colloidal inorganic nanoparticles. *Philosophical transactions. Series A, Mathematical, physical, and engineering sciences* **2010**, *368* (1915), 1333–1383. DOI: 10.1098/rsta.2009.0273.
- Stark, W. J. Nanoparticles in biological systems. *Angewandte Chemie (International ed. in English)* **2011**, *50* (6), 1242–1258. DOI: 10.1002/anie.200906684.

References

- Stefania Garbujo; Elisabetta Galbiati; Lucia Salvioni; Matteo Mazzucchelli; Gianni Frascotti; Xing Sun; Saad Megahed; Neus Feliu; Davide Prospero; Wolfgang J. Parak; Miriam Colombo. Functionalization of colloidal nanoparticles with a discrete number of ligands based on a “HALO-bioclick” reaction. *Chem. Commun.* **2020**, 56 (77), 11398–11401. DOI: 10.1039/D0CC04355A.
- Tenzer, S.; Docter, D.; Kuharev, J.; Musyanovych, A.; Fetz, V.; Hecht, R.; Schlenk, F.; Fischer, D.; Kiouptsi, K.; Reinhardt, C.; Landfester, K.; Schild, H.; Maskos, M.; Knauer, S. K.; Stauber, R. H. Rapid formation of plasma protein corona critically affects nanoparticle pathophysiology. *Nature Nanotech* **2013**, 8 (10), 772–781. DOI: 10.1038/nnano.2013.181.
- Thomaz, A. A. de; Almeida, D. B.; Pelegati, V. B.; Carvalho, H. F.; Cesar, C. L. Measurement of the hydrodynamic radius of quantum dots by fluorescence correlation spectroscopy excluding blinking. *The journal of physical chemistry. B* **2015**, 119 (11), 4294–4299. DOI: 10.1021/jp512214p.
- Verma, A.; Stellacci, F. Effect of surface properties on nanoparticle-cell interactions. *Small (Weinheim an der Bergstrasse, Germany)* [Online] **2010**, 6 (1), 12–21. <https://onlinelibrary.wiley.com/doi/10.1002/smll.200901158>.
- Wang, Z.; Ma, G.; Zhang, J.; Yuan, Z.; Wang, L.; Bernards, M.; Chen, S. Surface protonation/deprotonation controlled instant affinity switch of nano drug vehicle (NDV) for pH triggered tumor cell targeting. *Biomaterials* **2015**, 62, 116–127. DOI: 10.1016/j.biomaterials.2015.05.020.
- Wolfram, J.; Yang, Y.; Shen, J.; Moten, A.; Chen, C.; Shen, H.; Ferrari, M.; Zhao, Y. The nano-plasma interface: Implications of the protein corona. *Colloids and surfaces. B, Biointerfaces* **2014**, 124, 17–24. DOI: 10.1016/j.colsurfb.2014.02.035.
- Woythe, L.; Tito, N. B.; Albertazzi, L. A quantitative view on multivalent nanomedicine targeting. *Advanced drug delivery reviews* **2021**, 169, 1–21. DOI: 10.1016/j.addr.2020.11.010.
- Wu, A.; Gao, Y.; Zheng, L. Zwitterionic amphiphiles: their aggregation behavior and applications. *Green Chem.* **2019**, 21 (16), 4290–4312. DOI: 10.1039/C9GC01808E.
- Xu, M.; Soliman, M. G.; Sun, X.; Pelaz, B.; Feliu, N.; Parak, W. J.; Liu, S. How Entanglement of Different Physicochemical Properties Complicates the Prediction of in Vitro and in Vivo Interactions of Gold Nanoparticles. *ACS nano* **2018**, 12 (10), 10104–10113. DOI: 10.1021/acsnano.8b04906.

References

- Zhang, F.; Lees, E.; Amin, F.; Rivera Gil, P.; Yang, F.; Mulvaney, P.; Parak, W. J. Polymer-coated nanoparticles: a universal tool for biolabelling experiments. *Small (Weinheim an der Bergstrasse, Germany)* **2011**, *7* (22), 3113–3127. DOI: 10.1002/smll.201100608.
- Zhang, Y.-N.; Lazarovits, J.; Poon, W.; Ouyang, B.; Nguyen, L. N. M.; Kingston, B. R.; Chan, W. C. W. Nanoparticle Size Influences Antigen Retention and Presentation in Lymph Node Follicles for Humoral Immunity. *Nano letters* **2019**, *19* (10), 7226–7235. DOI: 10.1021/acs.nanolett.9b02834.
- Zijlstra, P.; Paulo, P. M. R.; Yu, K.; Xu, Q.-H.; Orrit, M. Chemical interface damping in single gold nanorods and its near elimination by tip-specific functionalization. *Angewandte Chemie International Edition [Online]* **2012**, *51* (33), 8352–8355. <https://onlinelibrary.wiley.com/doi/full/10.1002/anie.201202318>.